University of Lethbridge Research Repository

OPUS   **http://opus.uleth.ca**

Theses   Arts and Science, Faculty of

2010

Snowmelt energy balance in a burned forest stand, Crowsnest Pass, Alberta

Burles, Katie

Lethbridge, Alta. : University of Lethbridge, Dept. of Geography, 2010

**SNOWMELT ENERGY BALANCE IN A BURNED FOREST STAND,
CROWSNEST PASS, ALBERTA**

KATIE BURLES
B.A., Thompson Rivers University, 2008

A Thesis
Submitted to the School of Graduate Studies
of the University of Lethbridge
in Partial Fulfilment of the
Requirements for the Degree

[MASTERS OF SCIENCE]

Department of Geography
University of Lethbridge
LETHBRIDGE, ALBERTA, CANADA

Dedication

I would like to dedicate this thesis to my brother Alex. His strength, dedication, and growth in the past two years has been remarkable.

Abstract

Forested watersheds in western North America are subject to significant change from natural and anthropogenic disturbance, including wildfire. Forest canopy changes have subsequent impacts on sub-canopy snow processes. A simple, process-based point energy balance model was developed to quantify differences in energy balance characteristics between a burned and a healthy forest stand. Potential model uncertainties were identified using sensitivity analyses. Simulated snowmelt accurately recreated measured snowmelt, providing confidence in the model's ability to simulate energy balance processes in subcanopy environments where wind redistribution and sublimation are not major drivers of the local snowmelt energy balance. In the burned stand, sub-canopy snow accumulation was greater but melted more rapidly than in the healthy stand. The removal of forest canopy resulted in more energy available for snowmelt, including higher short-wave and lower long-wave radiation, and increased turbulent fluxes. Burned stands should be considered a separate land cover type in larger scale watershed models.

Acknowledgements

First I would like to thank my supervisor Dr. Sarah Boon, an inspiring snow scientist and forest hydrologist. Her support, friendship, and guidance has made this research enjoyable and I cannot express how appreciative I am of this opportunity to research something Sarah and I both agreed was important.

The financial support for this research was received from the University of Lethbridge, Natural Sciences and Engineering Research Council of Canada (NSERC), and a Tree Fund Scholarship to myself and by grants to my supervisor from the University of Lethbridge, Western Economic Diversification, Alberta Sustainable Resource Development (ASRD) Forest Management Branch, and the Alberta Water Research Institute. In kind support was also received from the Southern Rockies Watershed Project, University of Alberta Forest Hydrology Lab, and University of Lethbridge Mountain Hydrology Lab.

I would like to thank my thesis committee members: Dr. Stefan Kienzle and Dr. Larry Flanagan. Thesis committee meetings provided me the encouragement and direction I needed to complete my graduate program.

A successful field program was fundamental to my research. This research would not have been successful without the invaluable field support I received from the University of Lethbridge- Mountain Hydrology Lab, University of Alberta- Forest Hydrology Lab, Southern Rockies Watershed Project, and my friends and family. I extend my most sincere thank you to some of the most accomplished field personnel I have ever known and worked with. I would have never completed my field work without

Table of Contents

List of Figures

List of Tables

Chapter 1

Introduction

In the majority of Canadian watersheds, snow accumulation and melt in forested headwaters control the timing and magnitude of spring runoff, the main hydrologic event in snow-dominated watersheds. Forest cover in watersheds exerts a strong control over snow accumulation and melt, by intercepting snowfall and changing the sub-canopy micrometeorology (Link and Marks, 1999; Storck *et al*., 2002; Andreadis *et al.,* 2009). The snow surface energy balance in forested environments is highly complex, given the ability of the forest canopy to absorb and reflect incoming short-wave radiation, emit long-wave radiation, and alter snow surface albedo (Link and Marks, 1999). Forest canopy also increases land surface roughness, thereby reducing wind speeds (Gray and Prowse, 1993). Any changes to forest canopy structure will subsequently alter snow processes in forest environments.

Recent studies have identified forested areas of western North America as highly susceptible to natural disturbances such as insect infestation (Hicke and Jenkins, 2008) and wildfire (Littell *et al.*, 2009) under warmer air temperatures and prolonged drought conditions (Overpeck *et al*., 1990; Westerling *et al.*, 2003; Macias Fauria and Johnson, 2008). Understanding how forest cover changes with different types of natural disturbance, and its subsequent impact on snow accumulation and the rate and timing of snowmelt, is important for water supplies in disturbance-susceptible areas; however, this has received only modest attention in the literature.

Research has shown that disturbed forests have higher snow accumulation and more rapid melt than mature healthy forests (Koivusalo and Kokkonen, 2002; Gelfan *et al.*, 2004; Winkler and Boon, 2009; Boon, 2009), which can result in higher spring stream flow (Winkler *et al.*, 2005). This can cause severe flooding (Swanson *et al.*, 1998), disturb communities and/or productivity of aquatic ecosystems (Fausch *et al*., 2001; Dunham *et al*., 2003), and adversely affect the quantity and quality of water for downstream users (Swank *et al.*, 2001; Silins *et al.*, 2009b). Because forests are subject to a range of land uses and natural disturbances that result in a mosaic of stand types across watersheds (Jost *et al.*, 2007), it is necessary to understand the impact of each individual forest disturbance type. While forest disturbance generally opens the forest canopy, specific structural impacts vary between disturbance types, with different effects on snow processes. To date, there is a wealth of literature quantifying differences in snow process between open areas and forests (Koivusalo and Kokkonen, 2002; Spittlehouse and Winkler, 2002; Gelfan *et al*., 2004; Winkler *et al*., 2005). Natural disturbance effects are largely unknown, although this is changing with recent studies evaluating mountain pine beetle (*Dendroctonus ponderosae*) (MPB) (Boon, 2007; Boon, 2009; Bewley *et al.*, 2010).

Our understanding of post-wildfire snow processes is very limited: only two studies have examined wildfire impacts on snow accumulation (Farnes, 1996; Silins *et al.*, 2009a), and no studies have examined the post-wildfire snowmelt energy balance. This research is particularly timely because wildfire frequency and area burned in Canada have been increasing since the early 20th century (Podur *et al.,* 2002). By the end of the century, increases of 74-118% in forest area burned, and in wildfire duration and severity,

are predicted for Canadian forests (Flannigan *et al.,* 2005). These effects are especially pronounced in the mid-elevation areas of the Canadian Southern Rockies, which account for approximately 60% of recent wildfire increases (Westerling *et al.*, 2006).

The main goal of this thesis is to quantify differences in snow accumulation, snow surface energy balance, and the timing and magnitude of seasonal snowmelt in a burned relative to a healthy forest stand. The specific objectives of the thesis are to:

1) Design a field program to collect snow and meteorological data in the stands of interest;

2) Develop a snowmelt model to simulate the energy balance over a melting sub-canopy snow surface;

3) Run the model using collected field data as input, assess potential model uncertainties using sensitivity analyses and validate model output; and

4) Use model output to characterize the snowmelt energy balance in a burned compared to a healthy forest stand.

The 2003 Lost Creek fire area in the Crowsnest Pass, Alberta (AB) provides an ideal location to study hydrologic response to disturbance in a snowmelt-dominated watershed. The Crowsnest Pass is part of the headwaters of the Oldman River Basin (ORB) which has seen a mean annual temperature increase of 2ºC in the last century (Schindler and Donahue, 2006); natural and anthropogenic water demands in this semi-arid basin are extremely sensitive to changes in stream flow (Rood *et al.*, 2005). Two forest stands with similar topographic location and larger scale surrounding forest characteristics were evaluated: healthy (control) and burned. Snow and meteorological data were collected over the 2009 and 2010 spring snowmelt periods in both forest

stands, and were used to run a snowmelt energy balance model and validate model output.

Hydrological model accuracy is greatest, and uncertainty lowest, when the physics of the energy balance are simulated over relatively small research stands (Marks *et al.*, 1999); therefore, this study modelled the snowmelt energy balance at the stand scale. The model was developed specifically to use the collected field data, so snowmelt processes could be understood using direct field investigations, which have declined in the hydrology community (Sidle, 2006). This model was designed to quantify vegetation influences on snowmelt processes, and is applied specifically to assess the effects of wildfire on the sub-canopy snowmelt energy balance. This model is easily transferable to other environments because it is based on physically represented processes and clearly defined parameters that can be adjusted for other locations. Similar models have previously been applied to assess the effects of forest harvesting and mountain pine beetle infestation on sub-canopy snowmelt processes (Spittlehouse and Winkler, 2002; Boon, 2009). This stand scale research is important for the parameterization of numerical models designed to simulate watershed scale runoff response to forest disturbance, specifically when forests are composed of a variety of stand types. Although this research is small in scale, monitoring snow and meteorological variables at fine spatial and temporal scales allows for more detailed process-based understanding of differences in snow hydrology among varying landscapes.

This thesis has seven chapters, the first of which is this introduction chapter. Chapter 2 – Snow Accumulation and melt in forests, is a review of the pertinent literature. This chapter includes a summary of the current literature available, related to

the role of the forest canopy and its impact on snow accumulation, the snowmelt energy balance and the rate and timing of snowmelt, and our current knowledge of forest disturbance effects on snow processes. Chapter 3 – Study area, describes the hydrologic significance and biogeoclimatic characteristics of the study area, provides a background to the Lost Creek wildfire, and characterizes the specific location of both forest stands. Chapter 4 – Methods, outlines the development of the specific field program and snowmelt model used to calculate the energy balance over a melting sub-canopy snowpack. Chapter 5 – Modelling the snowmelt energy balance over a sub-canopy snowpack, presents and discusses model sensitivity and performance. This chapter is critical to the remainder of the thesis, as it is required to validate model output and confirm that the model can accurately simulate the rate and timing of snowmelt in both forest stands. Chapter 6 – Wildfire effects on the sub-canopy snowmelt energy balance, quantifies differences in snow accumulation, the snowmelt energy balance, and snowmelt between the burned and healthy forest stands. Chapter 7 – Conclusions, summarizes the main research findings and makes recommendations for the direction of future research.

Chapter 2

Literature review - Snow accumulation and melt in forests [*]

This chapter summarizes the current state of knowledge regarding snow hydrology processes in forest environments, focusing on the role of the forest canopy in snow accumulation, the snowmelt energy balance and the rate and timing of snowmelt. Given increasing rates of forest disturbance and the subsequent effects on forest canopies, this chapter presents our current knowledge of forest disturbance effects on snowmelt processes.

2.1 Introduction

Snow accumulation and melt dominate the hydrology of many western Canadian watersheds; spring snowmelt produces an annual hydrograph peak typical of most alpine fed rivers and streams (Pomeroy and Gray, 1995). The forested headwaters of many of these large watersheds play a major role in the hydrologic cycle, partitioning water into fluxes and stores such as snowmelt, transpiration, canopy interception loss, and soil moisture storage (Chang, 2003). Forests are currently undergoing significant changes in canopy structure as a result of natural and anthropogenic disturbances (Hélie *et al.*, 2005), with subsequent effects on forest hydrology and snow processes.

Recent studies have identified forested areas of western North America as highly susceptible to natural disturbances under greater air temperatures and prolonged drought

---

[*] A portion of this chapter has been accepted for publication: Boon, S. & Burles, K. 2010. Snow hydrology. In Singh, V., Singh, P., & Haritashya, U.K., Eds. *Encyclopedia of Snow, Ice, and Glaciers.* Heidelberg: Springer-Verlag.

conditions (Westerling *et al.*, 2003; Macias Fauria and Johnson, 2008). This includes

natural disturbances such as insect infestation (Hicke and Jenkins, 2008) and wildfire

(Littell *et al.*, 2009). Naturally disturbed areas affected by insect infestations such as

mountain pine beetle (MPB; *Dendroctonus ponderosae*) can be left as standing dead

timber, or managed via salvage harvesting, which results in complete removal of the

forest canopy. If left standing, dead trees provide a dry crown and litter layer that may

increase the risk of forest fire, particularly when coupled with predicted shifts in climate

(Intergovernmental Panel on Climate Change, 2008). The majority of beetle-killed forests

are located in snowmelt-dominated hydrologic regimes, within forest ecosystems

historically driven by fire (Hélie *et al.*, 2005). Wildfire frequency and area burned in

Canada have been increasing since the early 20th century (Podur *et al.*, 2002). By the end

of the century, increases of 74-118% in forest area burned, and increases in wildfire

duration and severity, are predicted for Canadian forests (Flannigan *et al.*, 2005).

Insect infestation, salvage harvesting, and wildfire open the forest canopy

(Winkler *et al.*, 2005; Boon, 2007; Carlyle-Moses, 2007), which then alters sub-canopy

hydrological processes such as snow accumulation, the energy balance, and snowmelt.

Thus, tree mortality as a function of natural or anthropogenic disturbance changes the

amount of snow accumulating on the ground surface and enhances snow surface energy

inputs (Adams *et al.*, 2010).

Properly managing water resources in forested headwaters with snowmelt-

dominated hydrologic regimes is critical to sustaining water supplies and water quality to

downstream ecosystems and users. It is known that increased snow accumulation

combined with more rapid melt conditions can result in high magnitude stream flows

which can cause flooding, alter aquatic ecosystems, and impact municipal water supplies (Winkler *et al.*, 2005). In Canada, forests cover the majority of the landmass (Buttle *et al.*, 2009), and are subject to a range of land use and natural disturbance that results in a mosaic of stand types across watersheds (Jost *et al.*, 2007). This high spatial variability in forest stand types makes it difficult to quantify the watershed-scale effects of forest cover change on snowmelt processes. Therefore, accurate modelling of the rate and timing of snowmelt in disturbed forests at the stand scale provides valuable process information required for modelling runoff from large forested watersheds.

2.2 Snow hydrology

Snow hydrology includes the study of precipitation in the form of snow and its role in the water balance during two distinct periods: snow accumulation and melt. The accumulation period is characterized by an increase in snow water equivalent (SWE) prior to the snowmelt period. During this time, net inputs of energy are negligible, while average air temperatures are decreasing and SWE is increasing. The melt period is initiated when net energy becomes positive, air temperatures begin to rise, and SWE begins to decrease. This process can be separated into three phases (Dingman, 2002):

1) *Warming:* average snowpack temperatures increase until the snowpack is isothermal at 0ºC.

2) *Ripening:* melting begins to occur but meltwater remains within the snowpack. At this time the snowpack is isothermal and said to be ripe (cannot hold any more liquid water; all available pore spaces are saturated).

3) *Output:* any energy inputs result in more melt and meltwater begins to leave the snowpack.

The average snowpack will not necessarily follow this exact sequence. In many cases, meltwater will occur on the snowpack surface prior to the snowpack becoming isothermal, in which case it will either percolate downwards through the snowpack and freeze, or the snow surface may refreeze until it becomes warm again and melting continues (Dingman, 2002). At the upper surface of the snowpack, where melt normally occurs, the rate and timing of snowmelt are determined by the amount of energy available (Pomeroy and Goodison, 1997). In forest environments, the snowpack – and snowmelt period – are influenced by the upper and lower boundary of the forest canopy and ground surface.

2.3 Snow accumulation in forests

Snow accumulation is characterized by its depth and density, which can vary significantly across spatial scales and across a range of environments. These variables are used to calculate SWE, a standardized term to quantify the depth of water contained within a snowpack.

Snow accumulation is governed by meteorology, topography, and vegetation. Regional and local meteorology are largely controlled by topography and vegetation. Higher elevations generally accumulate greater SWE (Hardy *et al.*, 2001) due to more frequent snow storms, lower air temperatures, and decreased evaporation and mid-winter melting events (Gray and Prowse, 1993). Slope and aspect can also affect snow accumulation: less snow will accumulate on slopes orientated in the prevailing wind

direction, while more snow will accumulate on leeward slopes and in depressions (Gray

and Prowse, 1993). In open areas, snow accumulates directly on the ground surface

without any interception. In forests, however, snow accumulation is controlled by the

interception capacity of the forest canopy, resulting in high variability in snow

accumulation.

The interception of snow by the forest canopy is a critical factor driving the

spatial distribution of the sub-canopy snowpack (Hedstrom and Pomeroy, 1998).

Snowfall intercepted by the needles and branches of trees can be stored; unloaded as

accumulated snow and meltwater to the ground surface; resuspended and redistributed by

high winds; or sublimated back into the atmosphere (Pomeroy and Goodison, 1997). The

primary cause of snow loss in forest regions is sublimation from the canopy (Schmidt *et

al.*, 1988; Lundberg and Halldin, 1994; Parviainen and Pomeroy, 2000) which accounts

for up to 45% of annual snowfall loss in western Canada (Pomeroy *et al.*, 1998). Figure

2.1 describes the disposition of winter snowfall in forests.

Increasing forest canopy density increases the interception efficiency of the forest

canopy (Suzuki *et al.*, 2008). Deciduous forests intercept less snow than coniferous

forests because they lose their foliage in the winter (Gray and Prowse, 1993). In

coniferous forests, specific tree characteristics such as branch orientation and strength,

needle configuration and orientation, mass, surface area, age, and density, as well as

meteorological conditions such as snowfall intensity and duration, wind speeds, and

temperature, affect snowfall interception (Schmidt and Troendle, 1992; Gray and Prowse,

1993). High winds can decrease snow accumulation on the forest canopy and increase

sub-canopy snow accumulation (Gray and Prowse, 1993). Higher temperatures increase

the elasticity of tree branches, making them less able to support the mass of intercepted snow (Schmidt and Pomeroy, 1990). Increasing air temperature, snowfall, time since snowfall, and initial canopy snow load prior to fresh snowfalls all decrease the interception efficiency of the forest canopy (Hedstrom and Pomeroy, 1998). If a forest canopy reaches its maximum snow holding capacity, snow will be unloaded onto the ground surface.
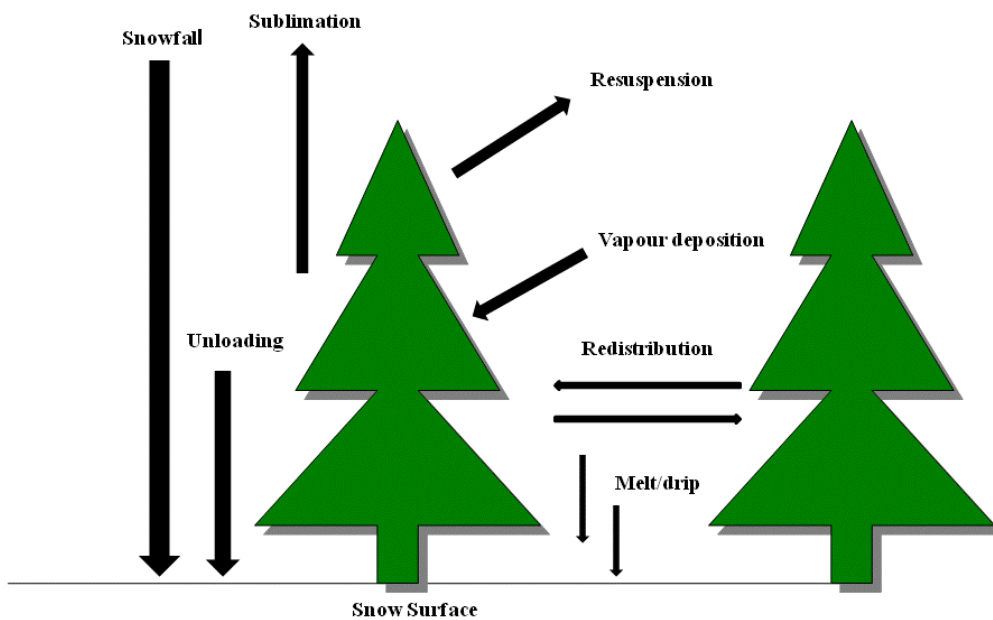
Figure 2.1: Disposition of winter snowfall in a forest environment (modified from Pomeroy and Schmidt, 1993)

Snow accumulated on the ground surface can also be redistributed by strong winds. Higher wind speeds are required to redistribute wet snow (7 to 14 m s^{-1}) than dry snow (4 to 11 m s^{-1}) because the top layer of the snowpack is more cohesive (Li and Pomeroy, 1997). Although blowing snow is not a large contributor to snow loss in boreal forests, it is significant in prairie and alpine environments (Pomeroy *et al.*, 2007).

2.4 Snowmelt modelling approaches

Once snow has accumulated on the ground, the rate and timing of snowmelt is determined mainly by the amount of available energy (Pomeroy and Goodison, 1997), which varies with topography (elevation, aspect), climate and meteorological conditions (maritime, continental; rain-on-snow events, chinooks), and vegetation cover (open, sub-canopy, shrub, glacier surface). South-facing slopes have higher melt rates than north-facing slopes given increased radiation inputs (Shook *et al.*, 1993), while lower elevations melt earlier than high elevations due to higher air temperatures (Gray and Prowse, 1993). In maritime climates, rain-on-snow events enhance snowmelt (Marks *et al.*, 1998; Floyd and Weiler, 2008), while in continental climates with frequent föhn (chinook) events, winter melt can occur (Hayashi *et al.*, 2005). Vegetation cover plays a significant role in altering the energy reaching the snow surface (Link and Marks, 1999); thus, melt processes are often divided into open versus forested environments. In open environments (prairie, clearcut, glacier surface), melt is driven by a combination of both radiative and turbulent fluxes (Gray and Landine, 1987; McGregor and Gellatly, 1996; Winkler *et al.*, 2005). In forested environments, however, turbulent fluxes are significantly reduced, and radiative fluxes are much more complex (Koivusalo and Kokkonen, 2002; Boon, 2009). Shrub environments, however, lie between open and forested environments, with reduced longwave radiation inputs relative to a forest, but only slightly reduced turbulent fluxes, and very similar shortwave radiation inputs to open environments.

2.4.1 Temperature index melt calculations

Snowmelt has historically been calculated using temperature index (degree-day) methods, where snowmelt is calculated as a function of average air temperature (Anderson, 1973):

$$MLT = M(T_a - T_m) \text{ when } T_a \geq T_m \tag{2.1}$$

$$MLT = 0 \text{ when } T_a < T_m \tag{2.2}$$

where MLT is snowmelt (m hr^{-1}), M is the melt factor or rate of melt per degree per unit time (m ºC^{-1} hr^{-1}), and T_a and T_m are the temperature of the atmosphere and melting temperature of the snowpack, respectively (ºC). This approach assumes that, during melt, snow temperature is at or near 0ºC, that energy inputs to the snowpack from long-wave and turbulent energy are linear functions of air temperature, and that solar radiation correlates well with air temperature (Braithwaite, 1984). The melt coefficient can be difficult to determine and is dependent on latitude, elevation, aspect, forest cover, and day of year, all of which must be empirically measured or assumed for various watersheds (Gray and Prowse, 1993).

Temperature index models are most commonly used because air temperature is the most readily available meteorological variable, and they have minimal computational requirements. However, these models are highly calibrated (Walter *et al.*, 2005) and are limited to larger spatial scales and longer periods (i.e., exceeding hourly and daily intervals). They are most commonly used in large scale watershed modelling with limited data sets. Examples of temperature index models include: HBV (Bergström, 1995), SRM (Martinec and Rango, 1986), UBC Watershed Model (Quick and Pipes, 1977), GENESYS (MacDonald *et al.*, 2009) and SWAT (Fontaine *et al.*, 2002). Although these

models represent snowmelt processes simplistically, they have been validated in large

scale watershed studies (Beven, 2001).

To improve the physical basis of degree-day models, researchers have defined

modified degree-day methods that incorporate additional variables such as snow surface

albedo (e.g., Hock, 1999; Pellicciotti *et al.*, 2008). While these models require additional

input data and are more computationally intensive than the standard temperature index

method, they remain more accessible than energy balance approaches, which can require

significant amounts of input data and processing time.

2.4.2 Energy balance melt calculations

Energy balance models are physically based and follow the fundamental physical

principles of conservation of mass and energy. Designed for short term forecasts under

more extreme conditions, and highly data intensive (Gray and Prowse, 1993), energy

balance models are the most thorough and accurate method for calculating stand scale

snowmelt in forest environments. The sub-canopy snowmelt energy balance consists of

the sum of energy fluxes from radiation, convection, conduction, and advection minus the

change in internal snowpack energy (Gray and Prowse, 1993). Figure 2.2 shows a

schematic of the vertical direction of energy fluxes during snowmelt.
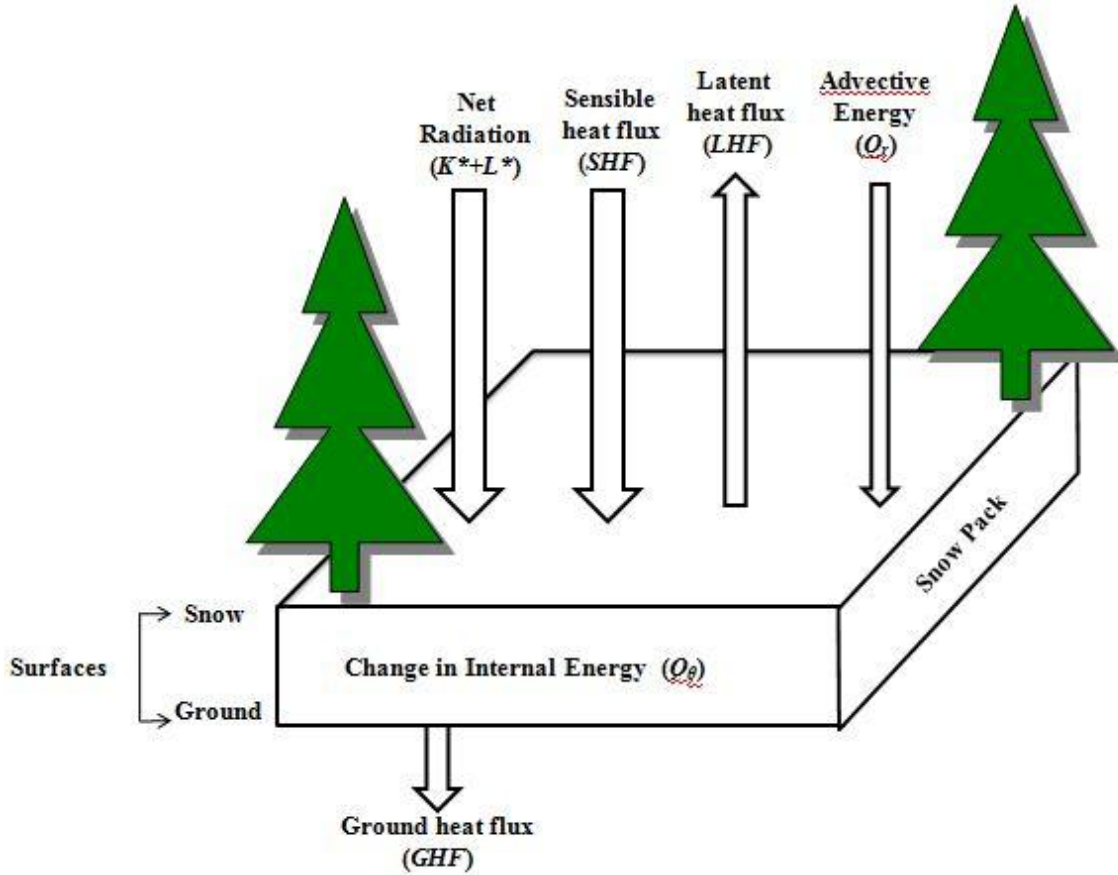
Figure 2.2: Schematic of the vertical directions of energy fluxes (modified from Gray and Prowse, 1993).

$$Q_m = Q^* + SHF + LHF + GHF + Q_r - Q_\Theta \qquad (2.3)$$

where Q_m is energy available for melt, Q^* is net radiation, SHF is convective transport of sensible heat between the air and snowpack, LHF is latent heat released through condensation of water vapour onto the snowpack or lost through evaporation, GHF is conduction of heat between the snowpack and the ground, Q_r is advective energy mainly heat transferred to the snowpack through rain, and Q_θ is change of internal energy in the volume per unit surface area per unit time (all in units of J m^{-2} d^{-1} or W m^{-2}).

Net radiation (Q^*) is the sum of net short-wave (K^*) and net long-wave (L^*) radiation fluxes and is the dominant energy flux contributing to snowmelt in forested environments (Link and Marks, 1999; Woo and Giesbrecht, 2000; Koivusalo and Kokkonen, 2002; Spittlehouse and Winkler, 2002). K^* is the total amount of incoming short-wave radiation ($K\downarrow$) minus outgoing short-wave radiation ($K\uparrow$).

$K\downarrow$ is representative of the total amount of solar radiation reaching the ground or snow surface. This includes the portion which is not reflected by clouds, or absorbed and scattered by the atmosphere (direct beam (S)) and the portion that is scattered by the atmosphere or surface objects such as trees (diffuse solar radiation (D)). $K\downarrow$ decreases with increasing percent forest canopy cover. In dense conifer forests only a small portion (approximately 10%) of above-canopy $K\downarrow$ is transmitted to the snow surface, although even leafless deciduous forests can only transmit approximately 50% of $K\downarrow$ (DeWalle and Rango, 2008). $K\downarrow$ is not limited to the snow surface, but can penetrate up to 10 cm into the snowpack (Brock *et al.*, 2000b), and reach the ground surface in shallow packs (DeWalle and Rango, 2008) increasing ground temperature (Buttle and McDonnell, 1987) which subsequently increases snowmelt rates.

$K\uparrow$ is the amount of solar radiation reflected by the Earth surface (Geiger *et al.*, 2003) and is a function of the snow surface albedo (α). $K\uparrow$ is highly dependent on the nature of the earth surface; typical values for α are given in Table 2.1. Albedo decreases as snow ages and melts, as it is affected by snow grain size (Wiscombe and Warren, 1980), and organic and inorganic debris accumulating on the snow surface (Link and Marks, 1999; Melloh *et al.*, 2001; Winkler *et al.,* 2010). Albedo can also change

significantly later in the melt season, when the snowpack becomes patchy and the

underlying ground surface is exposed (Liston, 1995).

Table 2.1: The range of albedo values for various surfaces (from Gray and Prowse, 1993).

Surface	Typical range in albedo
New snow	0.80-0.90
Old snow	0.60-0.80
Melting snow-porous-fine grained	0.40-0.60
Forests-conifers, snow	0.25-0.35
Forests-green	0.10-0.20
Water	0.05-0.15
Snow ice	0.30-0.55
Black ice: intact→candled→granulated	0.10→0.40→0.55

$K*$ in forest environments can be calculated and measured using several

techniques. In early studies the portion of $K\downarrow$ transmitted through the forest canopy was

calculated as a function of leaf-area index (LAI), the surface area of leaves/needles per

unit ground area (Jarvis *et al.*, 1976; Rauner, 1976; Baldocchi *et al.*, 1984). Other

approaches apply Beer's law-based models to calculate S, and a constant transmission

fraction for D to calculate $K\downarrow$ (Federer, 1971; Link and Marks, 1999). If short-wave

radiation data above the forest canopy are available, $K*$ can be modelled based on

average forest structure parameters:

$$K^* = K \downarrow \tau_c (1 - \alpha)$$
(2.5)

where canopy transmissivity (τ_c) is the proportion of $K\downarrow$ transmitted through the forest

canopy and is largely dependent on tree type, stand characteristics, stand age, and stand

productivity (Geiger *et al.*, 2003). The technique selected to model $K*$ is dependent on

17

the study and available meteorological data. Instead of modelling K^*, researchers also use measurements collected with net radiometers and pyranometers.

L^* is the sum of long-wave radiation emitted downward by the atmosphere ($L\downarrow$) minus the amount emitted upward by the earth's surface ($L\uparrow$). In the absence of clouds, $L\downarrow$ depends on atmospheric temperature and emissivity (ε_a), the latter of which is dependent on atmospheric distributions of temperature, water vapour, and carbon dioxide (Oke, 1987). Similar to $L\downarrow$, $L\uparrow$ from the snow surface is dependent on surface temperature and emissivity.

In forest environments L^* is the sum of $L\downarrow$ from the atmosphere, $L\downarrow$ from the canopy, $L\downarrow$ from the tree stems, and $L\uparrow$ from the snow surface:

$$L^* = \tau_L L\downarrow + (1 - \tau_L)\varepsilon_c \sigma T_c^4 + (H_t / H)\varepsilon_t \sigma T_t^4 - \varepsilon_{ss}\sigma T_{ss}^4 \qquad (2.6)$$

L^* is based on the Stefan-Boltzmann law and is a function of the sky view factor (τ_L) which is the proportion of hemisphere visible beneath the forest canopy, the hypothetical hemisphere surface area affected by long-wave radiation from the tree trunk (H_t) and the hypothetical hemispherical area emitting long-wave radiation to a point on the snow surface located at a distance from the tree trunk (H), the emissivity of the forest canopy, tree trunks, and snow surface (ε_c, ε_t, ε_{ss}), and the temperature of the forest canopy, tree trunks, and snow surface (T_c, T_t, T_{ss}).

$L\downarrow$ is a significant contributor to the energy available for snowmelt in forests, where a high proportion of incident $K\downarrow$ is absorbed by the canopy and emitted downward to the snow surface as long-wave radiation, and when low clouds occupy an area restricting the escape of long-wave radiation emitted by the ground or snow surface ($L\uparrow$) (Gray and Prowse, 1993). In coniferous forests, up to 90% of the short-wave flux incident

at the top of the canopy may be absorbed by the canopy (Gray and Prowse, 1993). T_c and T_t can be greater than T_a during periods of strong $K\downarrow$, increasing $L\downarrow$ onto the snow surface (Pomeroy *et al.*, 2009). Snow can more effectively absorb long- than short-wave radiation, resulting in higher snowmelt rates near tree trunks (Reifsnyder and Lull, 1965) and high spatial variability in those melt rates (Bohren and Thorud, 1973). Pyrgeometers can directly measure $L*$, but they emit radiation making it difficult to separate radiation emitted from the sensor and surrounding area and they are also relatively expensive compared to pyranometers (Duarte *et al.*, 2006). Therefore, they are not commonly used in field programs.

The turbulent fluxes of *SHF* and *LHF* represent the exchange of energy between the snow surface and overlying air due to differences in temperature and vapour pressure, respectively (Andreas, 2002). Under dense forest canopies, where wind speeds are low, turbulent heat transfers are small (Woo and Giesbrecht, 2000). However, *SHF* and *LHF* can dominate the snowpack energy balance, producing high short term melt rates, when strong warm winds occur (Moore, 1983).

While several methods are available to quantify turbulent heat exchange in forest environments, the suitability of the required instrumentation, site maintenance, and data processing depends on site specific conditions and the environments of interest. Eddy covariance (EC) is the most accurate method as it directly measures turbulent heat exchange using absolute values for eddy diffusivities (K_H and K_E) (Baldocchi *et al.*, 1988). However, EC can be difficult to use in remote complex terrain due to expensive instrumentation and rigorous equipment maintenance (McKay and Thurtell, 1978; Reba

et al., 2009), and is rarely used to measure turbulent heat transfers over sub-canopy

snowpacks.

An alternative method for calculating turbulent fluxes is the bulk aerodynamic

method. This method has been used extensively to calculate *SHF* and *LHF* at the snow

surface (Moore, 1983; Andreas, 2002), is less data intensive and has been used in a range

of environments including forested areas (Price and Dunne, 1976; Boon, 2009). The bulk

aerodynamic method requires measurements of T_a, wind speed (u), relative humidity

(*RH*), and atmospheric pressure at one height. This method uses bulk transfer coefficients

for sensible heat (D_H), and latent heat (D_E) instead of absolute values for the eddy

diffusivities (K_H, K_E). These fluxes are calculated as:

$$SHF = \rho_a C_{pa} D_H \left(T_a - T_{ss} \right) \qquad (2.7)$$

$$LHF = \rho_a \lambda_v D_E \left(\frac{0.622}{P} \right) \left(e_a - e_{ss} \right) \qquad (2.8)$$

where ρ_a is the density of air (kg m^{-3}), C_{pa} is the heat capacity of air (J kg^{-1} K^{-1}), D_H and

D_E are the bulk transfer coefficient for sensible and latent heat (m s^{-1}), T_{ss} is the

temperature of the snow surface (ºC), λ_v is the latent heat of vapourization (2.48 x 10^6 J

kg^{-1}), P is the atmospheric pressure (kPa), and e_a and e_{ss} are the atmospheric and snow

surface vapour pressure (kPa), respectively. The bulk transfer coefficients for latent and

sensible heat vary with atmospheric condition. Under neutral atmospheric conditions, D_H

= D_E:

$$D_H = D_E = \frac{k^2 u}{\left[ln \left(\frac{z_a}{z_o} \right) \right]^2} \qquad (2.9)$$

where k is von Karman's constant (0.40), u is the wind speed (m s^{-1}), z_a is the height of the wind measurement (m), and z_o is the roughness length of the snow surface (m). z_o values summarized by Moore (1983) varied between 0.0002 to 0.02 m, with the highest roughness lengths calculated over old snow.

Air temperatures over melting snow are generally >0ºC, resulting in stable atmospheric conditions (de la Casiniere, 1974). Two methods are available to correct the bulk transfer coefficients for stable atmospheric conditions over a melting snow surfaces: the Monin-Obukhov length scale (L) (Obukhov, 1971), and the bulk Richardson number (Rb) (Moore, 1983). The calculation of L requires the calculation of SHF to be incorporated into the stability correction which is already dependent on L. Studies that have used L must first calculate SHF for neutral conditions and then use this value to calculate L which is then used to recalculate SHF under stable and unstable atmospheric conditions (Brock and Arnold, 2000). However, Rb can be calculated directly using u and T_a, in which case the calculation of L is not needed (Moore, 1983; Greuell and Konzelmann, 1994; Boon, 2009).

Ground heat flux (GHF) is the energy exchange between the snow surface and the ground caused by conduction. In comparison to Q^*, SHF, and LHF, GHF makes a relatively small daily energy contribution (0 to 6 W m^{-2}) and many authors either do not consider it or apply a constant value when using the energy balance equation (e.g., United States Army Corps of Engineers, 1956; Melloh, 1999). Over short time periods, GHF effects on snowmelt are small and can be ignored (Gray and Prowse, 1993); however, over an entire winter season snowmelt can be influenced by the cumulative effects of GHF and should be considered (Pomeroy and Goodison, 1997).

GHF can be estimated using soil temperature and moisture data (Gray and Prowse, 1993):

$$GHF = k_G \left(\frac{\Delta T_s}{d_s} \right) \tag{2.10}$$

where k_G is the thermal conductivity of the soil (W m^{-1} K^{-1}), ΔT_s is the change in temperature of the soil (K), and d_s is depth of measurement below the ground (m). k_G depends on soil texture, soil density, and moisture content, and varies through space and time (Oke, 1987).

Advective energy (Q_r) is the energy supplied to the snowpack by rainfall during the snowmelt period, and is measured as the ratio between rainfall energy content while airborne before contacting the surface, and its energy content on reaching thermal equilibrium within the pack (Gray and Prowse, 1993). Three situations where rainfall can influence the snow surface energy balance are: (1) rainfall on an isothermal pack where the rain does not freeze, resulting in sensible heat additions; (2) rainfall on a frozen pack ($< 0°C$) at which point the rain freezes, releasing the latent heat of fusion; and (3) condensation on the snow surface due to high humidity associated with rain events (DeWalle and Rango, 2008). The advective energy from (1) and (2) can be calculated using:

$$Q_{r1} = \rho_w C_w P_r \left(T_r - T_{ss} \right) \tag{2.11}$$

$$Q_{r2} = P_r \rho_w \lambda_f \tag{2.12}$$

where ρ_w is the density of liquid water ($\sim$1000 kg m^{-3}), C_w is the heat capacity of water ($\sim$4190 J kg^{-1} K^{-1}), P_r is the rainfall intensity (m s^{-1}), T_r is the temperature of rain (K), T_{ss} is the temperature of the snow surface (K), and λ_f is the latent heat of fusion ($\sim$0.334 x

22

10^6 J kg^{-1}). Q_r can be large in maritime forests that are impacted by moist frontal systems (Marks *et al.*, 1998); rain-on-snow (ROS) events on deep coastal snowpacks can rapidly melt the snowpack and generate peak flow events (Floyd and Weiler, 2008).

Finally, Q_θ is the change of internal energy in the snowpack (Gray and Prowse, 1993). Within deep snowpacks internal energy changes can be relatively small in comparison to other energy fluxes and in most studies are considered negligible because the snowpack temperature during ablation is close to 0°C. However, if snow melts during the day and freezes overnight, large changes in internal energy can occur within shallow snowpacks and the upper layers of deep snow. Q_θ is calculated using:

$$Q_\Theta = \left(\rho_i C_i + \rho_w C_w + \rho_v C_v\right) \Delta T_{sd} s \qquad (2.13)$$

where ρ_i is the density of snow and ice (kg m^{-3}), C_i is the specific heat capacity of snow and ice (~2102 J kg^{-1} K^{-1}), ρ_v is the density of water vapour (kg m^{-3}), C_v is the specific heat capacity of water vapour (J kg^{-1} K^{-1}), ΔT_{sd} is the change in snow temperature (K), and s is the snow depth (m). Internal changes in snowpack temperature can also be measured using thermistor strings, or modelled using one-dimensional snow temperature and energy balance models such as SNTHERM (Jordan, 1991; Melloh, 1999).

Once the total energy available for melt (Q_m) is modelled, the depth of melt water can be quantified. Some researchers have successfully used snowmelt lysimeters to measure melt water output from the snowpack to validate the snowmelt energy balance (Storck *et al.*, 2002; Winkler *et al.*, 2005).

2.5 Forest disturbance effects on snow hydrology

The snow surface energy balance in a forested environment is highly complex, given the ability of the forest canopy (e.g., density, height to live crown, crown depth and diameter, tree condition) to absorb and reflect incoming short-wave radiation, emit long-wave radiation, and alter snow surface albedo (Link and Marks, 1999). The forest canopy also increases land surface roughness, thereby reducing wind speeds (Gray and Prowse, 1993). Any changes to forest canopy structure will alter the amount of energy available for snowmelt.

Forest disturbances are categorized as either anthropogenic or natural. Anthropogenic disturbances are associated with land use change, primarily forest clearing and harvesting. Natural disturbances include insect infestations, wildfire and disease, as well as blow down. In cleared forests the canopy is completely removed. In MPB-killed stands needles are shed to the snow and ground surface, but larger branches and stems remain intact for up to 10 years post-infestation (Mitchell and Preisler, 1998). Burned forest stands are a unique disturbance type, where needles and small branches are completely removed and all that remains are dead standing trunks and branches; however, burn severity can vary depending on wildfire intensity and duration. In MPB-killed and burned forests dead standing trees are retained that continue to intercept snowfall and short-wave radiation, and reduce wind speeds.

Currently, snow accumulation and melt processes are well understood in forests versus clearcuts (Koivusalo and Kokkonen, 2002; Spittlehouse and Winkler 2002; Gelfan *et al.*, 2004; Winkler *et al.* 2005). Opening of the forest canopy due to forest clearing ultimately results in an increase in snow accumulation of between 4 to 118% (Golding

and Swanson, 1986; Toews and Gluns, 1986). This variation is partially a result of the size of the forest clearing, which plays a large role in the amount of snow that accumulates on the ground surface. Small clearings will be sheltered by the surrounding forested area, whereas larger clearings can lose snow as a result of wind erosion and blowing snow (Pomeroy *et al.*, 2002). Melt rates in healthy forests can be 30-300% lower than nearby in cleared areas (Pomeroy and Granger, 1997; Murray and Buttle, 2003; Winkler *et al.*, 2005; López -Moreno and Stähli, 2008).

Studies evaluating the effects of natural disturbances such as MPB-killed and wildfire remain limited (Boon, 2007; Boon, 2009; Bewley *et al.*, 2010). Recorded increases in peak SWE in MPB-infested stands compared to clearcut forests range from 28 to 128% (Winkler and Boon, 2009), depending on the location, year, stand age, and level of attack. In mature, older green/red attacked stands, where the majority of foliage is intact, average SWE is 25% less than in the clearings. In mature, older grey attacked stands where over half of the foliage has been lost, average SWE is 13% less than in the clearings. Only one study has examined wildfire impacts on snow accumulation, and predicted a 37% increase in peak SWE in a lodgepole pine stand in Yellowstone National Park after a 1988 wildfire (Farnes, 1996). Melt rates in MPB-infested forests are lower compared with clearings, with average melt rates reduced by 31 and 38% for mature red/green and grey attack stands, respectively (Winkler and Boon, 2009). Boon (2009) found snowmelt rates were 14 to 17% greater in grey attack relative to healthy forest stands. No studies have evaluated snowmelt rates in post-wildfire regions.

Higher rates of snowmelt in disturbed forests are a result of enhanced snow surface energy inputs caused by opening of the forest canopy (Winkler *et al.*, 2005;

Koivusalo and Kokkonen, 2002; Boon, 2009). In disturbed forests, Q^* is driven by incoming shortwave radiation, as open forest canopies attenuate less incoming short-wave radiation (Ni *et al.*, 1997). Removing the forest canopy decreases canopy density and subsequently decreases the amount of $L\downarrow$ emitted from the canopy. Disturbance may result in negative values of L^*, because $L\uparrow$ from the snow surface is not compensated by $L\downarrow$ from the forest canopy (Boon, 2009). The lack of forest canopy will also decrease land surface roughness and increase wind speeds relative to healthy forests, which would enhance turbulent heat transfers. Studies have shown that turbulent heat fluxes are higher in forest clearings and MPB-killed stands than in forested areas (Koivusalo and Kokkonen, 2002; Boon 2009).

2.6 Summary

Seasonal snowpacks experience two main periods: snow accumulation and melt. At the stand and watershed scale, sub-canopy snow accumulation and melt is strongly influenced by the forest canopy. Forest disturbance ultimately opens the forest canopy which subsequently increases snow accumulation and alters the rate and timing of snowmelt compared to mature healthy stands. To date, snow processes in forest clearings are well understood and recent studies have improved our understanding of natural disturbance effects; however, studies of wildfire effects on the snowmelt energy balance and the rate and timing of snowmelt are lacking and require further investigation.

Chapter 3

Study Area

Research for this thesis was conducted in two forest stands situated in the Oldman River Basin headwaters, Crowsnest Pass, Alberta (AB), Canada; approximately 12 km south of Coleman at the northern edge of the 2003 Lost Creek wildfire. This chapter describes the hydrologic significance of the study area within the Oldman River Basin, defines the biogeoclimatic characteristics of the Crowsnest Pass region, and provides a background to the Lost Creek wildfire and the subsequent research goals of the Southern Rockies Watershed Project (SRWP). Finally, the specific location of forest stands where meteorological and snow data collection for this thesis took place are characterized.

3.1 Oldman River Basin

The Oldman River basin is located in southwestern AB with a small southern portion located in northwestern Montana (MT), USA (Figure 3.1).
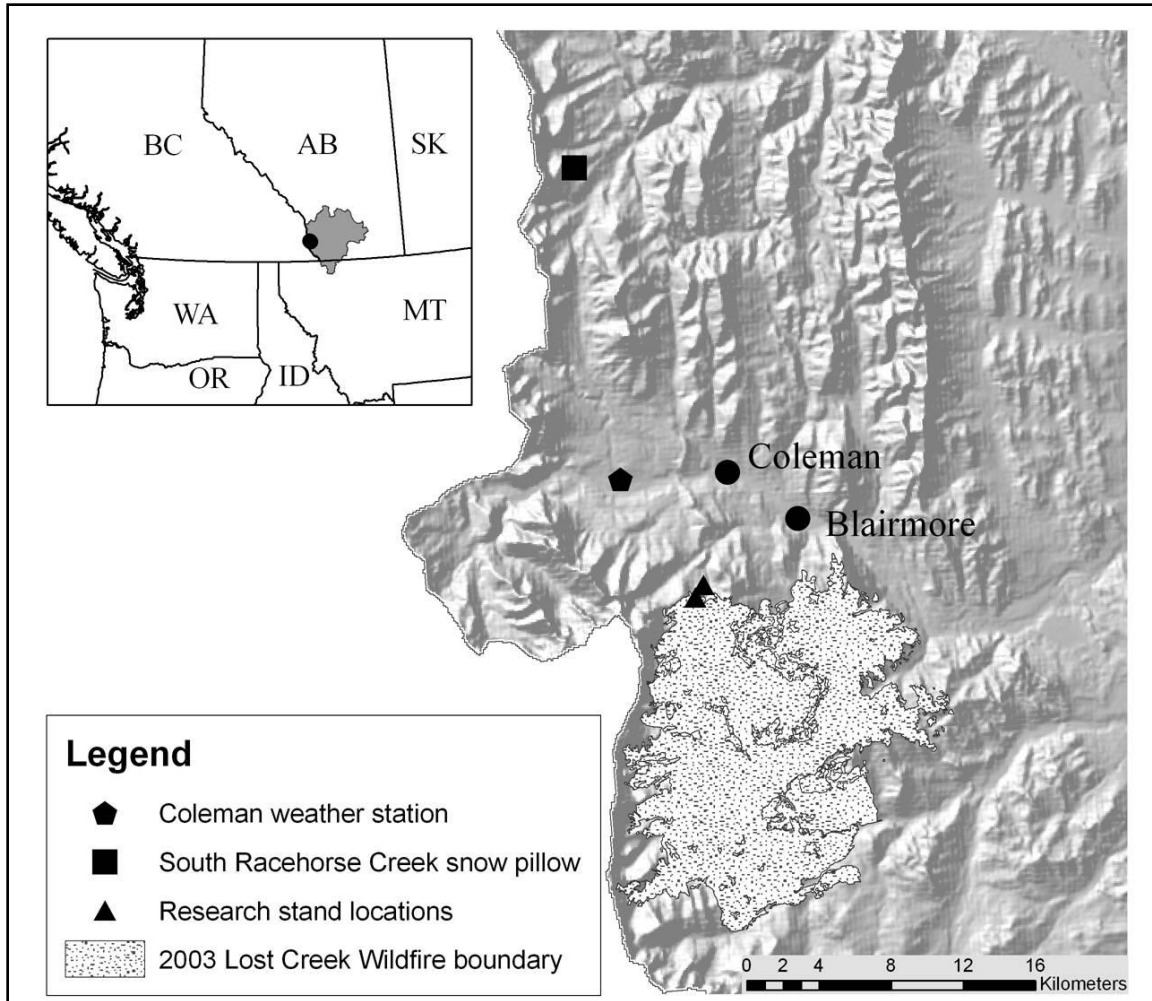
Figure 3.1: Location of the Oldman River Basin (inset), the nearest Federal meteorological station and Provincial snow pillow, the study stands, and the 2003 Lost Creek Wildfire boundary.

The catchment area is approximately 27000 km^2 at the confluence of the Oldman River and Bow River which, past this point, drains into the South Saskatchewan River. The main tributaries of the Basin, from north to south, are the Livingston, Oldman, Crowsnest, Castle, Waterton, Belly, and St. Mary Rivers. The western portion of the Basin is comprised of east facing slopes of alpine, subalpine, and montane deciduous and coniferous forests (Natural Resources Canada, 2007; Oldman Watershed Council, 2010). The central and eastern semi-arid portions, which form approximately 80% of the surface

area of the Basin, consist of Plains that support grassland and prairie vegetation (Oldman Watershed Council, 2010). The forested headwaters of the Oldman River, located in the Canadian Rockies, generate the majority of downstream streamflow from deep snowpacks that replenish and maintain surface and groundwater supplies (Schindler and Donahue, 2006), and provide water to the low lying semi-arid regions of the Basin. The Basin has three major reservoirs including the Oldman, Waterton, and St. Mary's, which store spring snowmelt and provide surface water for domestic water supply, irrigated agriculture, industry, water recreation, and fisheries in the semi-arid Southern Prairies region (Byrne *et al*., 2006).

Regional social and economic pressures result in high water usage and demand in Southern Alberta (AB). This region is also sensitive to drought, which can impact stream flow and water supply by increasing evapotranspiration, and reducing both snow accumulation and soil moisture recharge (Nkemdirim and Weber, 1998; Fang and Pomeroy, 2007). Currently, 97% of water license allocations in the Oldman River Basin are from surface water sources (Oldman Watershed Council, 2010). Ecological and human water demands in the semi-arid eastern portion of the Basin are extremely sensitive to changes in stream flow (Rood *et al*., 2005).

Global climate change models for the Canadian Southern Rockies region predict the following by the mid-21st century: decreased snow cover, especially in spring; increased midwinter warming events; earlier spring freshet; decreased soil moisture recharge; and lower base flows (Intergovernmental Panel on Climate Change, 2008). Increased spring temperatures will result in earlier snowmelt and lower water availability in the late summer months, potentially causing drought which is unfavourable for a

longer growing season (Saunders and Byrne, 1994). Southwestern AB has seen a mean

annual air temperature increase of 2ºC in the last century (Schindler and Donahue, 2006),

and recent studies have noted that higher air temperatures and prolonged drought are

drivers for increased tree mortality (Allen *et al.*, 2010), including insect infestation

(Hicke and Jenkins, 2008) and wildfire (Littell *et al*., 2009). The sensitivity of this region

to environmental change makes it an ideal location to conduct forest disturbance

research.

3.2 Crowsnest Pass

The Crowsnest Pass is located in the Oldman River Basin headwaters in the rain

shadow of the Canadian Rocky Mountains. The Crowsnest Pass is within the Montane

Cordillera Ecozone and the Northern Continental Divide Ecoregion (Natural Resources

Canada, 2007). Environment Canada's nearest climate station to the study area is located

in Coleman at 1341 m elevation, where annual average (1971-2000) air temperature is

3.5ºC (Figure 3.1). Monthly average air temperatures range from 14.5ºC in July and

August to -7.8ºC in January. Winter (Dec, Jan, Feb) extreme average maximum and

minimum daily air temperatures are 13.5ºC and -41.0ºC, respectively. Winter air

temperatures in the Crowsnest Pass are highly variable, largely due to chinook (föhn)

events which occur when cold continental air masses from northern Canada converge on

warm air in the west, creating strong, warm westerly winds (Nkemdirim, 1996; Hauer *et

al*., 2007). Annual precipitation at Coleman is approximately 57.7 cm, of which 30%

occurs as snowfall. The snow pillow measurement site closest to the research area is

Alberta Environment's South Racehorse Creek station, located at an elevation of 1920 m

(Figure 3.1). Annual average snow water equivalent (SWE) at this location peaks in early to mid-April at 40.0 cm, with the approximate date of snowpack removal at the end of May.

3.3 Lost Creek fire and Southern Rockies Watershed Project

The Lost Creek fire burned approximately 21,000 hectares in the headwater regions of the Castle and Crowsnest Rivers from July to August of 2003 (Kulig *et al*., 2009). This fire was one of the most severe forest fires to occur on the upper eastern slopes of Alberta in many decades.

The Southern Rockies Watershed Project (SRWP) was initiated in 2004 to evaluate post-wildfire hydrology, water quality and aquatic ecology (Silins *et al.*, 2009a). Seven watersheds (three burned, two burned and subsequently salvage logged, and two unburned) were instrumented for baseline hydrometeorological monitoring (Silins and Wagner, 2007). Snow surveys were completed annually in two watersheds and discharge, water quality, meteorological data, soil, and vegetation measurements have been collected at several stations. Preliminary results show that mean snowpack depth near the time of peak SWE and mean SWE are approximately three times greater in burned than in healthy unburned forests (Silins and Wagner, 2007). The processes driving these snow accumulation differences are poorly understood, highlighting the need for more detailed studies to evaluate the effects of wildfire on sub-canopy snow accumulation and melt.

Two of the seven SRWP instrumented watersheds were selected for study: North York (829 ha) was not burned during the wildfire, while South York (359 ha) was

severely burned. Both watersheds drain into the Crowsnest River, which flows into the Oldman River.

3.4 Study stands

During the winter seasons of 2009 and 2010, snow and meteorological measurements were collected in two forest stands: healthy (control) and burned (Figure 3.2). Both forest stands are located in the subalpine forest region (Alberta Sustainable Resource Development, 2010). Research stands and meteorological station locations were selected such that both stands had similar topographic characteristics (Table 3.1) and larger-scale surrounding forest cover. Both stands have north facing aspects, are located within 100 m elevation of each other, and are in close proximity (< 1 km) (Figure 3.3). The healthy (control) stand is at 1680 m elevation and the burned stand is at 1775 m elevation. Based on Alberta Sustainable Resource Development (ASRD) forest inventory maps, the pre-wildfire structural characteristics of both stands were similar. The burned stand is representative of the most severely burned forest in the Lost Creek fire area.
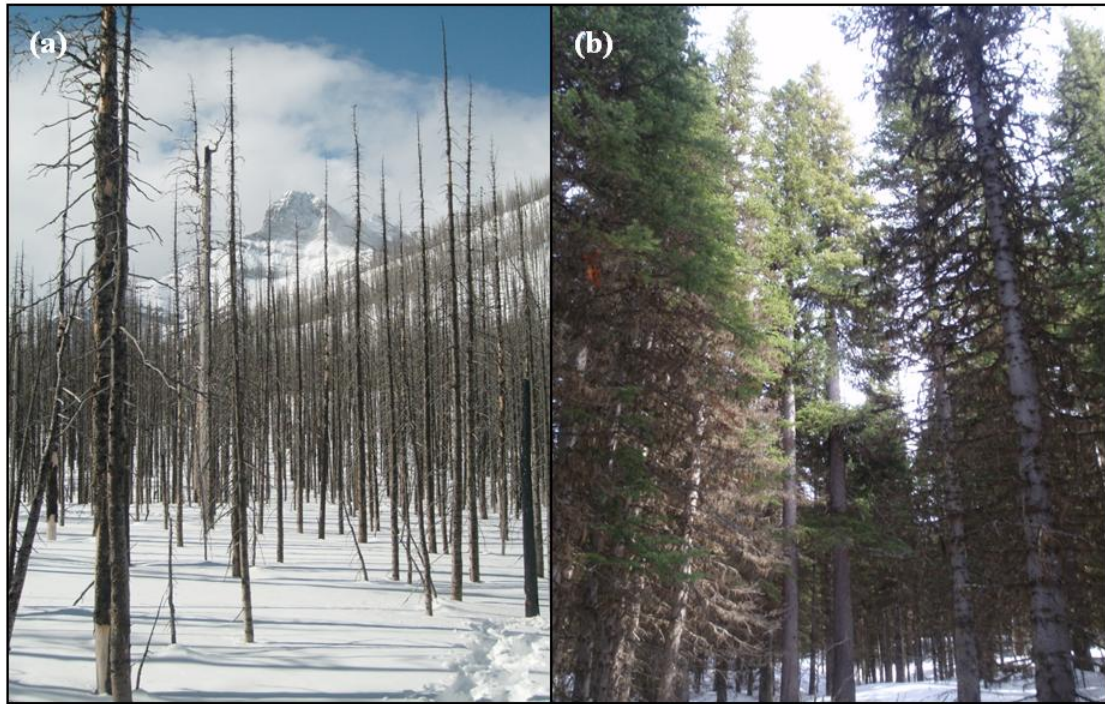
Figure 3.2: Photographs of forest stands: (a) burned and (b) healthy.

Table 3.1: Summary of study stand characteristics

	Burned stand	Healthy stand
Watershed	South York	North York
Aspect	NNE 45°	NNW 340°
Elevation (m)	1775	1680
UTM (11U)	0678687 N 5494107 E	0679102 N 5494786 E
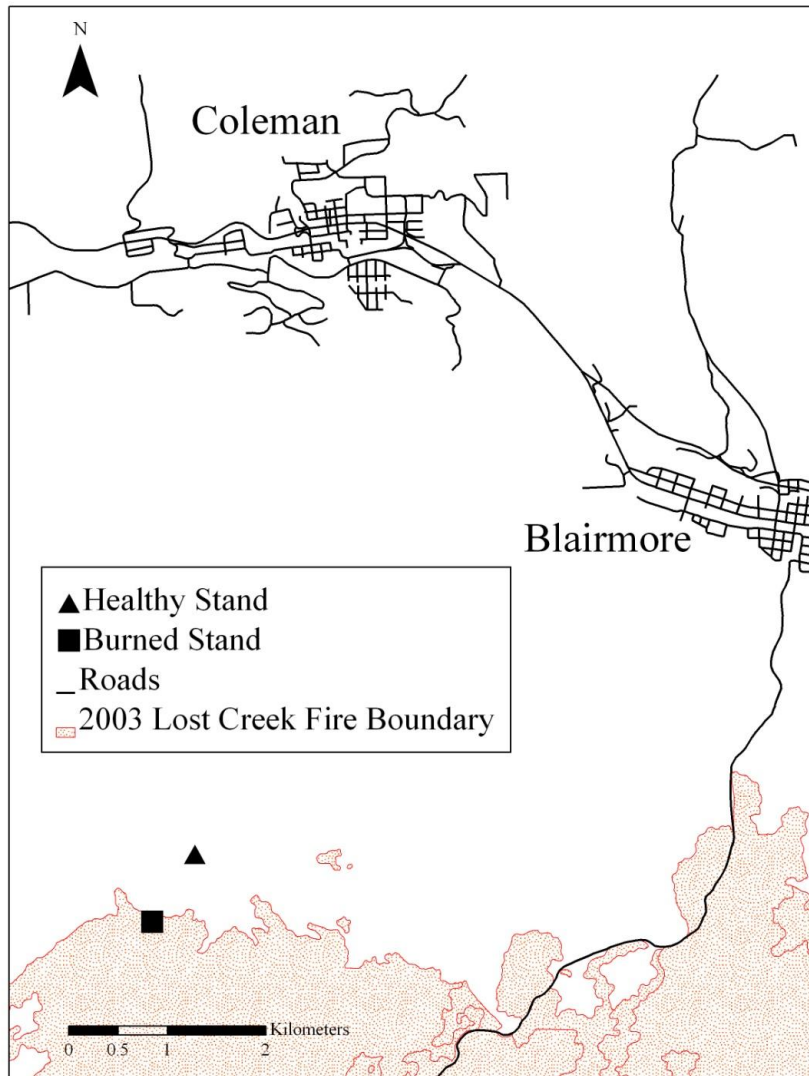
Figure 3.3: Study area region and location of the research stands.

Chapter 4

Methods

This chapter outlines the methods used to collect field data and develop a snowmelt model to calculate the energy balance over a melting sub-canopy snow surface. The specific objectives are to: 1) outline the field instrumentation and sampling program; 2) define the equations, assumptions, and parameters incorporated into the model; and 3) outline the methods for testing the sensitivity of the model to specific model inputs and the validation of model output using (1).

4.1 Field measurements

4.1.1 Meteorological and snowpack instrumentation

In October 2008, a 10 m Campbell Scientific (CSC) meteorological tower was installed in each of two forest stands to collect data required to calculate the snowmelt energy balance. Both meteorological towers recorded 20-minute and 24-hour averages of 1-minute readings of air temperature (T_a), relative humidity (RH), wind direction and speed (u), atmospheric pressure (P), incoming ($K\downarrow$) and reflected ($K\uparrow$) short-wave radiation, incoming ($L\downarrow$) and outgoing ($L\uparrow$) long-wave radiation, net radiation (Q^*), snow surface albedo (α), snow surface temperature (T_{ss}), internal snowpack temperature (T_{sd}), snow depth (s), soil heat flux at a fixed depth (G_d), soil moisture content (VWC), and soil

temperature (T_s), using CSC CR1000 data loggers. See Table 4.1 for the vertical position

and accuracy of the instrumentation.

Table 4.1: Instruments, accuracy and measurement height on each 10 m meteorological tower.

Variable	Instrument used for measurement	Accuracy	Height above (below) the ground (m)
Shielded T_a and RH	HMP45C212 (Vaisala Inc.)*	±0.01°C ±2% RH (0- 90%) ±3 RH (90 - 100%)	2.10
P	61205V (RM Young Company)*	±0.05 kPa	1.30
U	81000 Ultrasonic anemometer (RM Young Company)*	±0.05 m s^{-1}	1.98
$Q*$	NR Lite Net Radiometer (Kipp & Zonen)*	±10%	5.30
$Q*, K*, L*$, α	CNR1 Net Radiometer (Kipp & Zonen)*	±10%	3.20
T_{ss}	IRR-P infrared sensor (Campbell Scientific Canada Ltd.)*	±0.5°C T_{ss} (-40 - 70°C)	1.98
S	SR50A sonic ranging sensor (Campbell Scientific Canada Ltd.)*	1 cm	1.98
T_{sd}	Thermistor-based temperature acquisition cable (Beaded Stream)#	±0.5°C T_{sd} (-10 - 85°C)	0.00 – 2.00
T_s	TCAV soil temperature probes (Campbell Scientific Canada Ltd.)*	±3%	(0.02 and 0.06)
VWC	CS616 water content reflectometer (Campbell Scientific Canada Ltd.)*	±3%	(0.03)
G_d	HFP01SC soil heat flux plates (Hukseflux)*	±3%	(0.08)

*NOTE: * = instrument purchased from Campbell Scientific (Canada) Corp, Edmonton, Alberta, Canada; # = instrument purchased from Beaded Stream LLC, Anchorage, Alaska, USA*

4.1.2 Snow surveys

Peak snow accumulation and snowpack depletion were measured as snow water

equivalent (SWE) during the 2009 and 2010 snow seasons using a combination of snow

tube and snow pit measurements. Sampling technique selection was dependent on snow conditions, particularly the age, density, and depth of the snowpack.

Previous studies have determined that $n \geq 30$ density measurements give a power of approximately 0.9 to detect at least 30% differences in peak SWE between a mature and juvenile forest stand ($p = 0.05$) (Spittlehouse and Winkler, 1996). To maintain this level of statistical power or greater, snow density measurements were collected at 36 permanent snow survey stakes located on a grid (2500 m^2) at 10 m intervals in each stand. Snow depth measurements ($n = 121$) were collected at 5 m intervals within the same sampling grid, using a graduated metric snow probe. Average snow depth (cm) and density (g cm^{-2}) were multiplied to calculate stand scale SWE (cm). Snow surveys were completed in early and mid February, early March, and then weekly until complete snowpack removal.

In both field seasons, snow density was measured with both the standard Federal (GeoScientific Ltd, Vancouver, British Columbia, Canada) and Snow-Hydro (Snow-Hydro, Fairbanks, Alaska, USA) snow tubes. Both snow tubes are fitted with a cutting head that will cut through ice and consolidated snow layers within the snowpack and into the ground surface to obtain a dirt plug that helps to retain the snow sample (core). The length of each core must be >80% of snow depth at the sample point; in cases where the core was shorter, it was resampled. The Federal snow tube has a radius of 2.07 cm and a calibrated scale that allows SWE and snow density to be determined immediately by weighing the sample tube. Sampling with the Federal snow tube was most effective at the beginning of the snow season when the snowpack was relatively shallow with a fairly homogenous crystal structure. Sampling with the Snow-Hydro snow tube was most

effective when the snowpack became heterogeneous. This snow tube has a larger radius of 3.09 cm and is more successful at cutting through frozen and saturated layers; core lengths >90% of snow depth were easily obtained. However, the Snow-Hydro snow tube does not have a calibrated weighing scale; thus, samples were collected and weighed gravimetrically at the end of each snow survey to calculate snow density and SWE.

When the snowpack was too shallow (<20 cm) to use either snow tube, a bulk sampling method was applied. With this method, a snow sample was extracted with a 50 cm length of PVC pipe with a 5.08 cm radius. As the PVC pipe is not fitted with a cutting head, it is difficult to obtain a dirt plug; therefore, the snow around the PVC was removed and a shovel was inserted under the PVC to retain the sample. Snow-Hydro samples collected concurrently with the bulk method at ~50% of sampling locations across the snow survey grid indicated that the bulk method underestimated snow density by ~5% relative to the snow tube. When the snowpack was too deep (>140 cm) to use the Snow-Hydro tube and too heterogeneous to use the Federal tube, snow pits were dug to measure snow density. Density was sampled in two pits per stand at 10 cm depth intervals using a 250cc density cutter (SnowMetrics, Fort Collins, Colorado, USA) (e.g., Adams and Barr, 1974). Later in the snow season when the snowpack was shallower (~50 cm), additional snow pits were dug and three Snow-Hydro cores were collected near the pit wall to compare snow density measurements. Snow pits over-estimated snow density by ~5%, relative to the Snow-Hydro measurements.

4.1.3 Snowmelt lysimeters

Two 2.9 m^2 snowmelt lysimeters with 460 mL tipping buckets (each tip = 0.016 cm meltwater outflow) were installed in each of the burned and healthy forest stands in the fall of 2009 (Winkler, 2001; Winkler *et al.*, 2005). One lysimeter in each stand was installed within 2 m of the snow survey grid to be representative of the snow survey data. The second lysimeter in each stand was positioned within 25 m of the meteorological tower.

Lysimeters were constructed from 2.4 x 1.2 m sheets of marine grade plywood, with 15 cm sidewalls to minimize collection of meltwater flowing laterally at the base of the snowpack from the adjacent snowpack (Kattelmann, 1984). The plywood base was covered in several layers of clear fiberglass and painted white to mimic the thermal characteristics of the snowpack: low thermal conductivity and high α (Winkler, 2001). For field installation, organic material and understory vegetation were removed and the exposed mineral soil was levelled, then sloped to ensure ground contact with the entire lysimeter base and aid in drainage. The custom-built tipping buckets were connected to Hobo pendant event loggers (UA-003-64, Onset Computer Corporation, Pocasset, Massachusetts, USA) that recorded instantaneous bucket tips. Tipping buckets were placed in pits dug below the surface, on top of rocks and levelled to ensure good meltwater drainage. A drainage ditch was also dug from the pit to prevent localized pooling of water. Each pit was covered with an insulated plywood lid to prevent meltwater freezing.

The lysimeters were connected to the tipping bucket using standard ABS piping, with all pipe connections glued with ABS pipe glue and siliconed to prevent leakage.

Following installation, discharge tests determined no leaks and <10 mL water trapped in the ABS piping after each test. Piping was then covered in insulation and mineral soil to prevent overwinter freezing.

4.1.4 Forest mensuration

Forest structure characteristics were measured using standard forest mensuration techniques (BC Ministry of Forests and Range, 2007) to quantify differences between stands; data were also used to parameterize the snowmelt energy balance model described in Section 4.2. Measurements were collected in circular fixed area plots, with a plot center defined by one permanent snow sampling location in the centre of the snow survey grid, in each stand. The radius of each fixed plot was defined based on the plot area required to include > 40 and < 60 trees. Measurements of tree height (m) and height to base of live crown (m) were collected using a calibrated VL400 Vertex Laser (Haglof, Oscommerce Pacforest Supply Company, Springfield, Oregon, USA). Tree diameter at breast height (DBH; cm) was measured with a metric fabric diameter tape (Forestry Suppliers Inc, Jackson, Mississippi, USA). Tree species and crown condition (dead or alive) were recorded for each tree within the fixed plot. Stem density (number of trees per 100 m^{-2}) and canopy depth (m) were calculated from these data.

4.1.5 Classification of soils

Soil characteristics were quantified for use in the ground heat flux calculations outlined in Section 4.2.5. In July 2009, two soil pits were dug in each forest stand. Soil

depth and texture were measured *in situ*, and soil porosity and bulk density were measured in the lab for each soil horizon (A, B, and C) (see Klute, 1986). Soil samples were dried in an oven for 48 hours at 105°C to determine the bulk density. In the lab, soil samples were used to calibrate the soil VWC (%) measured from the soil water content reflectometer by incrementally adding a known volume of water to a known volume of soil.

4.2 Snowmelt model

Differences in snowmelt energy balance characteristics between the burned and healthy forest stands were calculated using the energy balance equation:

$$Q_m = L^* + K^* + SHF + LHF + GHF - Q_{cc} \qquad (4.1)$$

where Q_m is energy available for snowmelt, L^* is net long-wave radiation, K^* is net short-wave radiation, SHF is sensible heat, LHF is latent heat, GHF is ground heat, and Q_{cc} is the cold content of the snowpack (all in W m^{-2}). All energy balance components are considered positive when directed towards the surface, as per the snow research convention (e.g., Etchevers *et al*., 2004). Q_m is calculated as the residual of the surface energy balance fluxes minus the amount of energy required to raise the snowpack to the melting point (Q_{cc}) (0°C). Internal snowpack energy storage was not calculated directly; however, a post-hoc calculation of Q_{cc} was used to calculate the amount of energy required to raise the temperature of the snowpack to the melting point. Rain-on-snow (ROS) was not observed during the 2009 snowmelt period, while in 2010 it was observed twice in the healthy stand (May 9 and 26). The first was a morning snowfall event that melted out of the forest canopy as liquid rain, and the second was a small afternoon rain

event. These events did not cause rapid snow surface melting in the continuous snow depth record from the SR50A. Therefore, advective energy (energy supplied to the snowpack by rainfall) was not considered in the model.

4.2.1 Net long-wave radiation

Hourly $L*$ was quantified by calculating $L\downarrow$ from the atmosphere, forest canopy, and tree trunks, and $L\uparrow$ from the snow surface (all in W m^{-2}):

$$L* = \tau_L \varepsilon_a \sigma T_a + (1 - \tau_L) \varepsilon_c \sigma T_c^{\,4} + (H_t / H) \varepsilon_t \sigma T_t^{\,4} - \varepsilon_{ss} \sigma T_{ss}^{\,4} \tag{4.2}$$

To calculate $L\downarrow$ from the atmosphere, the sky view factor (τ_L: fraction of hemisphere visible from beneath the canopy) was calculated from hemispherical photos taken in close proximity to the meteorological station and the forest mensuration plot center using a Canon EOS 5D digital SLR camera with full-frame sensor and a Sigma 180º true fisheye lens on a leveled tripod. Hemispherical photos were processed using edge detection software (SideLook 1.1.01 for Windows, retrieved from www.appleco.ch) (Nobis, 2005) and Gap Light Analyzer (GLA) (Institute of Ecosystem Studies, Simon Fraser University, Burnaby, British Columbia, Canada) (Frazer *et al.*, 1999). The Stefan-Boltzmann (σ) constant used in Equation 4.2 is equal to 5.67 x 10^{-8} W m^{-2} K^{-4}. Emissivity of the atmosphere (ε_a) was calculated based on Prata (1996) for clear sky conditions:

$$\varepsilon_a = 1 - (1 + w) exp\left\{-(1.2 + 3.0w)^{0.5}\right\} \tag{4.3}$$

where w is the precipitable water content of the atmosphere (cm), estimated as (Leach and Moore, 2010):

$$w = 465 * \left[e_a / (T_a + 273.2)\right] \tag{4.4}$$

where e_a is atmospheric vapour pressure (kPa) and T_a is the air temperature (ºC).

To calculate $L\downarrow$ from the forest canopy, the emissivities of the forest canopy (ε_c) and tree trunks/stems (ε_t) were set to 0.96 (Link and Marks, 1999). Canopy and trunk temperatures (T_c and T_t, in ºC) were not measured directly, but were based on measured T_a. In continuous stands, T_a is a good surrogate for T_c (Pomeroy *et al.*, 2009); therefore in the healthy stand it was assumed that $T_c = T_a$. In discontinuous and/or dead forest stands, T_c and T_t values can be 4 to 38ºC greater than T_a, with the greater values measured during periods of high incoming short-wave radiation (Derby and Gates, 1966; Essery *et al.*, 2008; Pomeroy *et al.*, 2009). Thus in the burned stand where the forest canopy is discontinuous, it was assumed that both T_c and $T_t = T_a + 5$.

H_t/H was calculated as (Woo and Giesbrecht, 2000):

$$H_t/H = r_t \sin^2 \left\{ tan^{-1}\left(h - s / d_t\right)\right\}/ \pi d_t \tag{4.4}$$

where the ratio of the hypothetical hemispherical surface area receiving long-wave radiation from the tree trunk (H_t) to the hypothetical hemispherical area emitting long-wave radiation to a point on the snow surface (H) located at a distance (d_t, in m) from the tree trunk is a function of the tree radius (r_t, in m), height of the canopy above the ground (h, in m), and snow depth (s, in m). H_t/H was calculated using forest mensuration and snow data, and was based on average tree characteristics from each fixed area plot. Although H_t/H values are relatively insensitive to changes in s, they are very sensitive to d_t. As H_t/H can only be calculated for individual trees, the model assumes that, at any given point on the snow surface, $L\downarrow$ from trunks is emitted from the nearest tree trunk.

To calculate $L\uparrow$ from the snow surface, the emissivity of the snow surface (ε_{ss}) was set to 0.97 (Hardy *et al.,* 1997) and T_{ss} was measured directly.

43

4.2.2 Net short-wave radiation

Hourly net short-wave radiation, K^*, was simulated using:

$$K^* = K\downarrow \tau_c (1 - \alpha) \qquad (4.5)$$

In the absence of direct measurements of above-canopy $K\downarrow$, it was calculated using

measured $K\downarrow$ in the burned stand multiplied by 1.18 (based on 1 minus the sky view

factor in the burned stand $(1 - 0.82)$). Comparison of calculated above-canopy $K\downarrow$ with

above-canopy $K\downarrow$ measured over a two-week period in fall 2009 showed good

correspondence between the two. τ_c is the canopy transmissivity of short-wave radiation.

In the burned stand, τ_c was assumed to equal τ_L because there were no needles to restrict

transmission of incoming short-wave radiation ($K\downarrow$, in W m^{-2}). In the healthy stand,

however, τ_c was calculated using a 60-day average ratio of 20-minute measurements of

$K\downarrow$ above the forest canopy to $K\downarrow$ measured beneath the healthy forest canopy. Average

daily albedo (α) was calculated from CNR1 data in each stand.

4.2.3 Sensible heat

The hourly exchange of energy between the snow surface and overlying air due to

differences in temperature was calculated using the bulk aerodynamic method (Andreas,

2002):

$$SHF = \rho_a C_{pa} D_H (T_a - T_{ss}) \qquad (4.6)$$

where ρ_a is the density of air (kg m^{-3}), C_{pa} is the heat capacity of air (J kg^{-1} K^{-1}), and D_H is

the bulk transfer coefficient for sensible heat (m s^{-1}).

4.2.4 Latent heat

The hourly exchange of energy between the snow surface and overlying air due to differences in vapour pressure was also computed using the bulk aerodynamic method (Andreas, 2002):

$$LHF = \rho_a \lambda_v D_E \left(\frac{0.622}{P} \right) (e_a - e_{ss}) \qquad (4.7)$$

where λ_v is the latent heat of vapourization (2.48×10^6 J kg^{-1}), D_E is the bulk transfer coefficient for latent heat (m s^{-1}), P is atmospheric pressure (kPa), e_a is the atmospheric vapour pressure (kPa), and e_{ss} is the snow surface vapour pressure (kPa).

Assuming, under neutral conditions, that the bulk transfer coefficients for sensible heat (D_H), latent heat (D_E), and momentum (D_M) (all in m s^{-1}) are equal ($D_H = D_E = D_M$) they are given by (Moore, 1983):

$$D_E = D_H = D_M = \frac{k^2 u}{\left(\ln \dfrac{z_a}{z_o} \right)^2} \qquad (4.8)$$

where k is von Karman's constant (0.40), u is wind speed (m s^{-1}), z_a is the height of the wind measurement (m), and z_o is the roughness length of the snow surface (m). Maximum z_o values for seasonal snow covers (0.005) and undulating wet snow (0.007) (Moore, 1983) are most representative of the snow characteristics in the study stands; therefore, a value of 0.006 was used for this study.

The Richardson bulk stability parameter (Rb is dimensionless) was used to correct the bulk transfer coefficients (Equation 4.8) for stratified atmospheric conditions:

$$Rb = \frac{g (T_a - T_{ss})(z_a)}{T_k u^2} \qquad (4.9)$$

where g is the gravitational acceleration (m s^{-2}) and T_k is the mean temperature of the air layer (K). Atmospheric conditions are stable when $Rb > 0.3$, and unstable when $Rb < 0.3$ (Andreas, 2002).

During the snowmelt period, *SHF* (Equation 4.6) and *LHF* (Equation 4.7) were calculated using corrected bulk transfer coefficients (Price and Dunne, 1976):

$$D_{Ms} = D_M \,/(1+10Rb) \tag{4.10}$$

where $D_{Ms} = D_H = D_E$ and D_{Ms} is the bulk transfer coefficient for momentum under stable atmospheric conditions when $Rb > 0.3$.

When atmospheric conditions became unstable ($Rb < 0.3$), $D_{Mu} = D_H = D_E$ (Price and Dunne, 1976):

$$D_{Mu} = D_M \,(1-10Rb) \tag{4.11}$$

where D_{Mu} is the bulk transfer coefficient for momentum under unstable atmospheric conditions when $Rb < 0.3$. Unstable atmospheric conditions over melting snow are uncommon (de la Casiniere, 1974). In both 2009 and 2010, only 1 and 7% of hourly time steps were corrected for unstable conditions in the burned and healthy stand, respectively.

4.2.5 Ground heat flux

GHF is the energy exchange between the snow surface and the ground as a result of conduction. G_d (W m^{-2}) data from the heat flux plates were corrected for the heat capacity of a moist soil (C_s, in J kg^{-1} K^{-1}) and heat storage of a moist soil (S_H, in J m^{-2} s^{-1})

$$C_s = \rho_b C_d + \theta_v \rho_w C_w \tag{4.12}$$

$$S_H = \frac{\Delta T_s C_s d_s}{t} \tag{4.13}$$

$$GHF = G_d + S_H \qquad (4.14)$$

where ρ_b is the soil bulk density (kg m^{-3}) calculated as an average value from samples collected in each soil horizon (A, B, and C) of the soil pits dug in July 2009 (Klute, 1986); C_d is the heat capacity of a dry soil (~840 J kg^{-1} K^{-1}) (Hanks and Ashcroft, 1980); θ_v is the soil water content on a volume basis (dimensionless) using measured soil VWC data corrected for the specific soils found in the stands; ρ_w is the density of liquid water (~1000 kg m^{-3}); and C_w is the heat capacity of water (~4190 J kg^{-1} K^{-1}). To calculate S_H, ΔT_s is the change in soil temperature (in, K) over the output interval (t); d_s is the depth below the surface where G_d measurements were collected (m); and t is the output interval (s). S_H (in W m^{-2}, *also* J m^{-2} s^{-1}) was added to G_d to calculate GHF (W m^{-2}) at the soil surface (Equation 4.14).

4.2.6 Cold content of the snowpack

Once Q_m was determined, the cold content (Q_{cc}) of the snowpack was calculated and incorporated as a post-hoc calculation. Q_{cc} is the amount of energy (J m^{-2}) required to raise the average snowpack temperature to the melting point (Dingman, 2002):

$$Q_{cc} = -C_i \rho_w SWE(T_{sd} - T_m) \qquad (4.15)$$

where C_i is the heat capacity of ice (~2102 J kg^{-1} K^{-1}), T_{sd} is the average temperature of the snowpack (K), and T_m is the melting point temperature (273.2 K). SWE for each time step was calculated using continuous measured snow depth (m) from the SR50A and measured average snow density from snow surveys (kg m^{-3}). T_{sd} was calculated based on automated measurements of snow surface and soil temperature ($T_{sd} = (T_{ss} + T_s)/2$). In 2010, T_{sd} was measured with a thermistor string (TAC) in both stands. During the

snowmelt period, however, TAC measurements were problematic due to preferential melt around the sensor, which resulted in the thermistor string measuring T_a. Therefore, T_{sd} was calculated from average T_{ss} and T_s for both 2009 and 2010. Q_{cc} was then divided by the hourly output interval (in s), to convert it to W m^{-2} for use in Equation 4.1.

4.2.7 Snowmelt

Following calculation of Q_m minus Q_{cc}, hourly meltwater production (*MLT*, in m hr^{-1}) was calculated (Pomeroy and Goodison, 1997):

$$MLT = Q_m / (\rho_w \lambda_f B_i) \qquad (4.16)$$

where Q_m is in units of (J m^{-2} h^{-1} converted from W m^{-2}), λ_f is the latent heat of fusion (~0.335 x 10^6 J kg), and B_i is the thermal quality of snow (fraction of ice in a unit mass of wet snow; generally 0.95 - 0.97) (Male and Gray, 1981). B_i was set to 0.95 for the duration of the snowmelt period, as model output was relative insensitive to it. The model was initialized with maximum measured SWE, then run to complete snowpack removal. For snowfall events that occurred during the snowmelt period, the measured SWE record (m) using continuous measured snow depth (m) from the SR50A and measured average snow density from snow surveys (kg m^{-3}) was used to determine the amount of SWE that accumulated during these snowfall events. These values were then added to the simulated SWE record.

4.2.8 Data quality assessment and selection of input data

All instruments in the study stand were calibrated and installed as directed by the manufacturer (Campbell Scientific, Edmonton, Alberta, Canada); however, data

verification and quality control were necessary. NR Lite measurements of $Q*$ were corrected for wind speeds >5 m s^{-1}, and snow depth measurements were corrected for T_a, as per manufacturer's instructions. Measurements from the water content reflectometer were calibrated to the specific soils found in the stands (see Section 4.1.5). All recorded 20-min data greater than two standard deviations from the mean (duration of the snowmelt period) were removed and thus not used as input to the energy balance model. Less than 5% of data were removed, with sufficient data remaining to apply a 1-hour modelling interval. Due to snow accumulating on the CNR1 during and after snowfall, the CNR1 heater was used when $T_a < 1°C$ and $RH > 95\%$. Therefore, calculated short-wave radiation at the top of the forest canopy ($K\downarrow$) based on CNR1-measurements of $K\downarrow$ in the burned stand were removed when the heater were used. Missing hourly data were then infilled using the previous 3-day average of the corresponding 1-hour period. Less than 10% of hourly average above-canopy $K\downarrow$ data were infilled for both years.

Data inputs to the model were specifically matched to the field program; thus, the snowmelt energy balance model was not calibrated to improve model fit. Input variables include those simulated by the energy balance calculations described in the previous section (Table 4.2). Final model parameters listed in Table 4.3 were either measured or obtained from the literature.

Table 4.2: Variables used as input data in the model, and variables output by the model in both stands.

Input variables	Output variables
Air temperature (T_a, in ºC)	Net long-wave radiation ($L*$, in W m^{-2})
Snow surface temperature (T_{ss}, in ºC)	Net short-wave radiation ($K*$, in W m^{-2})
Relative humidity (RH, in %)	Latent heat flux (LHF, in W m^{-2})
Incoming short-wave radiation ($K\downarrow$, in W m^{-2})	Sensible heat flux (SHF, in W m^{-2})
Albedo (α, in ratio)	Ground heat flux (GHF, in W m^{-2})
Air pressure (P, in kPa)	Cold content of snowpack (Q_{cc}, in W m^{-2})
Wind speed (u, in m s^{-1})	Energy available for melt (Q_m, in W m^{-2})
Soil temperature (T_s, in ºC)	Snowmelt (MLT, in m)
Soil volumetric water content (VWC, in %)	
Soil heat flux (G_d, in W m^{-2})	
Maximum measured snow water equivalent (SWE, in m)	
Accumulated precipitation (SWE, in m)	

Table 4.3: Parameters used in the energy balance model for each stand in each year. Note the reference from which each parameter was obtained, or from which the equation to calculate each parameter was taken.

Parameter	Burned	Healthy	Referenced in literature or calculated
z_o	0.006	0.006	Moore, 1983
τ_c	0.82	0.09	Calculated from CNR1 $K\downarrow$ and $K\uparrow$ data
ε_{ss}	0.97	0.97	Hardy *et al.*, 1997
ε_t	0.96	0.96	Link and Marks, 1999
ε_c	0.96	0.96	Link and Marks, 1999
τ_L	0.82	0.18	Calculated as per Nobis, 2005; Frazer *et al.*, 1999
T_c (ºC)	$T_a + 5$	T_a	Pomeroy *et al.*, 2009
T_t (ºC)	$T_a + 5$	$T_a + 5$	Pomeroy *et al.*, 2009
H_t/H	0.018	0.035	Calculated as per Woo and Giesbrecht, 2000

4.3 Sensitivity analysis of model output

The sensitivity of model output (Q_m) to the under- or overestimation of model inputs was tested in the healthy stand in 2009 because snowmelt is most complex under a

healthy forest canopy (Link and Marks, 1999). Model parameters that were either calculated or taken directly from the literature were also tested. Tests were used to: (1) estimate the effect of input data error; (2) examine the relative stability of variables and parameters; and (3) estimate the effect of errors in variables and parameters on model output.

With the point-based snowmelt energy balance model used in this study, calculations of K^* and L^* require more parameterization than any other flux, therefore the sensitivity of all parameters used to simulate Q^* were tested. In addition, z_o was tested because of the large range of values given in the literature. Finally, the over- or under-estimation of T_{sd} was tested because it was based on average T_{ss} and T_s.

The model was run iteratively through a range of values for each of the variables and parameters. Ranges were either selected from the literature or were based on the full range of potential under- or over-estimations (i.e., the ratios τ_c and τ_L range from 0 to 1) (Table 4.4). After each model run, and prior to applying additional sensitivity tests, parameter values were returned to those used in the baseline simulation (Table 4.3). This ensured that any measured differences were a function only of the changed parameter. The sum of Q_m (MJ m^{-2} h^{-1}) from each model run was plotted against the variable or parameter value used in that run to quantify its relative sensitivity. Results were also compared with total Q_m calculated for the 2009 snowmelt period (3 April – 2 June) using the baseline model described in Section 4.2.

Table 4.4: Range, number of iterations, and iterative change used for sensitivity analysis of each parameter during the 2009 snowmelt period (3 Apr to 2 Jun) in the healthy stand. NOTE: a_t is the ºC added to T_a to represent T_c and T_t.

Parameter	Range	Number of iterations (Iterative change)
τ_c **(ratio)**	0.0 – 1.0	19 (0.05)
τ_L **(ratio)**	0.0 – 1.0	19 (0.05)
ε_{ss} **(ratio)**	0.94 – 1.0	31 (0.002)
ε_t **(ratio)**	0.94 – 1.0	31 (0.002)
ε_c **(ratio)**	0.94 – 1.0	31 (0.002)
T_c $(T_a + a_t)$ **(ºC)**	0.5 – 38.0	76 (0.5ºC)
T_t $(T_a + a_t)$ **(ºC)**	0.5 – 38.0	76 (0.5ºC)
H_t/H **(ratio)**	0.005 – 0.5	100 (0.005)
z_o **(m)**	0.0002 – 0.02	3 (0.0002, 0.002, 0.02)
(+ or -) T_{sd} **(ºC)**	-1.5 – 4.0	12 (0.5 ºC)

4.4 Model performance

Model performance was assessed by comparing measured and simulated: (1) Q^* and (2) rate and timing of snowmelt. Only time steps with corresponding measured Q^* data from both the CNR1 and NR Lite radiation sensors were compared to ensure the same sample size between all datasets. The simulation performance of the rate and timing of snowmelt was assessed by comparing continuous records of measured and simulated SWE. While snowmelt data from the lysimeters would have been the most accurate dataset to validate the model output, the success of the lysimeters in 2010 was compromised by the antecedent soil moisture conditions and event logger and/or tipping bucket failure. In the burned stand, saturated soils and poor soil infiltration resulted in flooding of the tipping buckets. In the healthy stand, both event loggers malfunctioned resulting in both lysimeters not recording any tips. Therefore, measured SWE was derived from the continuous snow depth record (SR50A) and snow survey density measurements averaged across each stand. SR50A measurements of snow depth were

representative of the average snow depth measured during snow surveys in each stand (Figure 4.1). While snow survey measurements are higher than SR50 measurements by an average of 17 cm in the burned stand during the snowmelt period, they follow the same trend.
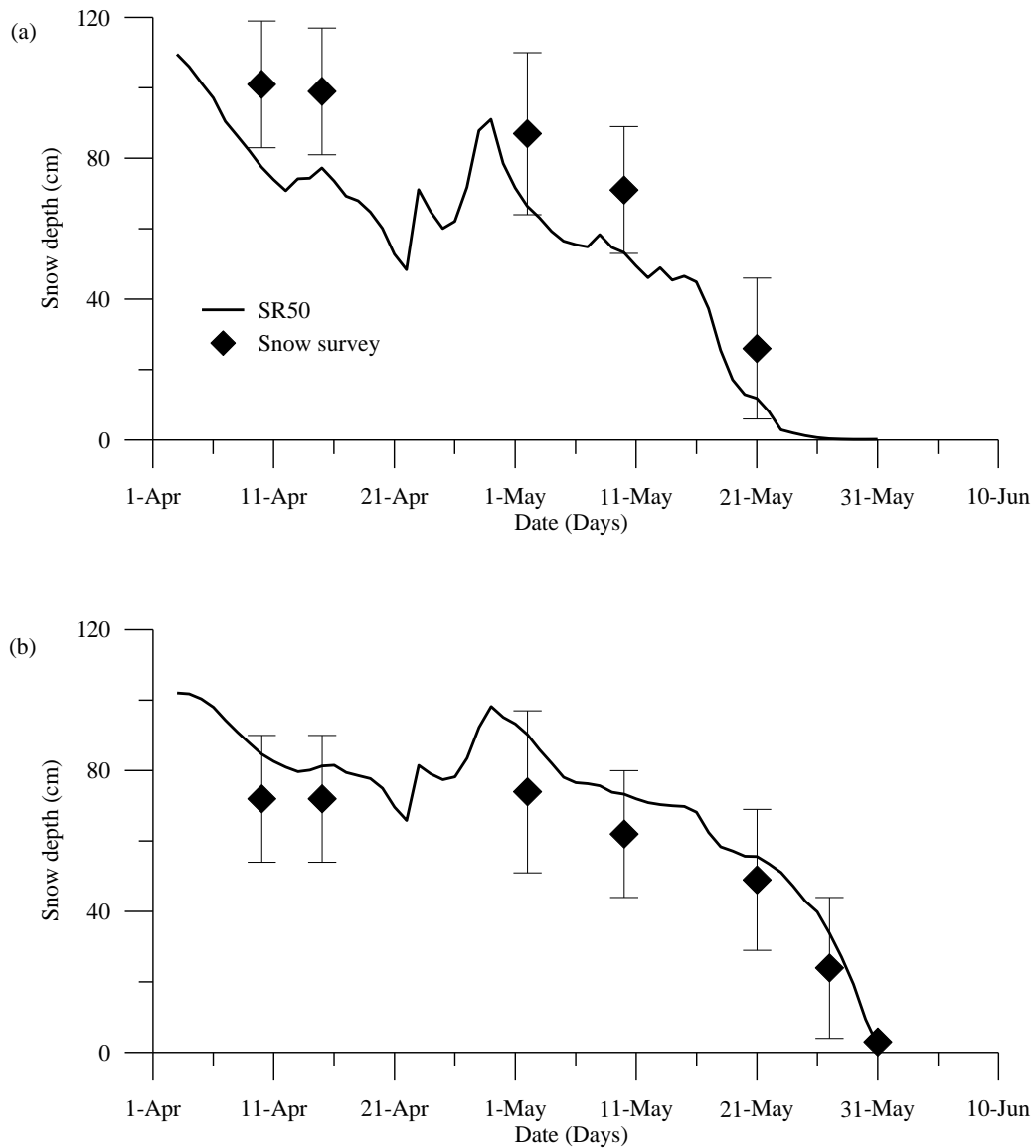
Figure 4.1: Average snow depth measurements from the SR50A and from the weekly snow surveys during the 2009snowmelt period: (a) burned and (b) healthy stand. Error bars denote one standard deviation from the average.

Descriptive statistics for measured and simulated $Q*$ and SWE were collated, and results were summarized to compare values. Goodness-of-fit between the measured and

simulated time series was determined using two quantitative measures of performance-coefficient of determination (r^2) and root mean square error (RMSE):

(1) r^2 describes the proportion of variance in the simulated values explained by the regression of measured versus simulated values (Krause *et al.*, 2005):

$$r^2 = \left(\frac{\Sigma_{i=1}^{n} (\chi_o - \overline{\chi_o})(\chi_s - \overline{\chi_s})}{\sqrt{\Sigma_{i=1}^{n} (\chi_o - \overline{\chi_o})} \sqrt{\Sigma_{i=1}^{n} (\chi_s - \overline{\chi_s})^2}} \right)^2 \qquad (4.17)$$

(2) RMSE is the measure of the square root of the variance of the residuals (average difference between the measured and simulated values):

$$RMSE = \sqrt{\frac{\Sigma (\chi_o - \chi_s)^2}{n}} \qquad (4.18)$$

Goodness of fit between measured and simulated SWE was also tested with the coefficient of efficiency (E) (Nash and Sutcliffe, 1970):

(3) E determines the predictive power of the simulated values:

$$E = 1 - \frac{\Sigma_{i=1}^{n} (\chi_o - \chi_s)^2}{\Sigma_{i=1}^{n} (\chi_o - \overline{\chi_o})^2} \qquad (4.19)$$

In Equations 4.17 to 4.19, n is the number of timesteps, χ_o is the measured hourly $Q*$ or measured SWE, χ_s is the simulated hourly $Q*$ or SWE, and $\overline{\chi_o}$ is the average measured hourly $Q*$ or measured SWE.

4.5 Defining the snowmelt period

The snowmelt period for each year was defined as the date of measured peak SWE to the date the snowpack was completely removed using the snowmelt simulation.

All between year and between stand comparisons of snow accumulation, snowmelt energy balance, and rate and timing of snowmelt were summarized for this period.

4.6 Differences between years and between stands

Differences in snow accumulation and snowmelt between the healthy and burned stands were graphically assessed using notched box plots of peak SWE (cm) and daily snowmelt (cm d^{-1}). Shapiro-Wilks' W test was used to confirm the data were normal (Shapiro *et al.*, 1968) and Levene's test was used to test the homogeneity of variances between comparisons (Hill and Lewicki, 2007). Overlapping notches between boxes indicates that the median values are not significantly different at $p = 0.05$ (Chambers *et al.*, 1983); this was confirmed using two tailed t-tests for independent samples.

Chapter 5

Modelling the snowmelt energy balance over a sub-canopy snowpack

This chapter presents and discusses the results of the sensitivity analyses and model performance tests to assess potential model uncertainties. The specific objectives are to: 1) define model sensitivity to parameters and variables selected in Chapter 4; 2) validate the simulated net radiation and snowmelt energy balance using data from Chapter 4; and 3) discuss model sensitivity and performance.

5.1 Sensitivity analysis

Note that the axes of the following figures are not standardized.

5.1.1 Forest canopy transmissivity and sky view factor

Although values of canopy transmissivity (τ_c) and sky view factor (τ_L) were calculated using published techniques (Sections 4.2.1, 4.2.2), the potential error associated with these estimates was high in the healthy stand (Figure 5.1 and 5.2). Values of τ_c and τ_L are used in the calculation of net short- and long-wave radiation, respectively. Although they are closely related, the sensitivity analysis was designed specifically to isolate and test the sensitivity of individual parameters. Therefore, these two parameters were not changed congruently.

In forest environments, forest canopy density can vary significantly over small spatial scales and subsequently affect snowmelt. The model was very sensitivity to

changes in τ_c used in the calculation of net short-wave radiation. An over-estimation of τ_c results in an over-simulation of Q_m (~34 MJ m^{-2} h^{-1} or 29% per 0.05 τ_c) (Figure 5.1).

(a)
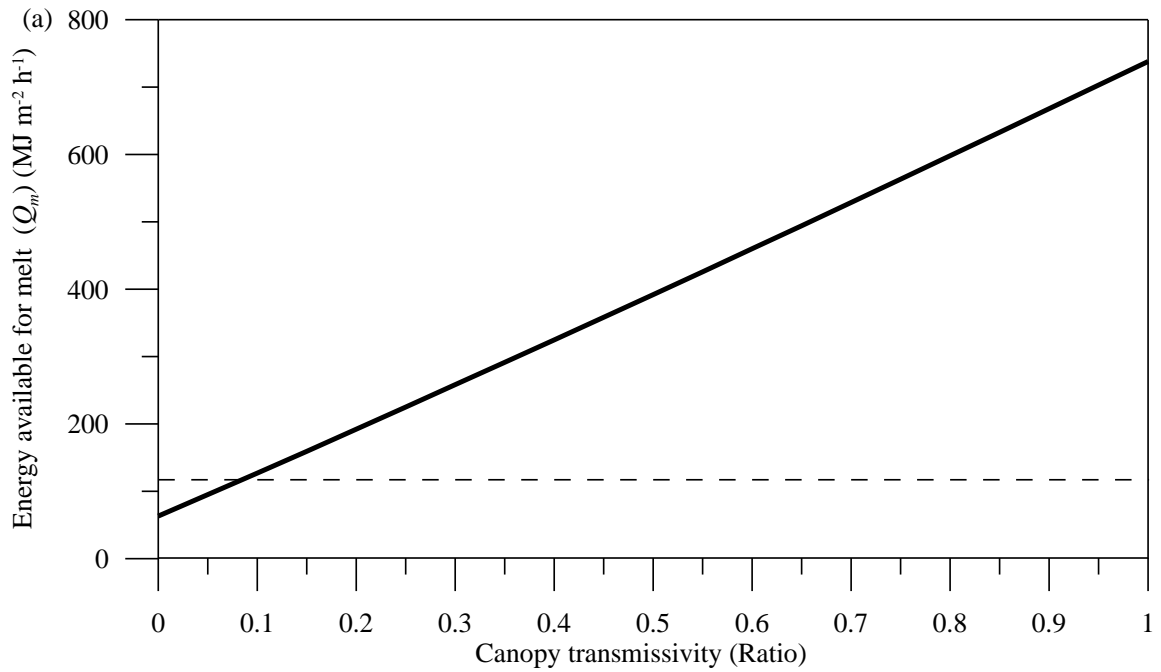
Figure 5.1: Sensitivity test results for the forest canopy transmissivity (τ_c) parameter in the healthy stand. The dashed line represents the total energy available for snowmelt (Q_m) in 2009 (117.25 MJ m^{-2} h^{-1}).

The model was also sensitive to values of τ_L used in the calculation of net long-wave radiation. An over-estimation of τ_L results in an under-simulation of Q_m (~6 MJ m^{-2} h^{-1} or 5% per 0.05 τ_c).
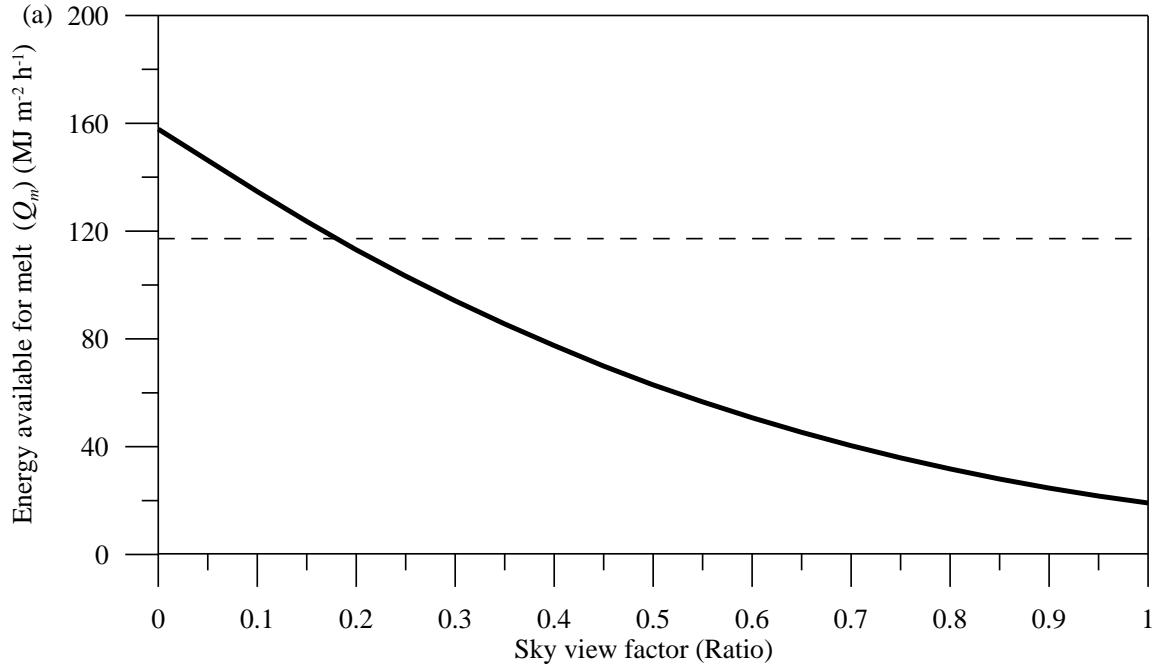
Figure 5.2: Sensitivity test results for the sky view factor (τ_L) parameter in the healthy stand. The dashed line represents the total energy available for snowmelt (Q_m) in 2009 (117.25 MJ m^{-2} h^{-1}).

5.1.2 Emissivity of the snow surface, tree trunks, and forest canopy

Calculations of long-wave radiation emitted by the snow surface, tree trunks, and forest canopy rely on values of ε_{ss}, ε_t, and ε_c, which are difficult to measure and in most models are estimated based on values from the literature. This could cause large over or under-estimations in model output (Figure 5.3) In forest environments, if ε_{ss} is over-estimated by even 0.01 over the snowmelt period, Q_m is reduced (~10 MJ m^{-2} h^{-1} or 8.5% per 0.01 ε_{ss}); the inverse is true for over-estimation of ε_c. The simulation appears relatively insensitive to ε_t.
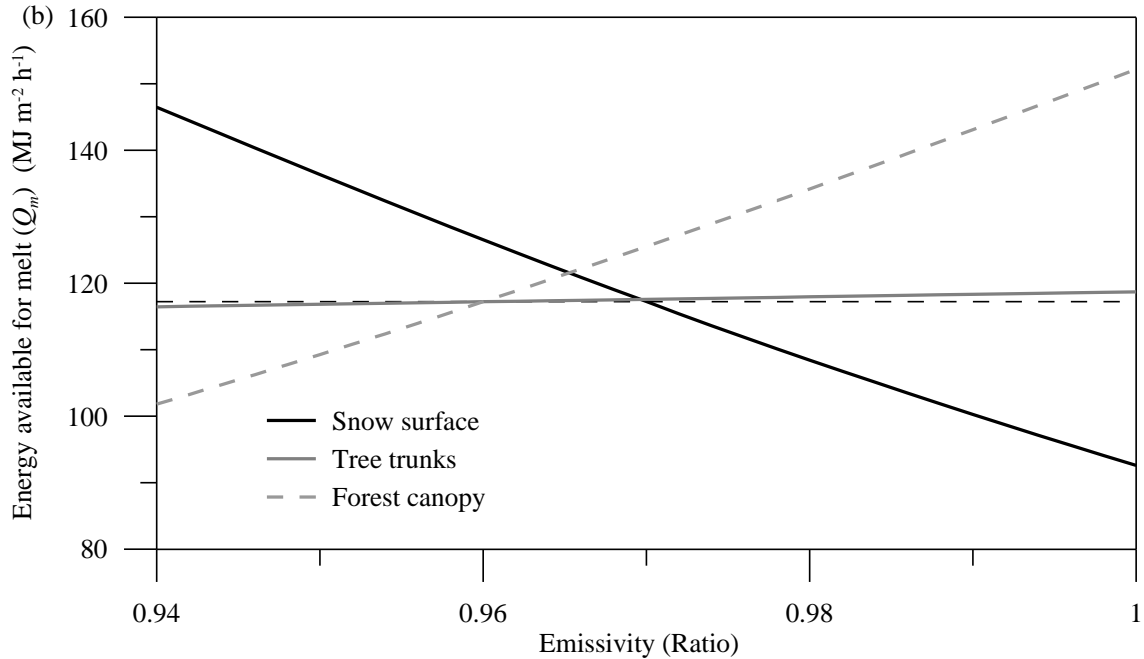
Figure 5.3: Sensitivity test results for the emissivity of the snow surface (ε_{ss}), tree trunks (ε_t), and forest canopy (ε_c) parameters in the healthy stand. The black dashed line represents the total energy available for snowmelt (Q_m) in 2009 (117.25 MJ m^{-2} h^{-1}).

5.1.3 Estimation of forest canopy and tree trunk temperature

Air temperature is generally a suitable surrogate for T_c under conditions of low $K\downarrow$ (Pomeroy *et al.*, 2009), but is more problematic under periods of high insolation. Previous studies have determined that T_c could be 0 to 30°C higher than T_a (Derby and Gates, 1966; Pomeroy *et al.*, 2003; Essery *et al.*, 2008). T_c and T_t were not measured directly for this study and were corrected based on T_a. Q_m is very sensitive to increases in T_c, but is relatively insensitive to increases in T_t (Figure 5.4). Although canopy and tree trunk temperatures of T_a + 30°C may seem unrealistic, the most extreme example is a well-exposed dead tree in a discontinuous forest stand which reached T_a + 38°C (Pomeroy *et al.*, 2009). Overall, the model is very sensitive to over-estimates of T_c; however, Q_m is less sensitive to over-estimates of 1 to 10°C (up to ~14 MJ m^{-2} h^{-1} or

11.9% per 1ºC increase in T_c) and more sensitive to over-estimates of 27 to 38ºC (up to ~21 MJ m^{-2} h^{-1} or 17.9% per 1ºC increase in T_c).
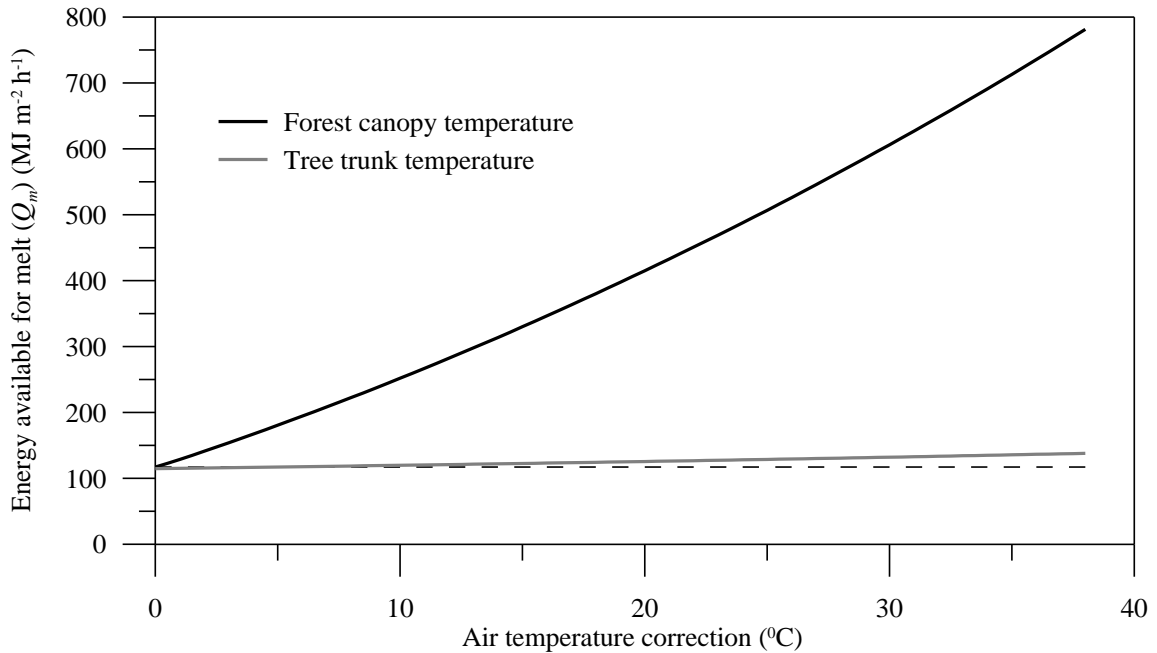
Figure 5.4: Sensitivity test results for the correction of forest canopy (T_c) and tree trunk temperature (T_t) based on the air temperature (T_a) in the healthy stand. The dashed line represents the total energy available for snowmelt (Q_m) in 2009 (117.25 MJ m^{-2} h^{-1}).

5.1.4 Long-wave radiation emitted from the tree trunks

It is difficult to quantify the physical processes affecting snowmelt around individual trees, where long-wave radiation emitted by tree trunks can cause localized melt. To calculate net radiation from tree trunks, the fraction of the $L*$ flux emitted from the tree trunk is estimated using H_t/H (Woo and Giesbrecht, 2000). Maximum H_t/H is determined to be 0.5, as only half of the hemisphere can receive radiation from a trunk. An average value was calculated (0.035) for the model using tree structure data from 2009 and snow depth data collected at specific points for both 2009 and 2010. The

simulation appears to be very sensitive to H_t/H, as a 0.01 increase in H_t/H increases Q_m by ~10 MJ m^{-2} h^{-1} or 8.5% (Figure 5.5).
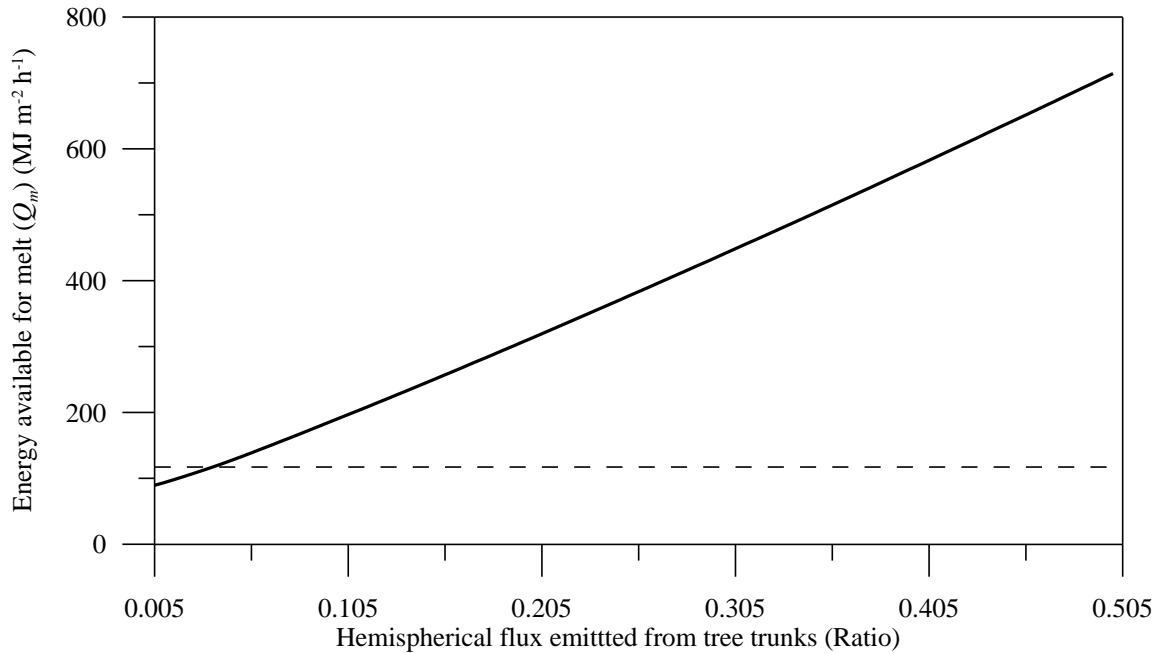
Figure 5.5: Sensitivity results for H_t/H in the healthy stand. The dashed line represents the total energy available for snowmelt (Q_m) in 2009 (117.25 MJ m^{-2} h^{-1}).

5.1.5 Snow surface roughness

In the absence of field measurements of z_o, a value was selected from the range given in the literature. Although other studies have noted that increasing roughness of the snow surface should be considered when the snowpack becomes patchy or understory vegetation appears (Metcalfe and Buttle, 1998), similar to Boon (2009) the healthy forest simulation of Q_m is relatively insensitive to z_o (Figure 5.6).
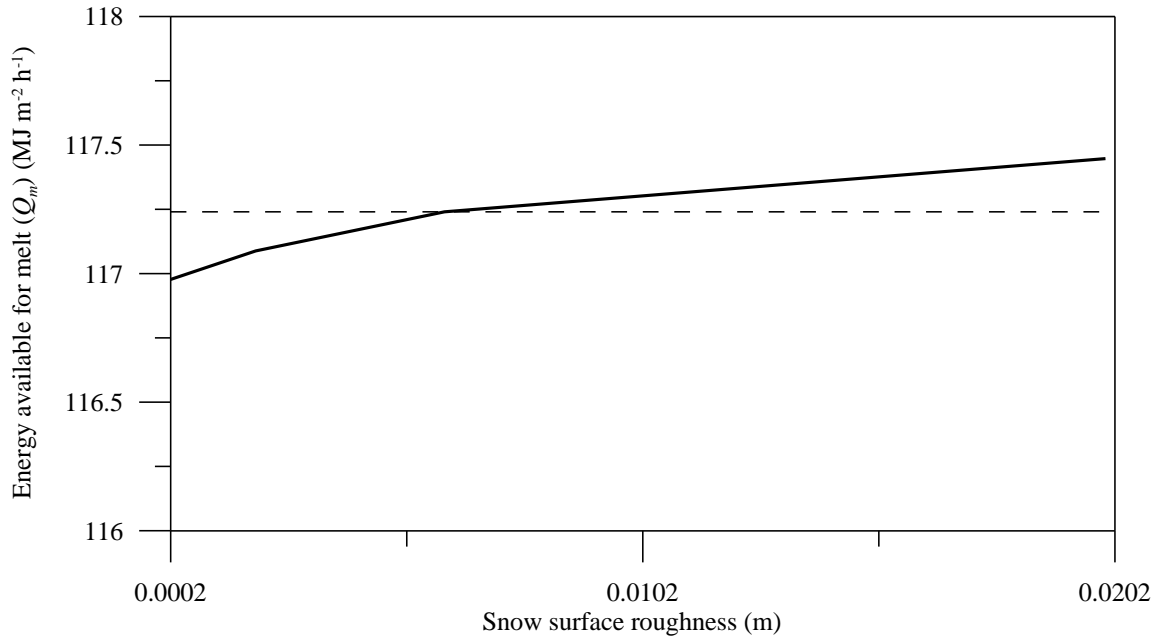
Figure 5.6: Sensitivity results for snow surface roughness (z_o) in the healthy stand. The dashed line represents the total energy available for snowmelt (Q_m) in 2009 (117.25 MJ m^{-2} h^{-1}).

5.1.6 Average snowpack temperature

Finally, simulation of model sensitivity to estimates of T_{sd} using average T_{ss} and T_s was tested. Q_m appears to be more sensitive to under- than over-estimation of T_{sd}. If the snowpack is colder than estimated ($<T_{sd}$), less Q_m would be available for melt because more energy would be required to raise the snowpack temperature to 0ºC before melt could occur. The greatest sensitivity is associated with under and over-estimation in the range of 0.5ºC (Figure 5.7).
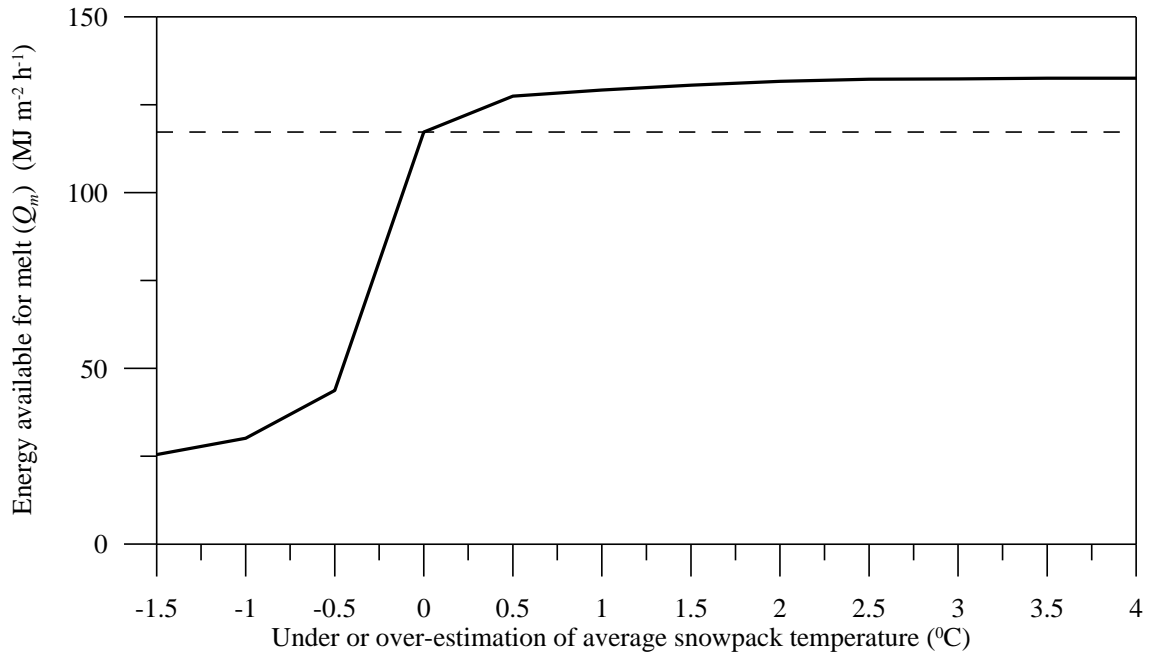
Figure 5.7: Sensitivity results for under or over-estimation of average snowpack temperature (T_{sd}) in the healthy stand. The dashed line represents the total energy available for snowmelt (Q_m) in 2009 (117.25 MJ m^{-2} h^{-1}).

5.2 Model performance

5.2.1 Net radiation

The model accurately simulated sub-canopy $Q*$ in the burned forest stand (Table 5.1). High coefficients of determination for both comparisons in both years indicate that the simulation explained over 80% of the variance in the measured data. Regression coefficients were less than unity for all comparisons, indicating a slight under-simulation of the $Q*$ trend. Positive y-intercepts suggest the simulated $Q*$ data was of a slightly higher magnitude than measured $Q*$ for all comparisons. The largest RMSE was

calculated for the NR Lite comparisons in both years, while lower RMSE values were calculated for CNR1 comparisons (Table 5.1).

Table 5.1: Simulated Q^* compared with Q^* measured by the CNR1 and NR Lite sensors in the burned stand (2009 and 2010 snowmelt periods: 3 Apr – 25 May; 13 Apr – 14 May).

	CNR1		NR Lite	
Year	**2009**	**2010**	**2009**	**2010**
n (hours)	1169	677	1191	768
Coefficient of determination (r^2)	0.87	0.84	0.81	0.88
Regression coefficient (standard error)	0.85 (0.01)	0.83 (0.01)	0.65 (0.01)	0.71 (0.01)
Regression intercept (standard error)	11.51 (1.19)	11.45 (1.76)	13.91 (1.43)	8.68 (1.39)
RMSE (W m^{-2})	39.97	38.05	67.31	53.44

Figure 5.8 presents average hourly simulated Q^*, with data from the CNR1 and NR Lite in the burned stand over the 2009 and 2010 snowmelt periods. Simulated Q^* shows the greatest divergence from measurements between 10:00 – 15:00 h, but is closest from 16:00 – 23:00 h and 0:00 – 9:00 h. Q^* is under-simulated when compared with NR Lite measurements (Figure 5.8), as evidenced by the RMSE (Table 5.1). Simulated Q^* was closest to CNR1-measured Q^*, as seen in the high slope and lower RMSE (Table 5.1). In 2009, the average hourly minimum and maximum difference between all comparisons was 0.55 and 95.21 W m^{-2}, respectively. In 2010, the average hourly minimum and maximum difference between all comparisons was 0.56 and 137.67 W m^{-2}, respectively. The maximum average hourly difference occurred at ~14:00 h in both years, when incoming short-wave radiation was greatest (Figure 5.8).
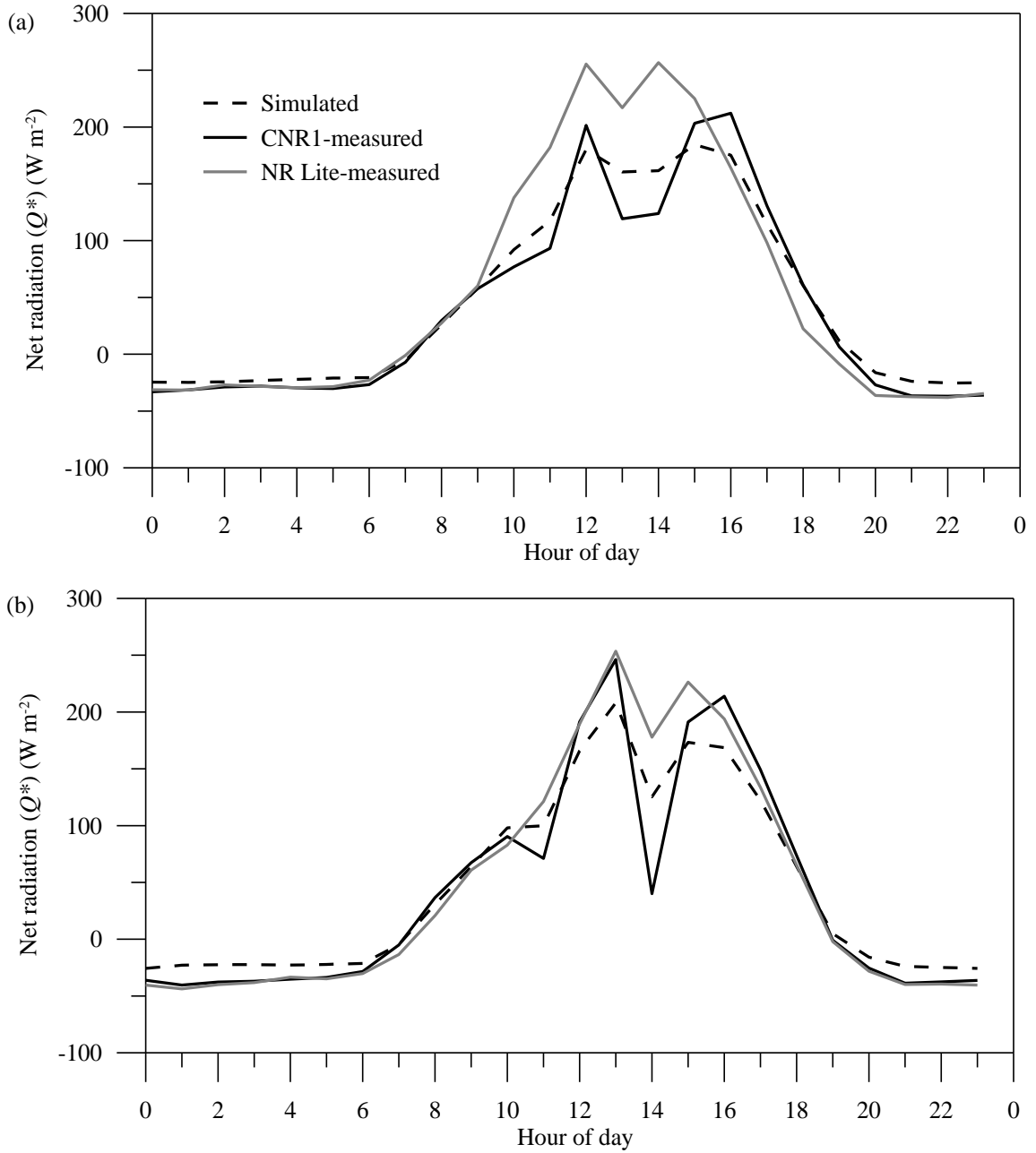
Figure 5.8: Average (2009 and 2010 snowmelt periods: Apr 3 – May 25; Apr 13 – May 14) hourly net radiation (Q^*) during the snowmelt period in the burned stand: (a) 2009 and (b) 2010.

The relationship between measured and simulated $Q*$ was weaker beneath the healthy forest canopy (Table 5.2). Although the coefficient of determination was low for all comparisons, results show stronger correlations with CNR1 than NR Lite values. Similar to the burned stand, regression coefficients were less than unity for all comparisons, indicating a slight under-simulation of the trend of $Q*$ in the healthy stand. The y-intercept for all comparisons was higher in the healthy than burned stand, and suggests the simulated $Q*$ data was of a higher magnitude than measured $Q*$ for all comparisons. For both years, calculated RMSE values were lower with the CNR1 than the NR Lite measurements. Although RMSE values for all comparisons were lower in the healthy than in the burned stand, average $Q*$ in the healthy stand was significantly lower; thus RMSE values formed a greater percentage of total net radiation. Thus, errors associated with the larger RMSE values in the burned stand were not as significant as those associated with the smaller RMSE values in the healthy stand.

Table 5.2: Simulated $Q*$ compared with $Q*$ measured by the CNR1 and NR Lite sensors in the healthy stand (2009 and 2010 snowmelt periods: Apr 3 – Jun 2; Apr 13 – May 28).

	CNR1		NR Lite	
Year	**2009**	**2010**	**2009**	**2010**
n (hours)	1246	941	1464	1104
Coefficient of determination (r^2)	0.54	0.58	0.46	0.47
Regression coefficient (standard error)	0.58 (0.02)	0.90 (0.03)	0.45 (0.01)	0.45 (0.01)
Regression intercept (standard error)	17.07 (0.73)	13.05 (0.77)	18.70 (0.66)	16.18 (0.72)
RMSE (W m^{-2})	28.07	27.20	39.31	38.80

Hourly averages of simulated and measured $Q*$ in the healthy stand during the 2009 and 2010 snowmelt periods did not compare as well as in the burned stand (Figure 5.9). Hourly averages of CNR1 and NR Lite-measured $Q*$ were more variable than the simulated $Q*$ in 2009, with the greatest average hourly peak $Q*$ values measured by the NR Lite (14:00 - 15:00 h) in both years. Simulated $Q*$ values are more comparable to CNR1 values in both years (Table 5.2). The minimum and maximum average hourly differences between simulated and CNR1-measured $Q*$ were 2.57 and 39.58 W m^{-2}. Figure 5.9 shows that the model over-simulates $Q*$ during periods of low solar angles, and under-simulates peak $Q*$ at midday (14:00 – 15:00 h).
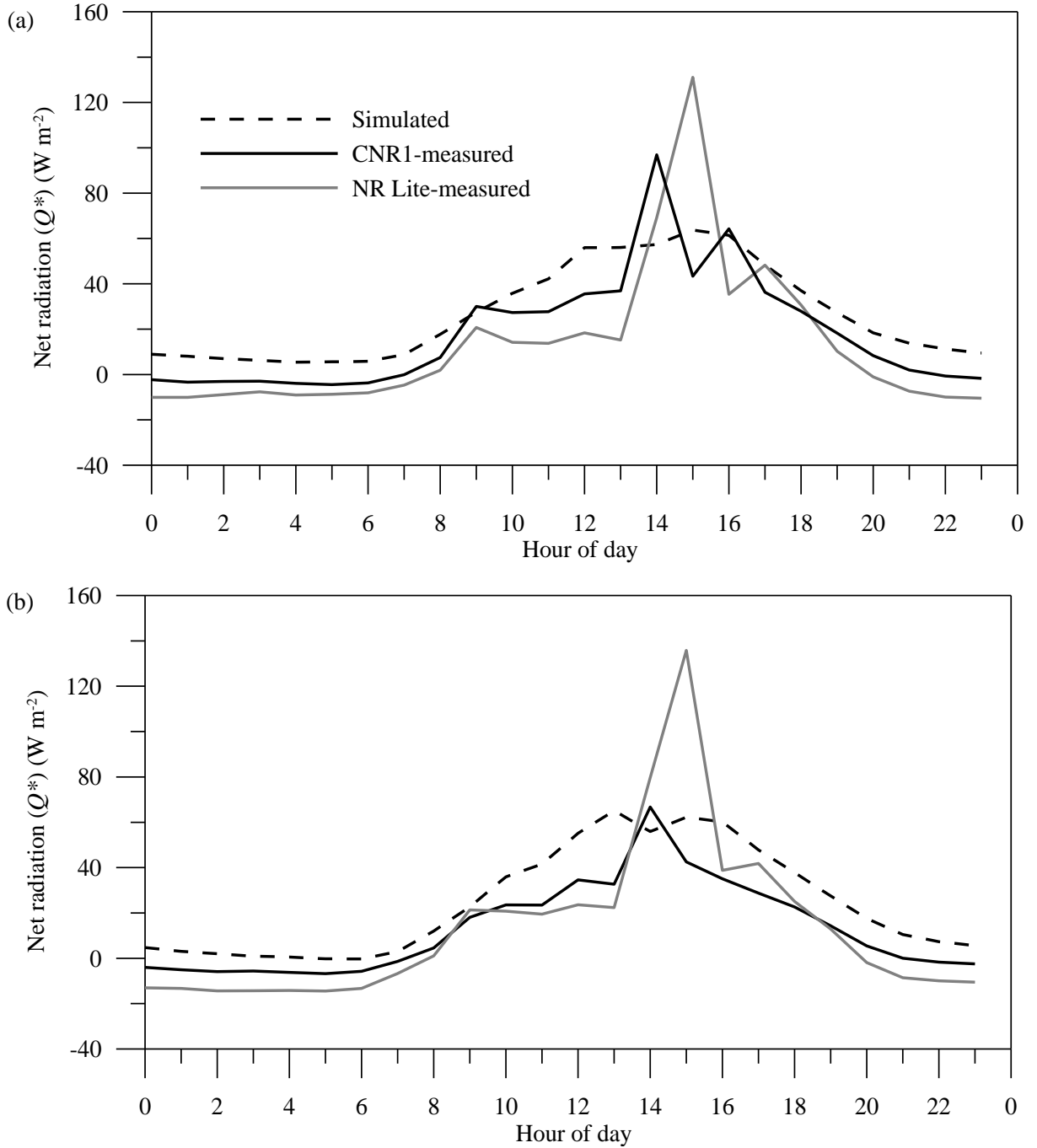
Figure 5.9: Average (2009 and 2010 snowmelt periods: Apr 3 – Jun 2; Apr 13 – May 28) hourly net radiation (Q^*) during the snowmelt period in the healthy stand: (a) 2009 and (b) 2010.

5.2.2 Rate and timing of snowmelt

For snowmelt simulations in the burned stand, mean hourly SWE over the snowmelt period was over-simulated by 19% in 2009 and under-simulated by 8% in 2010 (Table 5.3). The coefficient of determination for the burned stand was weaker in 2009 than 2010. The high coefficient of determination in 2010 indicates that simulated values explain the majority of variance in the measured SWE. The regression coefficient was less than unity indicating under-simulation of the trend of SWE in 2009. In 2010, regression coefficients were close to unity, indicating a slight over-simulation of the trend of SWE. The y-intercept was positive in 2009 suggesting the simulated SWE was of a higher magnitude than measured SWE, whereas in 2010 the y-intercept was negative suggesting the simulated SWE was of a lower magnitude than measured SWE. The E value was lower in 2009 than in 2010. The 2010 E value of 0.89 indicated that the predictive ability of the simulation was high. The 2010 simulation also had lower average model-prediction error, as indicated by the RMSE (Table 5.3).

Measured and simulated SWE are more closely associated for individual snowmelt events in 2010 than 2009 (Figure 5.10). Although in 2010 the energy balance model simulated the rate and timing of snowmelt with reasonable accuracy in the burned stand, the 2009 comparison was weaker.

Table 5.3: Simulated versus measured SWE in the burned stand (2009 and 2010 snowmelt periods: Apr 3 – May 25; Apr 13 – May 14).

		Burned Stand	
Year		**2009**	**2010**
n	Hours	1260	777
Maximum measured SWE	cm	31.29	23.49
Mean	Measured (cm)	19.17	10.66
	Simulated (cm)	23.29	9.84
	% difference	19%	-8%
Variance	Measured (cm)	50.95	33.57
	Simulated (cm)	52.40	41.82
	% difference	3%	22%
Coefficient of determination	r^2	0.66	0.96
Regression coefficient (standard error)	Slope	0.75 (0.02)	1.12 (0.01)
Regression intercept (standard error)	y-intercept	9.29 (0.32)	-2.50 (0.10)
Coefficient of efficiency	E	0.33	0.89
RMSE	cm	6.15	1.89
Date of complete snowpack removal	Measured (Date)	24 May	15 May
	Simulated (Date)	25 May	14 May
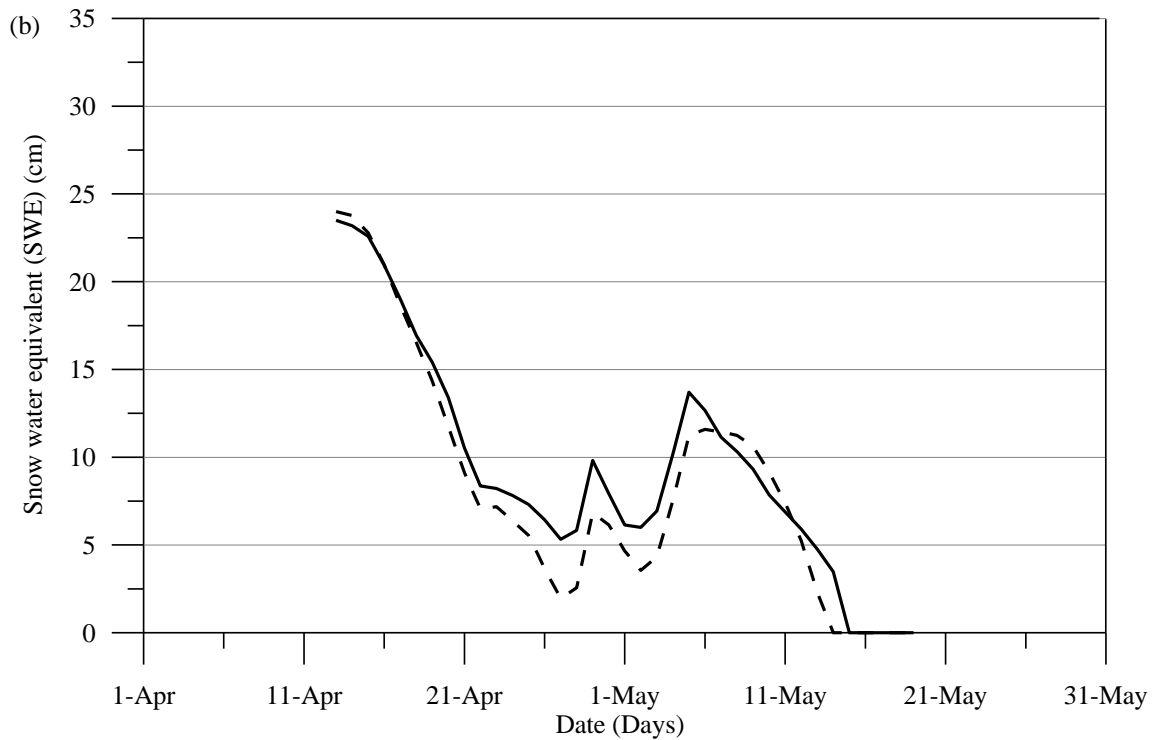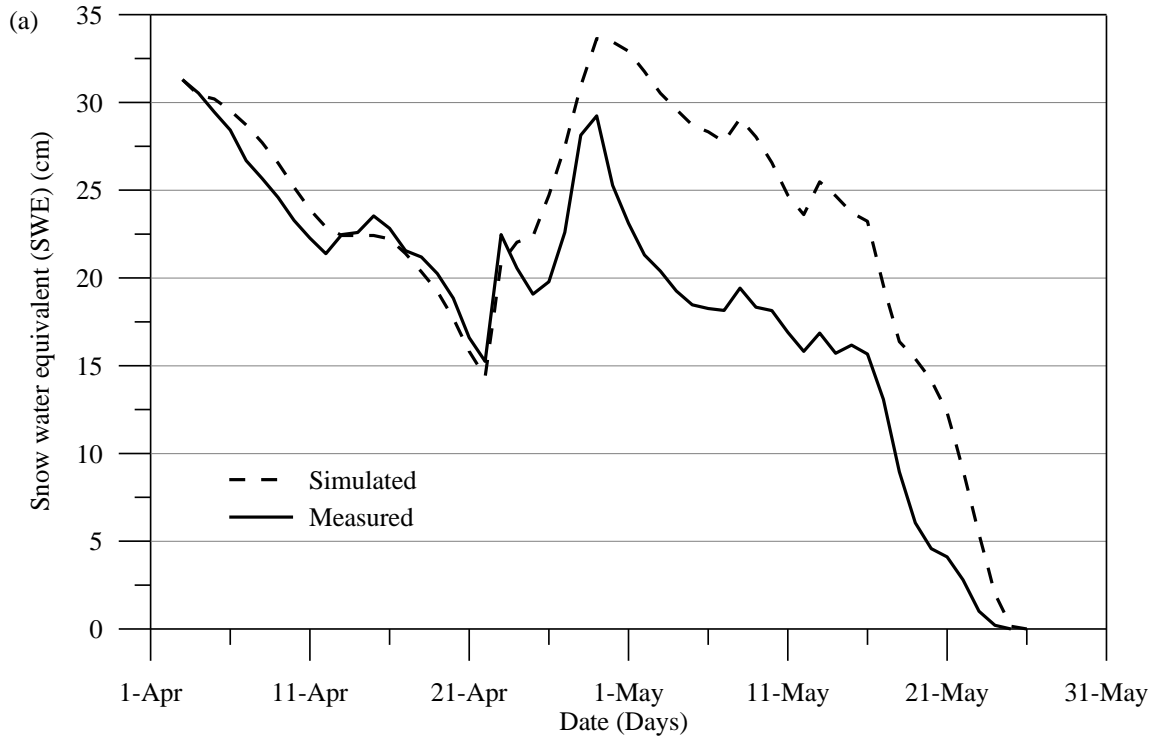
Figure 5.10: Simulated and measured snow water equivalent (SWE) in the burned stand: (a) 2009 and (b) 2010.

In the healthy stand, mean hourly SWE over the snowmelt period was under-simulated by 3% and 7% in 2009 and 2010, respectively (Table 5.4). As in the burned stand, the variance was higher for simulated relative to measured values for both 2009 and 2010. The coefficient of determination between measured and simulated SWE in both years indicates that – as in the burned stand in 2010 – simulated values explain almost all of the variance in the measured SWE. Regression coefficients were near or at unity, suggesting a very good simulation of snowmelt rates. In 2009 and 2010, y-intercepts were close to 0, suggesting that the simulated and measured values of SWE were of a similar magnitude. In the healthy stand, E values were high for both years, indicating the high predictive ability of the model (Table 5.4). The RMSE was lower in the healthy than the burned stand for both years, indicating low average model-prediction error in the healthy stand.

Measured and simulated SWE in the healthy stand in 2009 and 2010 showed close relationships between the rate and timing of snowmelt (Figure 5.11). The energy balance model simulated snowmelt in the healthy stand with a high level of accuracy.

Table 5.4: Simulated versus measured SWE in the healthy stand (2009 and 2010 snowmelt periods: Apr 3 – Jun 2; Apr 13 – May 28).

		Healthy Stand	
Year		**2009**	**2010**
n	hours	1453	1091
Maximum measured SWE	cm	24.61	19.21
Mean	Measured (cm)	20.17	12.65
	Simulated (cm)	19.50	11.85
	% difference	-3%	-7%
Variance	Measured (cm)	24.46	26.13
	Simulated (cm)	36.25	28.54
	% difference	39%	7%
Coefficient of determination	r^2	0.93	0.98
Regression coefficient (standard error)	Slope	0.99 (0.01)	1.02 (0.01)
Regression intercept (standard error)	y-intercept	0.09 (0.16)	-0.87 (0.06)
Coefficient of efficiency	*E*	0.95	0.96
RMSE	cm	1.39	1.08
Date of complete snowpack removal	Measured (Date)	31 May	28 May
	Simulated (Date)	02 Jun	28 May
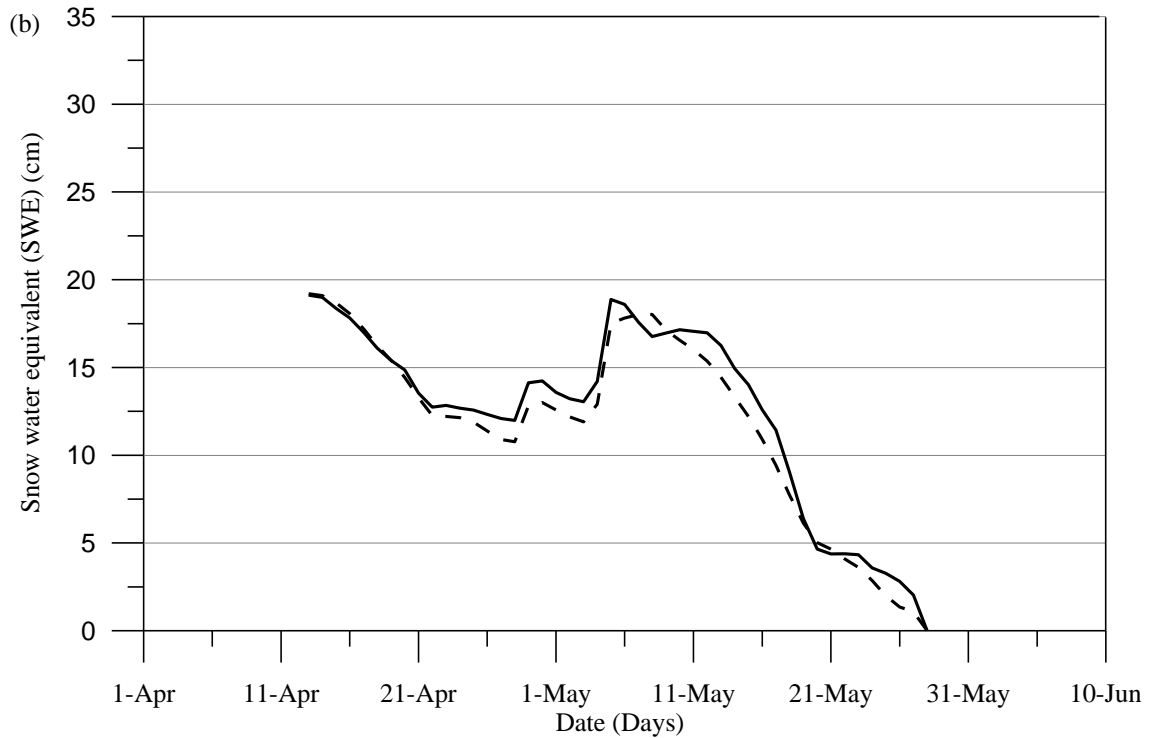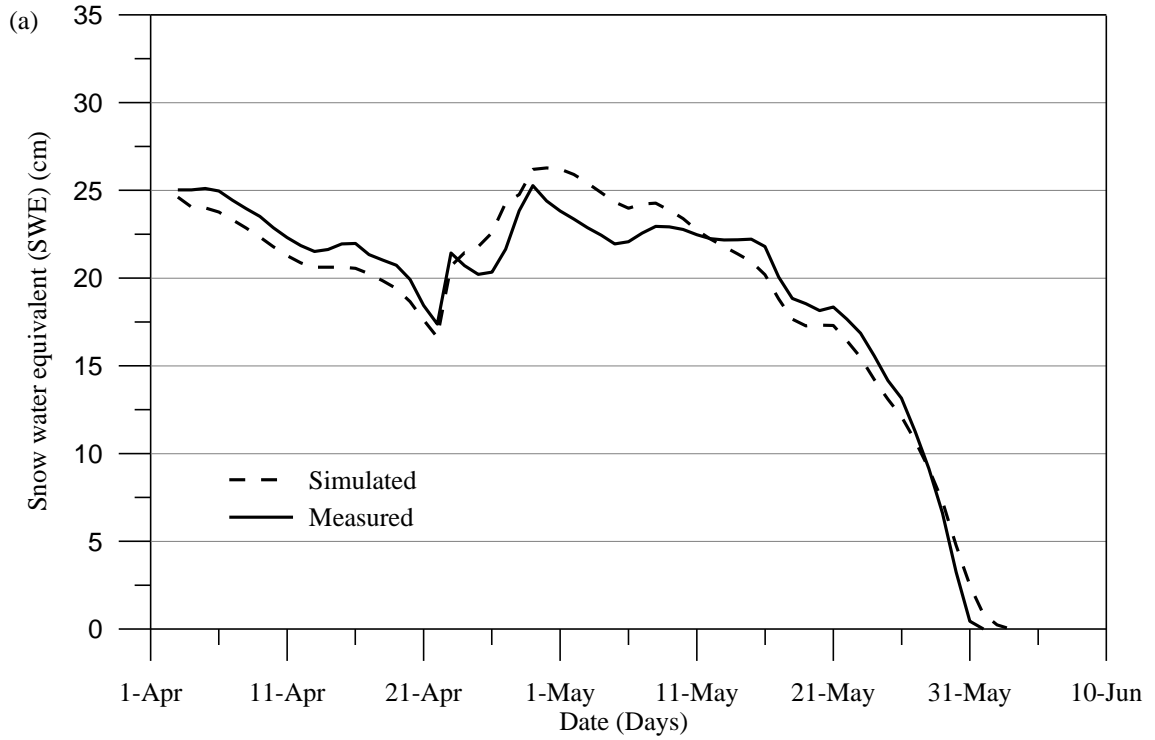
Figure 5.11: Simulated and measured snow water equivalent (SWE) in the healthy stand: (a) 2009 and (b) 2010.

5.3 Discussion of model sensitivity and performance

The most challenging issue inherent in modelling is quantifying the source and amount of uncertainty, as model accuracy is affected by uncertainties in model representation of inputs, process descriptions, and model assumptions and parameters (Sivapalan *et al.,* 2003). Modelled Q_m is most sensitive to the parameters used in the simulation of Q^*, the largest contributor to snowmelt in forest environments. Q^* was simulated based on a combination of parameters measured in the snow survey grid (τ_c, τ_L, H_t/H) and selected from the literature (ε_{ss}, ε_c, ε_t), and variables measured at the meteorological tower (T_a, T_{ss}, α, $K\downarrow$). The largest potential error in the calculation of Q_m is associated with τ_c, highlighting the model's sensitivity to changes in the forest canopy. The measured under-simulation of Q^* at peak $K\downarrow$ could be the result of over-estimating canopy density (under-estimating τ_c); however, that would also result in an under-simulation during periods of reduced $K\downarrow$, which was not evident. The under-simulation of Q^* is likely due to the model not accurately representing short-wave radiation transmission through the complex canopy matrix during daylight hours.

Model output of Q_m was also very sensitive to ε_c, ε_{ss}, T_c, and H_t/H, which are used to calculate L^*. Accurate values of these parameters are fundamental to simulating L^*, especially in the healthy stand where $L\downarrow$ is emitted by the canopy. Q^* was over-simulated during low periods of Q^*. This could be the result of under-estimating τ_L, which would have over-estimated the amount of $L\downarrow$ emitted by the forest canopy.

In the healthy stand, Q^* appears to be under-simulated when the solar angles are highest (14:00-15:00). Transmission of short-wave radiation through the canopy varies with canopy leaf area and the size and distribution of canopy gaps. Thus $K\downarrow$ measured at

high time resolution (e.g., hourly) would be noisy due to the interaction between sun angle and the arrangement of branches in the vicinity of the sensor, whereas coarser time resolutions would average these local variations (Roujean, 1999). Poor comparisons between simulated and measured hourly Q^* may, therefore, be a function of these noisy measurements in the healthy stand. In the burned stand, however, the fit between simulated and measured Q^* was stronger, likely because the forest canopy had been removed and there was less variability in forest structure parameters. In both stands and in both years, simulated Q^* values were more comparable to CNR1- than NR Lite-measured values, likely because the CNR1 independently measures the four components of Q^* ($K\downarrow$, $K\uparrow$, $L\downarrow$, $L\uparrow$), and is more accurate than older net radiometers such as the NR Lite (Blonquist *et al.*, 2009).

Sensitivity analyses showed that the model was most sensitive to a 0.5ºC over- or under-estimation of T_{sd}, which also corresponds with the resolution of T_{ss} and T_{sd} sensors used in this study. Although calculating T_{sd} from T_{ss} and T_s may not accurately represent average T_{sd} under specific circumstances, it represents a best approximation of this value given the available data set. Direct measurements of snowpack temperature are difficult to obtain as *in situ* instruments often experience preferential melt, thus providing T_a rather than T_{sd} values. This highlights the importance of accurately measuring T_{sd} and considering internal snowpack processes in snowmelt models.

Model validation of SWE was used to test the temporal correspondence between simulated and measured values. The energy balance model simulated snowmelt accurately in both forest stands; however, the 2009 comparison in the burned stand was weaker. In 2009, snowmelt in the burned stand was simulated well until the snowfall

76

event on April 22, after which snowmelt was under-simulated (Figure 5.12 (a)).

Immediately after this snowfall, T_{ss} decreased by ~15°C in < 1 day (April 24) (Figure

5.12). This dramatic decrease subsequently decreased average snowpack temperature (T_{sd}

= (T_{ss} + T_s)/2); thus, more energy was required to raise the average snowpack temperature

to the melting point (0°C) (Figure 5.12 (c)).

In the healthy stand in 2009, snowmelt was also under-simulated immediately

following snowfall events. Very few studies have quantified the effects of snowmelt

season snowfall events on snowpack cold content, particularly the ability of fresh

snowfalls to either insulate the melting pack or allow penetration of cold air temperatures.

Snow is an excellent thermal insulator, with new snow (density of ~0.14 kg m^{-3}) having

the lowest average thermal conductivity (0.07 W m^{-1}K^{-1}) (Sturm *et al.*, 1997). It is likely

that the low T_{ss} did not penetrate far into the snowpack during this short period. The

under-simulation of snowmelt is therefore a result of T_{sd} being colder than in reality,

leading to an over-calculation of Q_{cc} and subsequent under-simulation of Q_m.
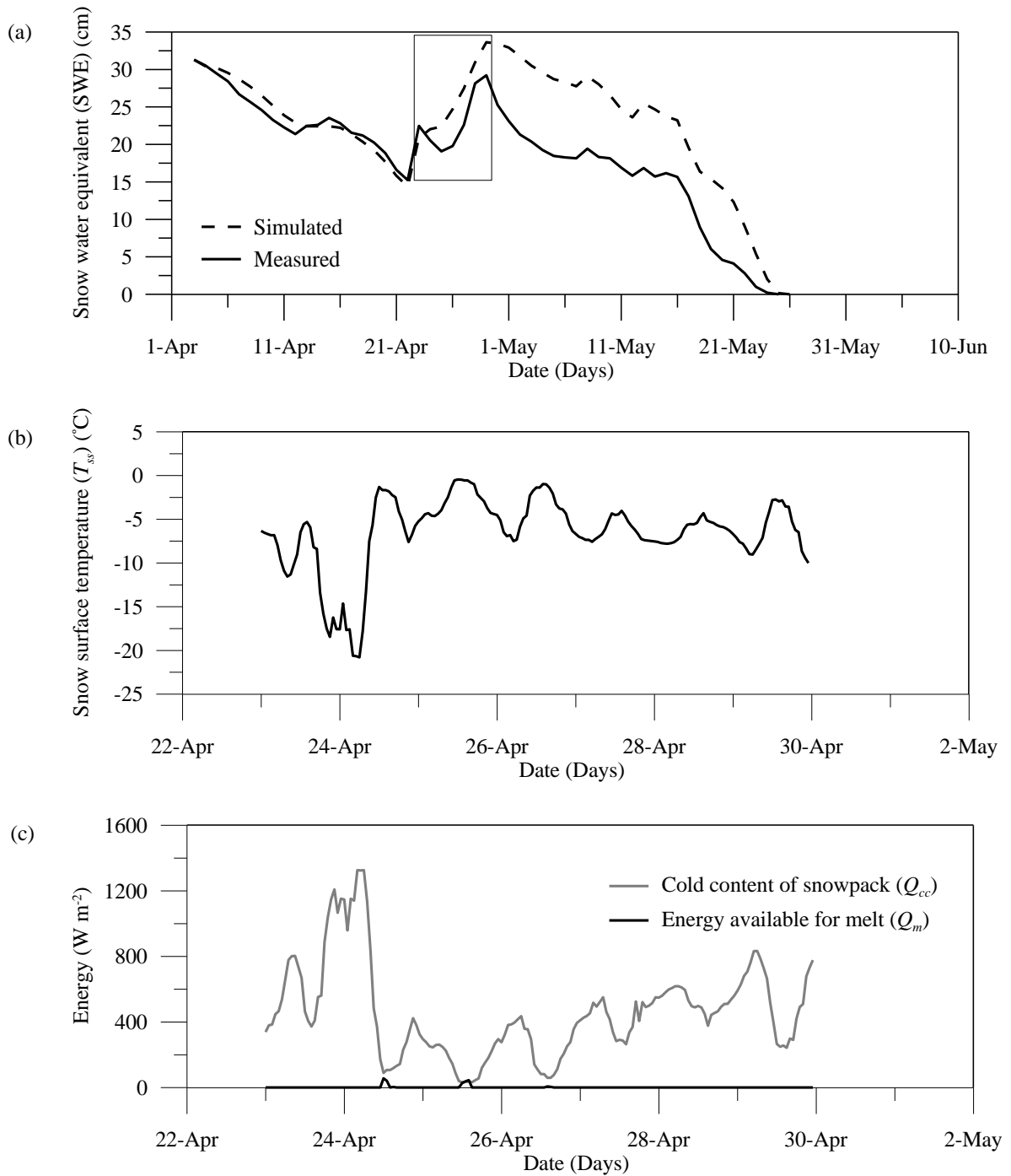
Figure 5.12: Under-simulation of snowmelt during a period of cold snow surface temperatures (T_{ss}),high cold content of the snowpack(Q_{cc}) and low energy available for snowmelt (Q_m): (a) 2009 simulated and measured snow water equivalent (SWE) in the burned stand. Inset represents the Apr 23 – 29 time period. (b) T_{ss} in the burned stand (Apr 23 – 29). (c) Q_{cc} and Q_m in the burned stand (Apr 23 – 29).

Following the two snowfall events in both years, snowmelt was significantly under-simulated. While this could be a result of over-estimating Q_{cc} as described above, it could also be a result of the failure of the model to include snow redistribution processes. Average hourly wind speeds in the burned stand were up to 96% greater than in the healthy stand as a result of the discontinuous forest canopy in the burn. Field observations note significant wind redistribution of snow, resulting in some snow loss by sublimation (Pomeroy *et al.*, 2002). In 2010, wind redistribution was not as significant because snowfall events in 2010 fell onto a warmer snowpack. Cohesion between snow particles is greater with higher T_{ss} (Hosler *et al.*, 1957; Schmidt, 1980); thus, fresh snowfalls would have adhered to the existing snow surface. Also, higher wind thresholds are required to transport warm wet snow (7 to 11 m s^{-1}) than cold dry snow (4 to 11 m s^{-1}) (Li and Pomeroy, 1997). As most snowfall events in 2010 occurred during higher air temperatures, snow transport would have been limited, resulting in reduced wind redistribution in 2010 than in 2009.

The energy balance model simulated the timing of snowpack removal accurately in both forest stands, although snowmelt rates were over-simulated at the end of the melt season. This may be a function of comparing snowmelt measured at a point (SR50A) with snowmelt simulated with radiation data integrated over a much larger area (~3200 m^2; Campbell Scientific (Canada) Corp., 2008). The large footprint of the CNR1 sensor would have incorporated lower albedo values caused by observed spatial heterogeneity in the shallower snow cover at the end of the snowmelt period, with patchy snow cover characterized by large snow free areas around trees and more snow in open areas. While this spatial heterogeneity was greater in the healthy stand, simulated SWE in the burned

stand would be more sensitive to input albedo values given its overall greater Q^*. Thus, although SR50A measurements were representative of the average snowpack in each stand, the spatial variability in snowmelt rates is difficult to extrapolate from a single point, making it difficult to quantify the exact date of snowpack removal. Given that the model simulated the date of complete snowpack removal within one to two days in both stands in both years, I have confidence in the simulated rate and timing of snowmelt in the burned and healthy stands.

In conclusion, sensitivity analyses of modelled Q_m and the comparison of simulated and measured Q^* values highlight the complexity in quantifying K^* and L^* at the snow surface in sub-canopy environments. This study shows that accurate calculation and selection of parameters is fundamental to accurately model Q^*. Although snowmelt is under-simulated following snowfall events as a result of over-simulation of Q_{cc} and/or the failure to include redistribution processes and is over-simulated at the end of the snowmelt period because of the spatial heterogeneity of the shallow snowpack at the end of the melt period, overall the energy balance model accurately modelled snowmelt processes without calibration.

Chapter 6

Wildfire effects on the sub-canopy snowmelt energy balance

A comprehensive field program (described in Chapter 4) was executed to collect meteorological and snow data in a burned and healthy forest stand. The snowmelt energy balance model (also described in Chapter 4) used the collected field data as input. Results from Chapter 5 determined that the model accurately simulates the rate and timing of snowmelt in a burned and healthy forest stand without calibration. Therefore, it can be assumed that the model provides accurate surface energy balance fluxes used to calculate the energy available for melt. This chapter characterizes the snowmelt energy balance in a burned relative to a healthy forest stand in 2009 and 2010. The specific objectives of the chapter are to: 1) compare forest structure, soils, meteorology, snow accumulation, modelled energy balance components, and the rate and timing of snowmelt between the burned and healthy stands; 2) discuss the differences in snow accumulation, the snowmelt energy balance, and the rate and timing of snowmelt between years and between stands; and 3) compare results from this study with results from other forest disturbance-related studies.

6.1 Forest structure and soils

The forest canopy and ground surface represent the boundary conditions for energy fluxes occurring at the top and bottom of the snowpack. Thus it is important to quantify forest structure, forest floor, and soil characteristics in each forest stand.

Both forest stands possess similar topographic characteristics. The healthy (control) and burned stands have similar north facing aspects, are located in close proximity (< 1 km apart), and are within 100 m elevation (1680 and 1775 m, respectively). Based on Alberta Sustainable Resource Development (ASRD) vegetation inventory maps, both stands are located in the subalpine forest region and had similar pre-wildfire structural characteristics. In the fall of 2009, six years after the wildfire, post-wildfire forest structure was characterized using forest structure data collected from both hemispherical photos and fixed-area plots covering 201 and 79 m^2 in the burned and healthy stands, respectively (Table 6.1).

Table 6.1: Summary of forest structure characteristics in each stand

		Burned	Healthy
Tree height (m)	**Average**	8.6	9.9
	Range	1.6-20.3	1.6-28.7
Canopy depth (m)	**Average**	n/a	9.1
	Range	n/a	4.3-11.9
Canopy transmissivity (τ_c)	**Average**	0.82	0.09
Sky view factor (τ_L)	**Average**	0.82	0.18
Tree density (per 100 m^2)		23.4	67.5
Basal area (m^2 ha^{-1})		49.6	127.1
Diameter at breast height (DBH) (cm)	**Average**	13.6	12.5
	Range	2.2 - 43.3	2.6 – 44.1

In both stands, the dominant tree species was subalpine fir (*Abies lasiocarpa*), with a small portion of white spruce (*Picea glauca*) and lodgepole pine (*Pinus contorta var. latifolia*). Average tree height and diameter at breast height (DBH) were similar for both stands, suggesting the approximate age and size of trees is comparable between stands. The range of tree heights was larger in the healthy relative to the burned stand

likely because taller trees experience higher rates of blowdown during high winds observed in the burned stand. Forest canopy depth averaged 9.1 m for the healthy stand. No canopy data were collected for the burned forest stand as it was completely removed during the wildfire and the trees in this stand are primarily burned trunks with no branches. Tree density was approximately three times lower in the burned compared to the healthy stand due to the large number of fallen trees following the wildfire. Forest structure parameters τ_c and τ_L were also significantly higher in the burned relative to the healthy stand (Figure 6.1).
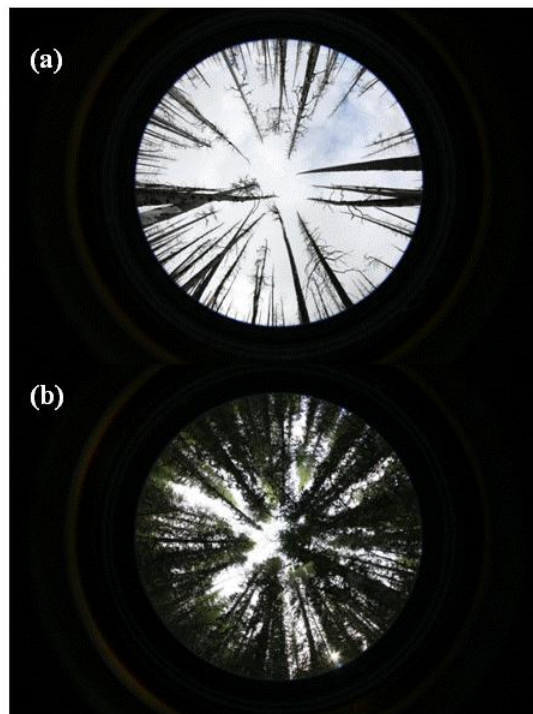
Figure 6.1: Examples of hemispherical photos taken in the each stand: (a) burned and (b) healthy.

Both forest stands had similar topographic and forest structure characteristics, confirming that they would have been classified as the same forest type before the wildfire. Thus, the main current difference between stands can be attributed to lower tree density and forest canopy removal as a result of tree mortality caused by the 2003 Lost Creek wildfire.

Soil texture and type in both stands was a silty clay Brunisol, commonly found below coniferous forests (Agriculture and Agri-Food Canada Soil Classification Working Group, 1998). The healthy stand had a thick litter-humic-fibric (LHF) horizon of up to 14 cm composed of decomposing bryophytes, small herbaceous plants, needles and branches, and a ~10 cm A horizon. The burned forest stand, six years post-wildfire, had very little LHF and a less than 4 cm A horizon, as the wildfire burned all organic matter on the forest floor down to the mineral soil layer (Silins *et al.*, 2009a). The bulk density was higher and the porosity lower in the burned than healthy stand for the A and B soil horizons.

6.2 Meteorology

Trends in daily average T_a, T_{ss}, and u were similar between stands in both years, suggesting that both stands responded similarly to large scale weather conditions (Figure 6.2). However, average daily T_a, T_{ss}, and u were observed to be more episodic during the snowmelt period in 2009 than 2010.
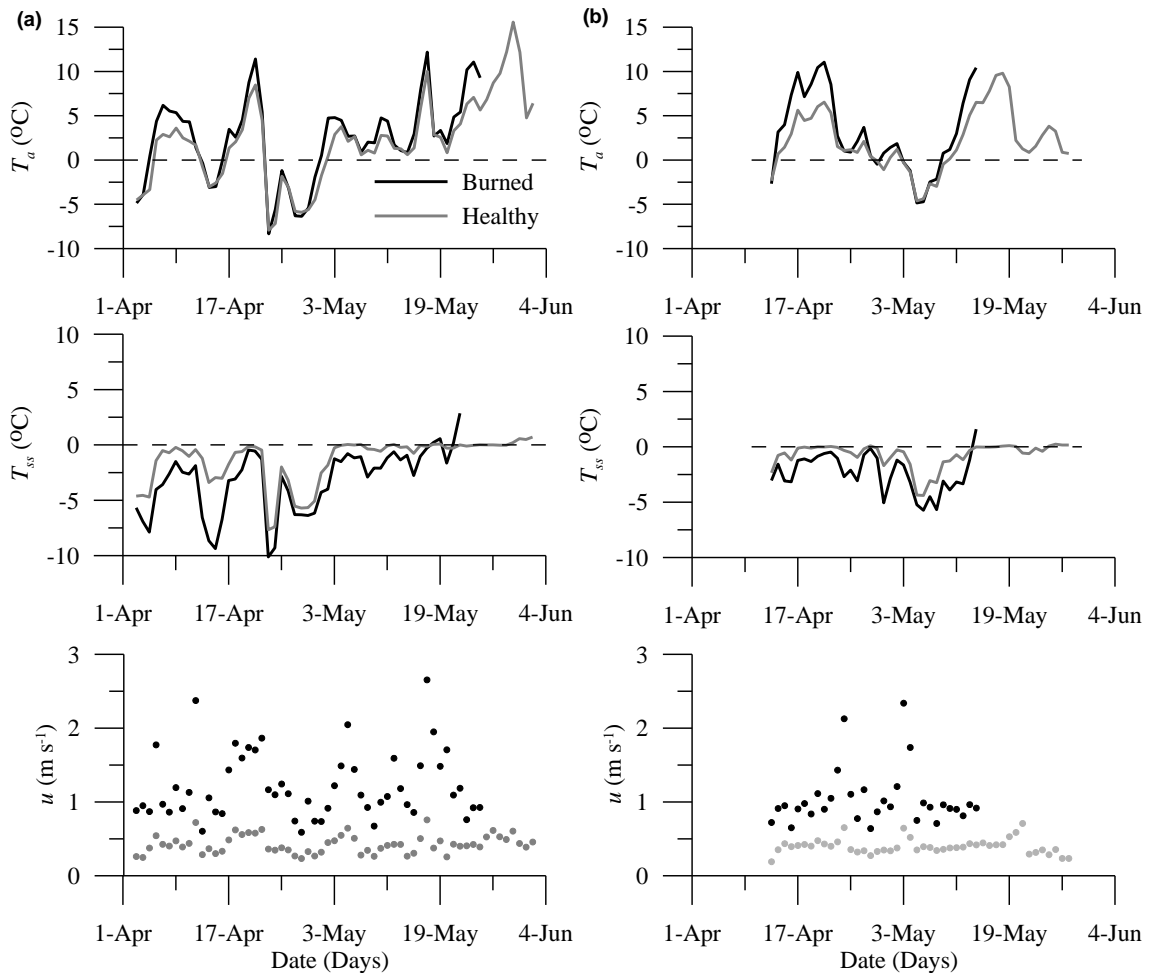
Figure 6.2: Daily average air temperature (T_a), snow surface temperature (T_{ss}), and wind speed (u) in each stand: (a) 2009 and (b) 2010.

Average hourly air temperature (T_a) was comparable between stands in 2009, but was slightly higher in the burned than in the healthy stand in 2010 (Table 6.2). Minimum hourly T_a was lower in 2009 than in 2010 in both stands. Average hourly T_{ss} was lower in the burned than in the healthy forest stand in both years, and minimum snow surface temperature (T_{ss}) was lower in 2009 than in 2010 in both stands. Average hourly wind speed (u) in each stand was similar in both years, but was more variable and of higher magnitude in the burned than in the healthy stand. The range of hourly above-canopy short-wave radiation ($K\downarrow$) was slightly greater in 2010 in both stands. In the healthy

stand, average hourly $K\downarrow$ was slightly greater in both years due to the longer snowmelt period. Average hourly relative humidity (*RH*) and vapour pressure (e_a) did not vary significantly between years; however, values of both were measured to be higher in the healthy stand. Maximum and minimum hourly e_a were similar between years and stands. In both stands, average hourly soil temperature (T_s) was ~0°C in both years (Table 6.2). Average hourly soil volumetric water content (VWC) was higher in 2010 than in 2009 in both stands, and average hourly VWC was overall greater in the healthy than in the burned stand.

Table 6.2: Average and range of hourly meteorological conditions in both stands (2009 burned and healthy snowmelt period: Apr 3 – May 25; Apr 3 – Jun 2, and 2010 burned and healthy snowmelt period: Apr 13 – May 14; Apr 13 – May 28).

		Burned		**Healthy**	
		2009	**2010**	**2009**	**2010**
T_a (°C)	**Average**	2.3	3.0	2.1	2.2
	Range	-13.2 – 16.1	-7.7 – 16.7	-13.9 – 21.6	-7.1 – 18.5
T_{ss} (°C)	**Average**	-2.6	-2.4	-1.3	-0.7
	Range	-20.8 – 6.9*	-13.7 – 6.8*	-13.4 – 1.6	-7.0 – 0.4
u (m s^{-1})	**Average**	1.2	1.0	0.4	0.4
	Range	0.1 – 3.9	0.2 – 3.9	0.1 – 1.2	0.1 – 1.1
Above canopy $K\downarrow$ (W m^{-2})	**Average**	195.7	199.6	207.0	200.4
	Range	0.0 – 1015.9	0.0 – 1091.5	0.0 – 1080.5	0.0 – 1091.5
RH (%)	**Average**	61.8	63.1	72.3	77.1
	Range	17.6 – 100.0	17.5 – 100.0	19.5 – 100.0	25.6 – 100.0
e_a (kPa)	**Average**	0.41	0.42	0.48	0.51
	Range	0.1 – 0.6	0.1 – 0.6	0.1 – 0.6	0.2-0.6
T_s (°C)	**Average**	0.1	0.3	0.2	0.3
	Range	-0.4 – 5.2	0.0 – 0.6	-0.2 – 5.3	0.0 – 2.1
VWC (%)	**Average**	16.0	32.2	34.7	42.9
	Range	9.4 – 26.3	26.5 – 59.7	16.4 – 44.3	34.4 – 50.6

*NOTE: * = high measurements of average hourly snow surface temperature (T_{ss}) occurred at the end of the snowmelt period when the ground surface was observed to be partially exposed.*

6.3 Snow accumulation

2009 was an average snow year, with peak snow water equivalent (SWE) at South Racehorse Creek (1920 m elevation) at 94% of normal conditions (Alberta Environment, 2009). Within the research stands, large snowfall events occurred in late-November through early January, with no subsequent events observed until early March. Peak SWE was observed on April 3, based on the continuous snow depth record from the SR50A and density measurements collected during the snow surveys.

2010 was a below average snow year, with peak SWE at South Racehorse Creek at 86% of normal conditions (Alberta Environment, 2010). The snow accumulation period was characterized by smaller snowfall events that began in early October and continued through mid-January. Similar to 2009, very little new snow accumulated from mid-January through mid-March, but a large snowfall event was observed at the end of March. Peak SWE (calculated from the SR50A data and snow density measurements) was observed on April 13, approximately 10 days later than in 2009.

Peak SWE comparisons between years and between stands were also completed using SWE data collected during snow surveys on April 1, 2009 and March 31, 2010. While these datasets were normally distributed, some comparisons had unequal variances. As the difference in variances is small, two tailed t-tests conducted for both equal and unequal variances yielded similar p-values. Notched box plots and two tailed t-tests showed significant differences in peak SWE both between years and between stands ($p < 0.001$) (Figure 6.3).
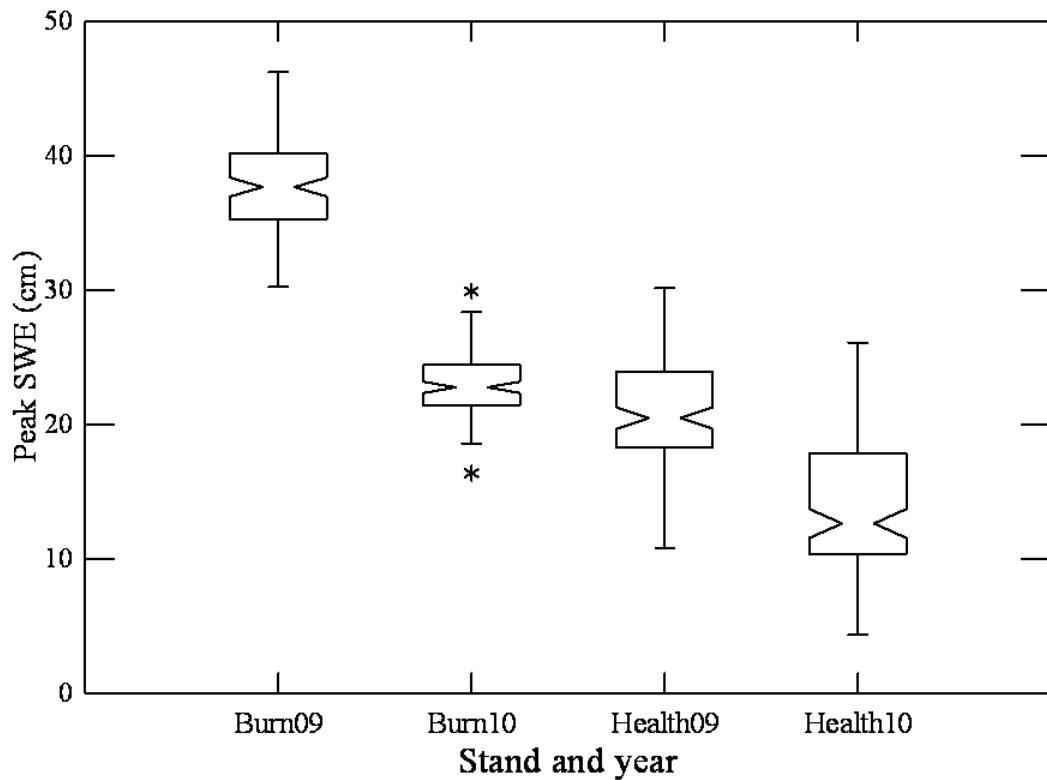
Figure 6.3: Notched box plots of peak SWE from annual snow survey data (April 1, 2009; March 31, 2010). Data were derived from average snow density ($n = 36$) and individual snow depth measurements ($n = 121$) in each stand. The box denotes the 25th and 75th percentile of the data (inter-quartile range; IQR), the notch represents the median, the bars show non-outlier maximum and minimum values, and the asterisks indicate outliers. Outliers are defined as > 1.5 times the IQR.

Maximum measured SWE was 49 and 41% higher in 2009 than in 2010 in the burned and healthy stands, respectively. Maximum observed SWE was 58 and 50% greater in the burned than in the healthy stand in 2009 and 2010, respectively. As snow surveys were designed to detect > 30% differences in SWE between stands, the observed differences were greater than the sampling error.

6.4 Modelled snowmelt

6.4.1 Total energy available for snowmelt and cold content

Total energy available for snowmelt (Q_m) became positive in both stands approximately 1-2 days after peak SWE (April 3, 2009; April 13, 2010), in both years. The snowmelt period was longer in 2009 than in 2010, requiring 20% more energy to melt the snowpack in both stands. Average hourly Q_m in the burned and healthy stands followed a similar trend; however, the magnitude of Q_m was lower in the healthy stand (Figure 6.4).
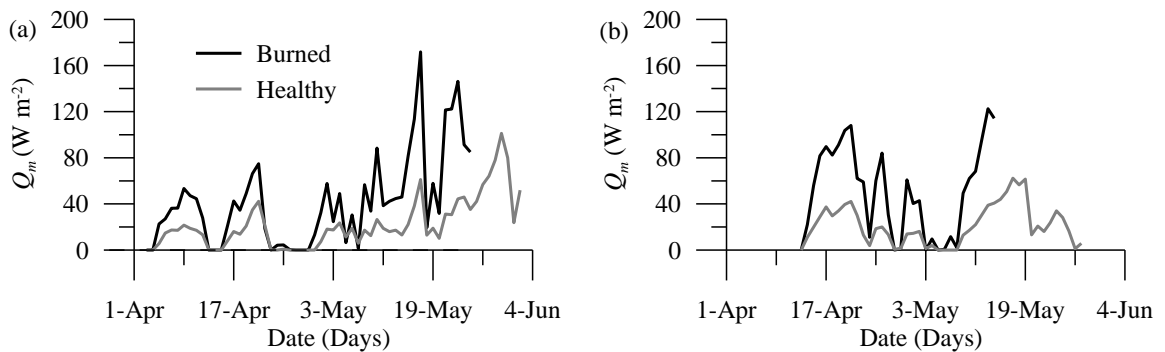
Figure 6.4: Daily average energy available for snowmelt (Q_m) in each stand from snowmelt energy balance model calculations: (a) 2009 and (b) 2010.

Average daily T_a was < 0°C more frequently and T_{ss} was lower at the onset of snowmelt in 2009 relative to 2010 (Figure 6.2), resulting in a greater cold content of the snowpack (Q_{cc}) in 2009. Thus, more energy was required to raise the average daily snowpack temperature (T_{sd}) to the melting point in each stand (Figure 6.5). At the onset of snowmelt in 2010, higher average daily T_a and T_{ss} in both stands (Figure 6.2) resulted in the majority of Q_m contributing to snowmelt.
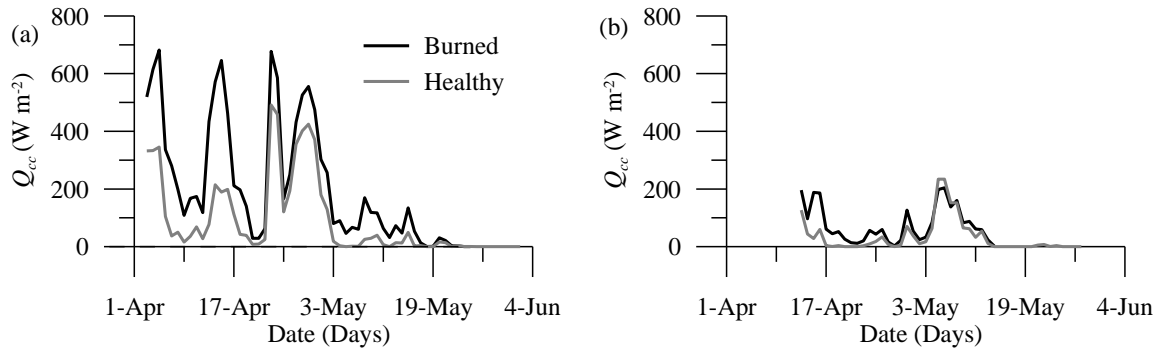
Figure 6.5: Daily average cold content of the snowpack (Q_{cc}) in each stand: (a) 2009 and (b) 2010.

6.4.2 Energy balance fluxes

Differences in forest structure (Table 6.1) and associated micrometeorological conditions (Table 6.2) between stands resulted in approximately 30% more energy available for melt, and energy balance fluxes of a greater magnitude, in the burned than in the healthy stand in both years (Figure 6.6).
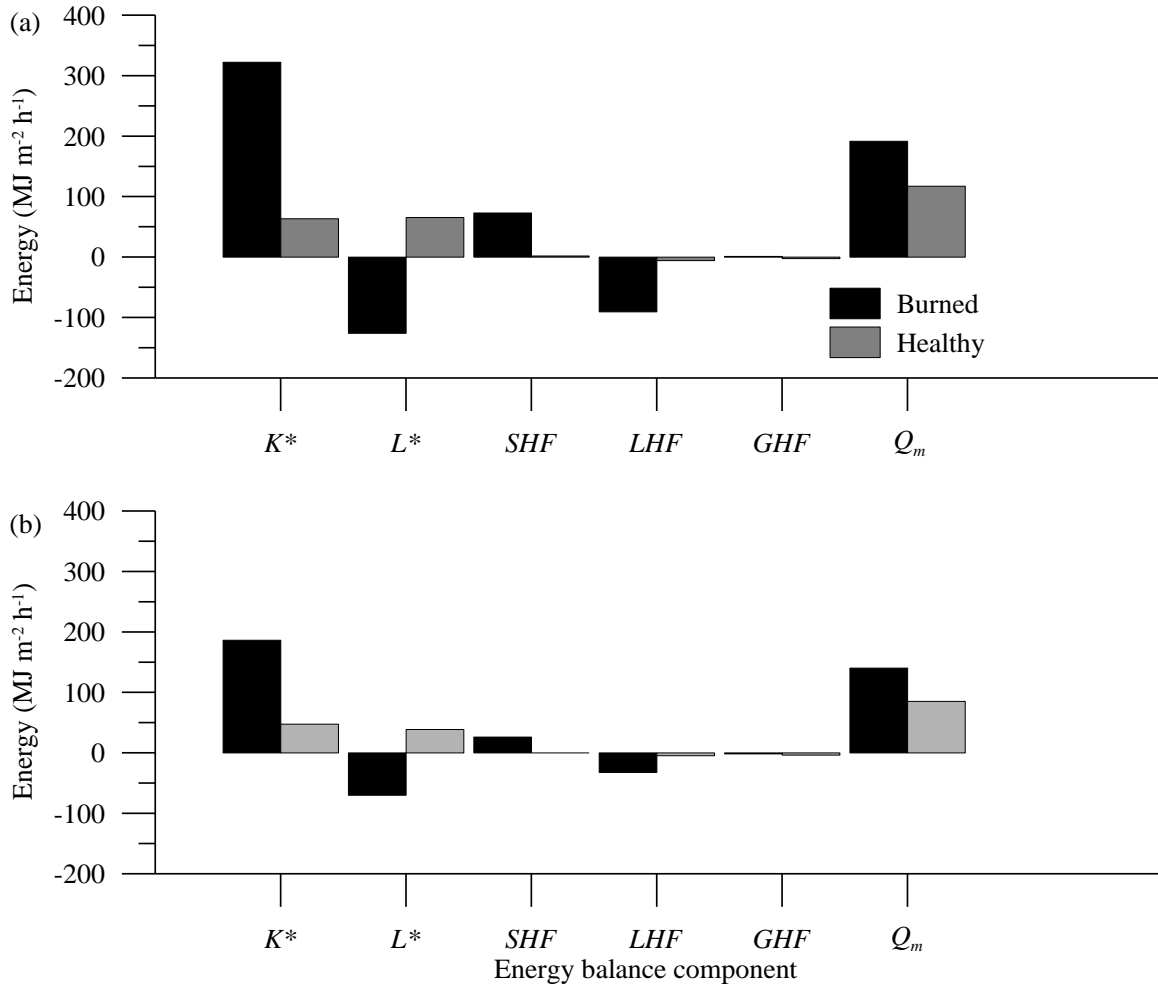
Figure 6.6: Total energy balance fluxes (2009 and 2010 snowmelt periods: Burned: Apr 3 – May 25; Apr 13 – May 28, Healthy: Apr 3 – Jun 2; Apr 13 – May 28) (in MJ m^{-2} h^{-1}) in each stand for each component of the calculated energy balance: (a) 2009 and (b) 2010.

Snowmelt was largely driven by net short-wave radiation (K^*) and sensible heat flux (SHF) in the burned stand, and a combination of K^* and net long-wave radiation (L^*) in the healthy stand. Contributions of individual energy balance components to snowmelt were similar between 2009 and 2010 in both stands (Figure 6.7 and 6.8).
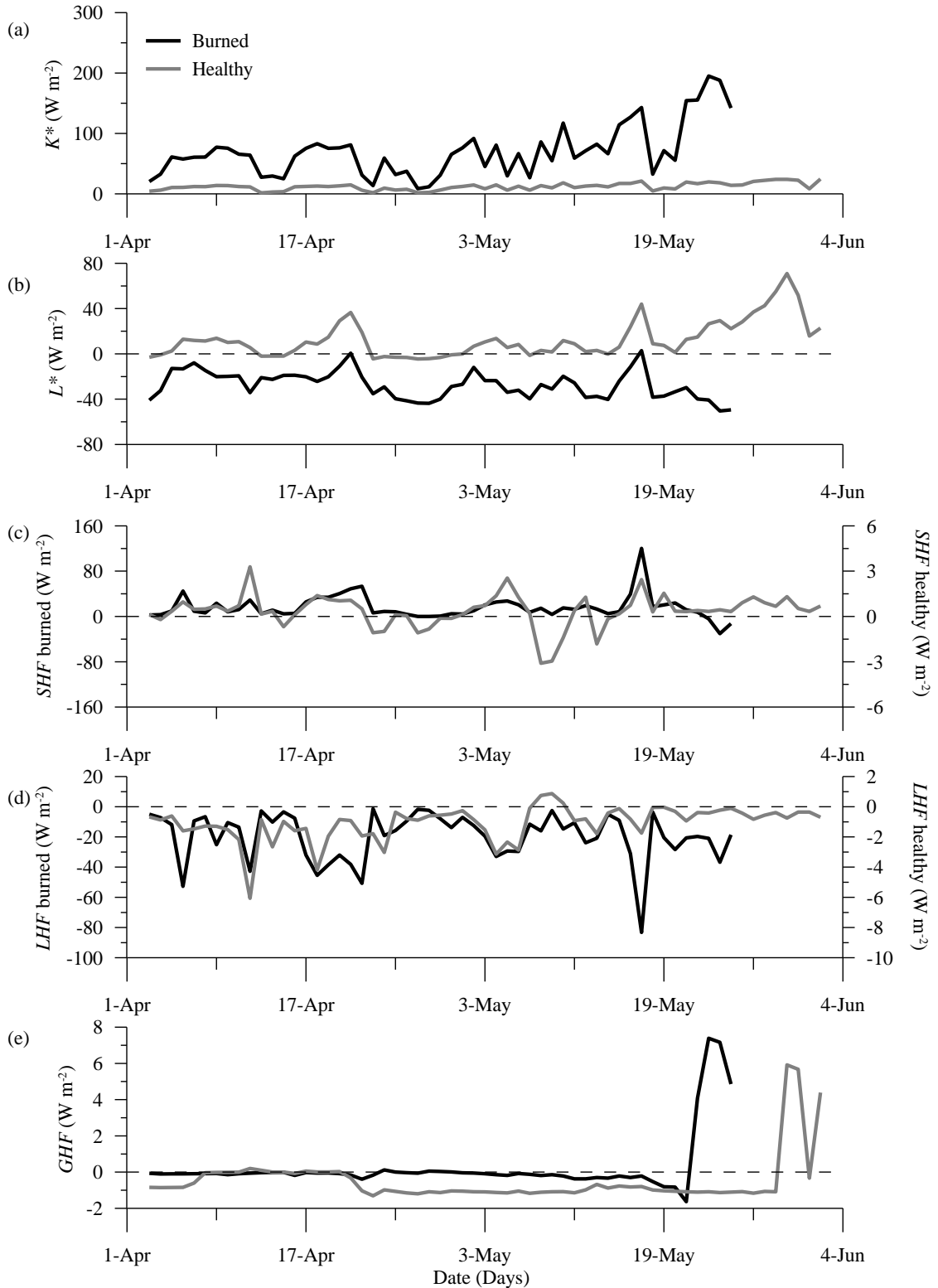
Figure 6.7: Daily average simulated fluxes of: (a) net short-wave radiation (K^*), (b) net long-wave radiation (L^*), (c) sensible heat (SHF), (d) latent heat (LHF), and (e) ground heat (GHF) during the 2009 snowmelt period in the burned (Apr 3 – May 25) and healthy stand (Apr 3 – Jun 2).
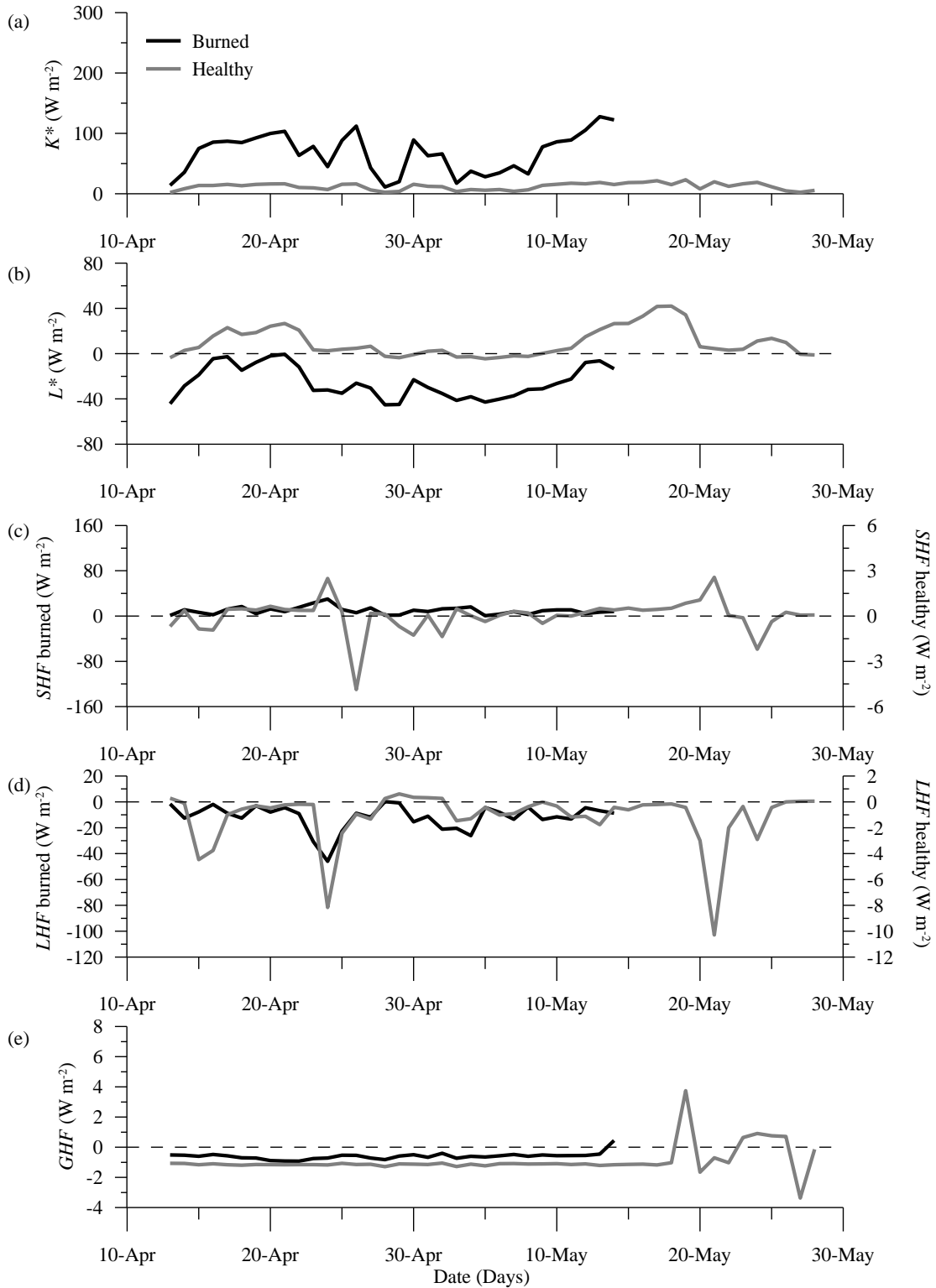
Figure 6.8: Daily average simulated fluxes of: (a) net short-wave radiation (K^*), (b) net long-wave radiation (L^*), (c) sensible heat (SHF), (d) latent heat (LHF), and (e) ground heat (GHF) during the 2010 snowmelt period in the burned (Apr 13 – May 14) and healthy stand (Apr 13 – May 28).

93

Daily average K^* at the onset of snowmelt was slightly lower in 2009 than in 2010. This could be a combination of: (1) cloudier conditions that resulted in lower $K\downarrow$ above the forest canopy in 2009, as observed in the average hourly $K\downarrow$; and (2) daily average snow surface albedo (α) being ~18 and 14% higher in 2009 than in 2010 in the burned and healthy forest stands, respectively (Figure 6.9).
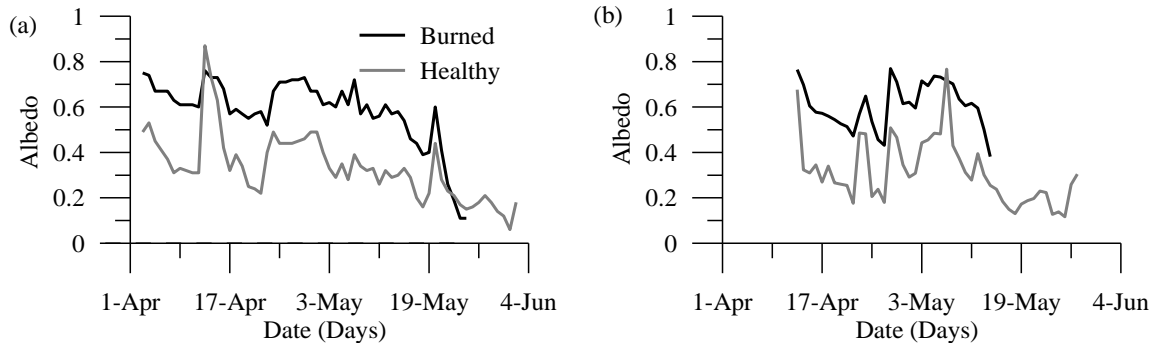
Figure 6.9: Measured albedo (α) in each stand: (a) 2009 and (b) 2010.

Total L^* in the burned stand was 35% lower in 2009, and in the healthy stand was 31% higher in 2009 relative to 2010. Although the trend of L^* was similar between stands, overall it was 211% more negative in the burned relative to the healthy stand.

Daily average SHF in each stand was less positive and average daily latent heat flux (LHF) less negative in 2010 than in 2009 (Figures 6.7 and 6.8). Although hourly average u and hourly average gradients of air temperature and vapour pressure between the snow surface and overlying air were comparable between years in each stand (Table 6.2), daily average T_a, T_{ss}, and u were less episodic during the snowmelt period in 2010 relative to 2009 (Figure 6.2). Episodes of greater u were observed more frequently resulting in more enhanced turbulent heat transfers in 2009 than in 2010. Overall, turbulent heat fluxes were up to two orders of magnitude lower in the healthy than in the

94

burned stand. In the burned stand, total *LHF* was 150% more negative and total *SHF* was 191% more positive than in the healthy stand in both years.

Ground heat flux (*GHF*) was small and did not significantly contribute to the total energy available for snowmelt in either stand in either year (Figure 6.4). *GHF* values were slightly more positive in 2009 than in 2010 in both stands, due to greater hourly maximum T_s and lower volumetric water content (VWC) (Table 6.2).

6.5 Rate and timing of snowmelt

The 2009 snowmelt period lasted approximately two months, with complete snowpack removal observed at the end of May. The 2010 snowmelt period began approximately ten days later than in 2009, and was 21 and 15 days shorter than the 2009 melt period in the burned and healthy stands, respectively (Table 6.3). The trends of both snowmelt periods were similar to the record from the South Racehorse Creek snow pillow. Greater Q_m in the burned than in the healthy stand resulted in a shorter snowmelt period in the burned stand in both years. Average snowmelt rates were slightly greater in 2010 than in 2009 in the burned stand, but were more comparable between years in the healthy stand. The ratio of snowmelt in the healthy relative to that in the burned stand was slightly higher in 2010 (0.45) than in 2009 (0.44).

Table 6.3: Summary of snowmelt timing, duration, and rate for 2009 and 2010 in each stand.

	Burned		Healthy	
	2009	**2010**	**2009**	**2010**
Measured start of snowmelt (date)	Apr 3	Apr 13	Apr 3	Apr 13
Simulated snow removal (date)	May 25	May 14	Jun 2	May 28
Simulated snowmelt duration (days)	52	31	61	46
Average snowmelt rate during snowmelt period (cm d^{-1})	1.28	1.54	0.56	0.70

Notched box plots and two tailed t-tests identified significant differences in snowmelt rates between stands in both years ($p < 0.001$). Although average hourly snowmelt rates in the burned stand were greater in 2010 than in 2009, the difference was not statistically significant ($p = 0.371$). No significant difference was observed between years in the healthy stand ($p = 0.885$) (Figure 6.10). In the burned stand, non-outlier maximum melt rates were greater in 2010; however, more outlier values were observed in 2009.
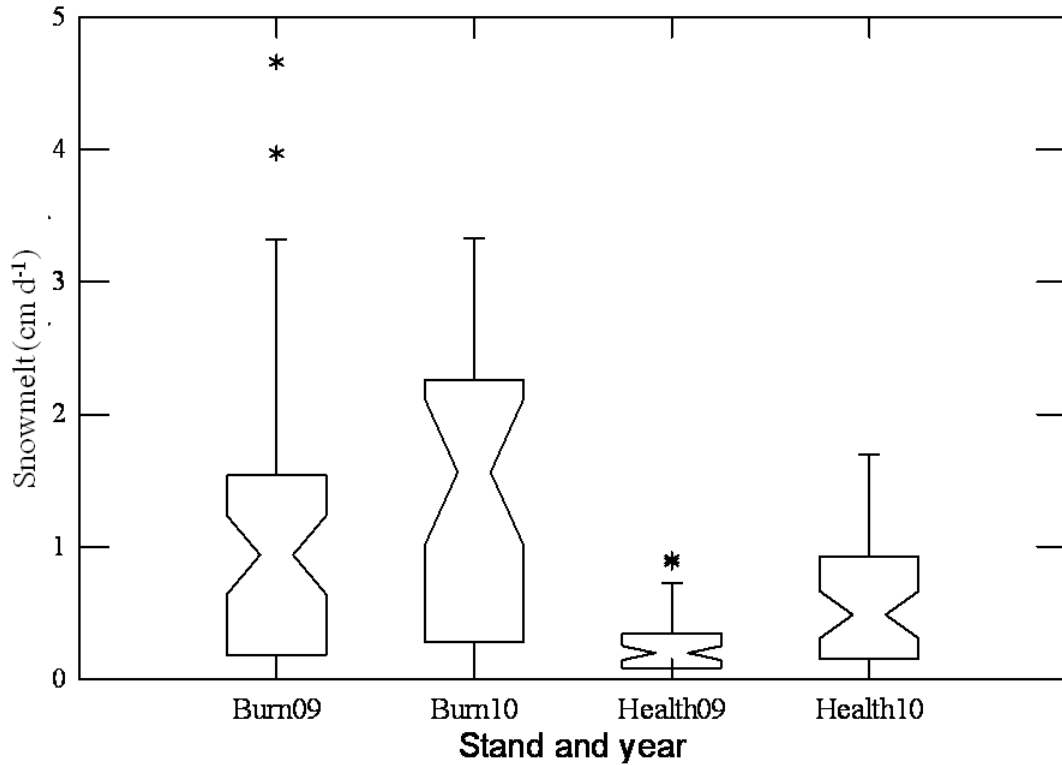
Figure 6.10: Notched box plots of daily snowmelt rate (cm d^{-1}) based on simulated values in each stand in each year. Note that the snowmelt period varied between stands and years. Values are based on daily simulated snowmelt rates from the energy balance model (n = simulated snowmelt duration in days; Table 6.3). The box denotes the 25th and 75th percentile of the data (inter-quartile range; IQR), the notch represents the median, the bars show non-outlier maximum and minimum values, and the asterisks indicate outliers. Outliers are defined as values > 1.5 times the IQR.

6.6 Discussion

6.6.1 Differences between years

Snow accumulation, the snowmelt energy balance, and snowmelt rates vary with seasonal snow and meteorological conditions. This research allowed for the comparison of snow processes in both average (2009) and below average (2010) snow years. Since peak SWE was greater and the snowmelt period was 21 and 15 days longer in 2009 than in 2010, more energy was required to melt the snowpack. Thus, more total energy from all components of the energy balance was required during the 2009 snowmelt period. However, notable differences in the trends of individual energy fluxes between years were affected by seasonal meteorological conditions.

In 2009, at the onset of snowmelt, T_a and T_{ss} were relatively low resulting in a greater Q_{cc} than in 2010. Thus, more energy was required to warm the snowpack to the melting point, leaving less energy to contribute to snowpack melting. In 2010, Q_{cc} was significantly lower throughout the snowmelt period; thus, Q_m was greater at the onset of snowmelt than in 2009. This was largely driven by annual meteorological conditions, including more frequent cloud free conditions, lower α, higher T_a and T_{ss}, and more constant u in 2010 than in 2009. These conditions resulted in higher Q^* and reduced turbulent heat fluxes in 2010 than in 2009.

Despite the variability in meteorological conditions, both stands behaved similarly in terms of the relative contribution of each energy balance component to the total energy available for snowmelt. Additionally, snowmelt rates were not significantly different between 2009 and 2010 in both forest stands. This suggests that, regardless of annual meteorological and snow conditions, the two stands maintained their differences in the

amount of energy available for snowmelt and the rate of snowmelt between years. Since greater differences were observed between forest stands than between years during this two year study, the remainder of the chapter focuses on differences between stands.

6.6.2 Differences between stands

Given the close proximity of the two study stands, they are exposed to very similar weather conditions and receive the same total precipitation. Thus, the higher peak SWE in the burned than in the healthy stand in both years is directly related to forest canopy differences. Lower snow accumulation in the healthy stand is likely due to snow being intercepted by the healthy forest canopy and subsequently sublimated from the canopy surface. The greater maximum observed SWE (58 and 50%) in the burned than the healthy stand suggests that in both years, approximately half the total snowfall was sublimated from the healthy forest canopy. This is consistent with studies indicating that up to 45% of annual snowfall in western Canada is sublimated from the canopy (Pomeroy *et al.*, 1998). While snow surface sublimation and wind redistribution in the burned stand did not completely offset the greater accumulation due to reduced interception, greater wind speeds as well as reduced stem and canopy density in the burned stand suggest that sublimation and wind re-distribution likely play a role in snow accumulation differences between stands. Model results also indicate the significance of these processes during the 2009 snowmelt period (Chapter 5), suggesting that they be considered in future studies.

The largest contributor to Q_m was K^* in both stands. In the burned stand, the lack of forest canopy and lower tree density resulted in more $K\downarrow$ reaching the snow surface (higher τ_c). Snow surface albedo (α) was lower on average in the healthy stand, likely

because field observations during snow surveys noted more litter accumulated on the snow surface in the healthy than in the burned stand. Consequently, lower $K\downarrow$ being transmitted through the canopy in the healthy stand meant α played a minimal role in $K*$. More $K\downarrow$ was absorbed by the forest canopy (lower τ_L) in the healthy stand, resulting in greater $L\downarrow$ emission from the forest canopy and tree trunks onto the snow surface, contributing to melt. In the burned stand, however, $L\uparrow$ from the snow surface was not compensated by $L\downarrow$ from the forest canopy (higher τ_L) given the burn severity and substantial forest canopy loss. The resulting negligible $L\downarrow$ values and higher $L\uparrow$ led to overall negative $L*$.

Pomeroy *et al*. (2009) highlighted the importance of evaluating the emission of $L\downarrow$ by standing dead trees impacted by wildfire and mountain pine beetle (MPB) and its importance in the snowmelt energy balance. Although forest canopy and tree trunk temperature (T_c and T_t) were not directly measured to quantify the absolute contribution of $L\downarrow$ from burned trees, model output suggests that $L\downarrow$ did not contribute significantly to Q_m in the burned stand. However, in both years, when T_a was $> 10^{\circ}$C, increased $L\downarrow$ was observed and $L*$ approached 0 W m^{-2}. Field observations during snow surveys also noted snow-free areas observed around blackened trees were larger than those around burned trees that had shed their bark and become a silver-grey colour. The lower α of the blackened trees relative to the silver-grey coloured stems would likely absorb more $K\downarrow$, resulting in higher T_c and T_t and subsequently higher $L\downarrow$ to the snow surface. This suggests that $L\downarrow$ from burned trees could offset $L\uparrow$ from the snowpack in years with high $K\downarrow$ and/or T_a, reducing energy loss from the pack. However, additional field data collection is required to validate this hypothesis.

L* contributions to snowmelt may also change significantly over the years post-wildfire. Forest mensuration completed in the summer of 2009 noted significant blowdown in the burned stand. Field observations in 2010 indicate that additional blowdown occurred since measurements were completed in 2009. Thus, the simulation of *Q** in 2010 may be missing key forest structural changes between years that would assist in the interpretation of *L** data and forest structure impacts on *Q** over time. In future studies, forest mensuration should be completed after each snow season to assess potential changes in forest structure and subsequent changes to *Q**.

The removal of the forest canopy and blowdown of dead trees reduced land surface roughness resulting in higher wind speeds in the burned relative to the healthy stand. This enhanced *SHF* and *LHF*, increasing their role in the snowmelt energy balance. Greater temperature gradients between the snow surface and overlying air, as well as greater *u* (Table 6.2) were measured in the burned than in the healthy stand and resulted in more significant turbulent fluxes. In years with higher intensity *u*, greater turbulent heat transfer would be expected from burned than in healthy stands. Although differences in peak SWE between stands suggest that more intercepted snow was sublimated from the healthy than the burned forest canopy. Enhanced *LHF* in the burned stand suggests that there was more sublimation from the snow surface during the snowmelt period in the burned than in the healthy stand.

While *GHF* did not significantly contribute to Q_m in either forest stand, it was greater in the burned stand due to higher bulk density, lower hourly average VWC, and higher hourly maximum T_s than in the healthy stand. Because the forest floor in the burned stand was burned to the mineral soil, the LHF, A, and B horizons were completely

removed. Even six years post-wildfire, very little new soil had developed, resulting in a higher soil bulk density and lower porosity in the burned than the healthy stand. The lower VWC measured in the burned than the healthy forest stand was likely a result of the lower soil porosity. Also, higher soil temperature in the burned than the healthy stand could be a function of the lower VWC in the burned stand: air has a lower heat capacity than water, thus less energy is required to increase the temperature of a dry versus a wet soil.

Changes in forest structure resulted in higher snow accumulation and more energy available for snowmelt in the burned than in the healthy stand in both years, resulting in significantly higher melt rates in the burned stand. These greater melt rates resulted in complete snowpack removal nine and fifteen days sooner in the burned than in the healthy forest stand in 2009 and 2010, respectively.

6.6.3 Implications for disturbance research

Inter-annual hydro-climatic variability plays a significant role in snow accumulation and melt; therefore, it is difficult to make comparisons with other studies conducted under different geographic, snow, and meteorological conditions. However, comparing the ratio of snow accumulation and melt between controls (clearings or healthy stands) to different disturbance types reduces the influence of year and geographic location (Winkler and Boon, 2009). Most studies compare ratios of forest (disturbed or healthy) to clearings, making it difficult to compare results of this research to the literature. Where ratios of healthy to disturbed forests were not available, either the range or the absolute percent difference was used to make comparisons between studies.

The ratio of peak SWE in healthy versus burned forest stands (0.55 and 0.60) compares well with the lower range of healthy versus cleared forest stands (0.60 -1.0) (Golding and Swanson, 1986; Toews and Gluns, 1986; Faria *et al.*, 2000). Because wildfire completely removes the forest canopy, snowmelt rates are higher than those in mountain pine beetle-killed stands, and are closer to those reported for cleared forest areas. Comparison of the ratio of snowmelt rates in the healthy to the burned stand (0.44 and 0.45) indicates that the burned stand has significantly higher values than those reported for healthy to MPB-killed grey attack stands (0.85 - 0.83) (Boon, 2009). Melt rates in the burned stand (1.28 and 1.54 cm d^{-1}) were higher than the range of melt rates for MPB-grey attack (0.21 to 0.97 cm d^{-1}), where over half of the foliage has been lost and for green/red attack to grey attack (0.25 to 0.85 cm d^{-1}), where the majority of foliage is intact (Winkler and Boon, 2009). Interestingly, the absolute difference in snowmelt rates were 46 and 44% lower in the healthy relative to the burned stand, which are comparable to the lower range of studies that found snowmelt to be 30-300% lower in healthy than in cleared stands (Pomeroy and Granger, 1997; Winkler *et al.*, 2005; López-Moreno and Stähli, 2008).

The dominant energy balance component contributing to snowmelt in the healthy stand was Q^*, similar to studies in boreal forests (Price and Dunne, 1976; Link and Marks, 1999). As in beetle-killed and cleared stands, wildfire disturbance resulted in negative L^*, as $L\uparrow$ from the snow surface was not compensated by $L\downarrow$ from the forest canopy (Boon, 2009); therefore, the dominant energy balance component contributing to snowmelt in the burned stand was K^*. Results are similar to those from other studies in mature forest environments, which found that turbulent heat transfers played a very small

role in the snowmelt energy balance of healthy forest stands and a larger role in the snowmelt energy balance of disturbed forest stands (Koivusalo and Kokkonen, 2002; Boon, 2009).

Approximately 30% more Q_m was simulated in the burned relative to the healthy stand in both years. Link and Marks (1999) concluded that in boreal forests, land use changes may have larger impacts than climate shifts on seasonal snowpacks given the significant impact of forest canopies on Q^*. This study also suggests that forest canopy removal increased the amount of energy available for snowmelt in burned forests, particularly increasing K^* and turbulent heat transfers. In the burned stand, greater hourly average T_a and T_{ss} at the onset of snowmelt and smaller SWE resulted in higher average snowmelt rates, with complete snowpack removal occurring twelve days earlier in 2010 than in 2009. In the healthy stand, greater hourly average T_a and T_{ss} was also measured at the onset of snowmelt and the snowpack was shallower in 2010 than in 2009; however, average snowmelt rates were more comparable in both years and complete snowpack removal in 2010 occurred within five days of 2009. Results between 2010 and 2009 suggest that the burned stand was more sensitive to interannual variability in meteorological and snow conditions than in the healthy stand. Therefore, it may also be more sensitive to predicted increases in air temperature and reductions in snowfall under climate change; however, additional research is required to incorporate a larger range of hydro-climatic variability and confirm this hypothesis.

In conclusion, this study provides insights into the effect of the forest canopy and forest disturbance on snow accumulation and melt. In the burned stand, more snow accumulated on the ground surface, there was more energy available for snowmelt, the

snow melted more rapidly, and complete snowpack removal occurred sooner than in the healthy stand. Although results are comparable to cleared forest stands, standing dead trees in burned forest stands will continue to attenuate incoming short-wave radiation, wind speed, temperature, and snow accumulation on the surface. Thus, burned forest stands should be considered a separate land cover type in larger scale watershed models.

Chapter 7

Conclusion

Given predicted climate change, Canadian forests will experience an increase in
forest area burned, and in wildfire duration and severity (Westerling *et al.*, 2003;
Flannigan *et al.*, 2005). Although research quantifying wildfire effects on the forest
canopy and its subsequent impacts on snow accumulation have had some mention in the
literature (Farnes, 1996; Silins *et al.*, 2009b), the rate and timing of snowmelt and the
snowmelt energy balance in burned forests are poorly understood. Research has shown
that disturbed forests have higher snow accumulation and more rapid snowmelt than
mature, healthy forests (Koivusalo and Kokkonen, 2002; Gelfan *et al.*, 2004; Winkler and
Boon, 2009). Therefore, understanding snow processes in wildfire disturbed watersheds
is important for managing water supplies in disturbance-susceptible regions. The purpose
of this thesis was to quantify snow accumulation, snow surface energy balance, and the
timing and magnitude of seasonal snowmelt in a burned relative to healthy forest stand
during two snow seasons. Chapter 1 outlined the specific objectives for this research:

1) Design a field program to collect snow and meteorological data in the stands of
   interest;

2) Develop a snowmelt model to simulate the energy balance over a melting sub-
   canopy snow surface;

3) Run the model using collected field data as input, assess potential model
   uncertainties using sensitivity analyses and validate model output; and

4) Use model output to characterize the snowmelt energy balance in a burned compared to a healthy forest stand.

The two forest stands selected for this research were representative of a larger, relatively homogeneous forest region in the sub-alpine forest of the Crowsnest Pass, southwestern Alberta. Forest mensuration and hemispherical photos were used to quantify differences in forest structure between stands. Before the 2003 Lost Creek wildfire, the two forest stands had similar topographic and forest structure characteristics. After the fire, therefore, the main differences between stands were lower tree density and forest canopy removal in the burned stand. High resolution meteorological data indicated that the two stands reacted similarly to large-scale weather conditions.

A field program was designed to collect meteorological and snow data during the snow accumulation and melt periods. Snow survey data were collected using a combination of snow tube samples, bulk sampling, and snow pits. Measured meteorological variables included: air temperature, relative humidity, wind direction and speed, atmospheric pressure, incoming and reflected short-wave radiation, incoming and outgoing long-wave radiation, net radiation, snow surface albedo, snow surface temperature, internal snowpack temperature, snow depth, soil heat flux at a fixed depth, soil moisture content, and soil temperature. Snowmelt lysimeters (e.g. Storck *et al*., 2002; Winkler *et al*., 2005) were also installed in 2009 to measure melt water outflow from the snowpack; however, their success was compromised by antecedent soil moisture conditions and event logger and/or tipping bucket failure.

Meteorological data were used as input to a simple, process-based snowmelt model (e.g., Spittlehouse and Winkler, 2002; Boon, 2009) and snow data were used to

validate model output. The snowmelt model was based on the basic energy balance equation and was designed to simulate sub-canopy snowmelt at a point. The model was parameterized using forest and snow measurements as well as values from the literature and validated with measured snow water equivalent derived from the continuous snow depth record and density measurements from snow surveys.

Model output of energy available for snowmelt was relatively insensitive to values that remain constant throughout the modelling period (parameters) such as snow surface roughness, as well as input data (variables) of tree trunk temperature. However, model output was very sensitive to certain parameters including canopy transmissivity, sky view factor, emissivity of the snow surface and canopy, the hemispherical long-wave radiation flux emitted from tree trunks, and the canopy temperature variable. This highlighted the complexity of calculating net short- and long-wave radiation at the snow surface in sub-canopy environments.

While the model accurately simulated net radiation in the burned stand, net radiation measurements in the healthy stand were complicated by the complexity of the forest canopy in the vicinity of the radiation sensor. In the healthy stand, net radiation appears to be under-simulated when the solar angles are highest (14:00 – 15:00), which may be a function of noisy measurements of incoming short-wave radiation beneath the forest canopy. Net radiation was over-simulated in the healthy stand during periods of low solar angle, which could result from over-estimation of parameters and variables used to calculate long-wave radiation. The higher correlation between simulated and measured net radiation in the burned stand is likely due to forest canopy removal and reduced variability in measured incoming short-wave radiation.

The predictive ability of the model was high ($E > 0.89$) and showed high correlation between simulated and measured snow water equivalent ($r^2 > 0.93$) for most comparisons in both stands and both years; however, the 2009 comparison in the burned stand was not as strong ($E = 0.33$; $r^2 = 0.66$). This was the result of two issues: (1) snowmelt was under-simulated following new snowfalls as a result of over-simulating snowpack cold content; and (2) failure to include snow redistribution and/or sublimation processes.

Over-simulating snowpack cold content was a result of an under-estimation of average snowpack temperature when temperatures dropped immediately following snowfall events. Although our method of calculating average snowpack temperature as an average of snow surface temperature and soil temperature may not accurately represent average snowpack temperature under specific circumstances, it represents a best approximation of this value given the available data set. Results suggest that internal snowpack processes are important to monitor when modelling snowmelt processes.

Field observations noted significant wind redistribution of snow, resulting in some snow loss by sublimation. These processes occur when wind speeds are high and the snowpack is cold and dry, which characterized the 2009 snowmelt season in the burned stand.

In most comparisons snowmelt was over-simulated at the end of the snowmelt period, likely a result of comparing snowmelt measured at a point with snowmelt simulated using radiation data integrated over a much larger area. This large area incorporated lower albedo areas caused by observed spatial heterogeneity in the shallower snow cover at the end of the snowmelt period. Thus, the over-simulation of

snowmelt rates was greater in the burned stand, as higher net radiation made it more sensitive to changing albedo.

Generally, simulated snowmelt accurately represented measured snowmelt. This snowmelt energy balance model therefore shows strong potential as a hypothesis-testing tool to better understand the effects of forest cover change on snowmelt, provided snow redistribution and sublimation are not major drivers of the local snowmelt energy balance.

Similar to other disturbance research, this thesis confirmed that changes in forest structure result in changes to snow accumulation, snowmelt energy balance, and the rate and timing of snowmelt (Koivusalo and Kokkonen, 2002; Gelfan *et al.*, 2004; Winkler *et al.*, 2005; Boon, 2009). Despite the variability in meteorological conditions between years, both stands behaved similarly in terms of the relative contribution of each energy balance component to the total energy available for snowmelt, and snowmelt rates were not significantly different. Therefore, rather than focusing on between-year differences, this thesis focused on the differences between plots.

The burned stand had significantly different snow accumulation and melt patterns than the healthy stand in both years. Significantly more snow water equivalent accumulated at peak in the burned than the healthy stand in both years ($p < 0.001$). Snowmelt was largely driven by net short-wave radiation and sensible heat flux in the burned stand, and a combination of short-wave radiation and net long-wave radiation in the healthy stand. Short-wave radiation was the largest contributor to snowmelt in both forest stands, with 107% greater inputs in the burned than in the healthy stand. The removal of forest canopy caused the long-wave flux to be 211% more negative in the

burned than in the healthy stand. Higher wind speeds and surface-atmosphere temperature gradients resulted in 150% more positive sensible heat fluxes and 191% more negative latent heat fluxes in the burned than in the healthy forest stand. Ground heat flux contributions to snowmelt were minimal, but were observed to be 123% higher in the burned stand, corresponding with warmer ground temperatures and lower soil moisture. Snowmelt rates were significantly greater in the burned than in the healthy stand ($p < 0.001$). The snowpack in the burned stand melted more rapidly, resulting in complete snowpack removal earlier than in the healthy stand.

Understanding differences in snow processes between disturbance types is very important to water resource managers, particularly when the forested areas consist of a mosaic of stand types (Jost *et al.*, 2007). Ratios of snow accumulation in the healthy to burned stand (0.55 and 0.60) were comparable to the lower range of healthy to cleared forest stand ratios (0.60 – 1.00) (Golding and Swanson, 1986; Toews and Gluns, 1986; Faria *et al*., 2000). This study simulated greater snowmelt rates in the burned stand than those observed in mountain pine beetle (MPB) killed stands five years after death (Winkler and Boon, 2009), and in the lower range of those observed in cleared forest stands (Pomeroy and Granger, 1997; Winkler *et al.*, 2005; López-Moreno and Stähli, 2008). Although snow accumulation and melt results are comparable to cleared forest stands, standing dead trees in burned forest stands will continue to attenuate incoming short-wave radiation, wind speed, and snow accumulation on the snow surface. Therefore, burned forest stands should be considered a separate forest type when simulating watershed scale runoff with stand scale data used to parameterize larger watershed-scale models.

Link and Marks (1999) concluded that in boreal forests, land-use changes may have greater impacts on seasonal snowpacks than climate shifts given the significant impact of forest canopies on net radiation. This thesis also suggests that forest canopy removal increased the amount of energy available for snowmelt in burned forests, particularly increasing short-wave radiation and turbulent heat transfers. In the burned stand, greater hourly average air and snow surface temperature at the onset of snowmelt, in combination with a shallower snowpack, resulted in higher average snowmelt rates and complete snowpack removal occurred twelve days earlier in 2010 than in 2009. In the healthy stand, the difference in meteorological and snow conditions between years was the same as in the burned stand; however, average snowmelt rates were more comparable between years, and complete snowpack removal in 2010 occurred within five days of 2009. Results between 2010 and 2009 suggest that the burned stand was more sensitive to interannual variability in meteorological and snow conditions than in the healthy stand. Therefore, it may also be more sensitive to predicted increases in air temperature and reductions in snowfall under climate change; however, additional research is required to incorporate a larger range of hydro-climatic variability and test this hypothesis.

Higher snow accumulation and more rapid melt in burned relative to healthy mature healthy forests could reduce infiltration of meltwater into the soil profile, causing spring runoff to primarily follow surface or near surface pathways (Murray and Buttle, 2005). These conditions may promote higher runoff peaks from snow-dominated watersheds, which may have severe hydrologic implications such as severe flooding (Swanson *et al.*, 1998), disturbed communities and/or productivity of aquatic ecosystems (Fausch *et al*., 2001; Dunham *et al*., 2003), and adverse effects on the quantity and

quality of water for downstream users (Swank *et al.*, 2001; Silins *et al.*, 2009b). This research not only improves our understanding of snow accumulation and melt in a burned forest stand, but also contributes valuable information to forest watershed management. Although burned stands are comparable to cleared stands, standing dead stems continue to exert controls on snow accumulation and melt processes. Retaining standing dead stems instead of salvage harvesting disturbed forests may be a more viable option for minimizing adverse hydrologic effects. Post-wildfire salvage harvesting may exacerbate the effects of wildfire on spring runoff.

Although the model developed in this thesis simulated snowmelt with a high level of accuracy and provided key information on differences in the snowmelt energy balance between the burned and healthy forest stand, the following research recommendations and additional considerations are provided to improve snowmelt modelling at the stand-scale in both disturbed and healthy forest environments.

1) Model output of total energy available for snowmelt is very sensitive to parameters used in the calculation of net radiation. Thus, stand specific values of canopy transmissivity, canopy and tree trunk temperature, and forest structure should be measured for all types of forest stands instead of selecting values from the literature.

2) The field program could be adjusted to improve the accuracy of model output by providing better data for model parameterization and validation. For example:

   a. Internal snowpack processes should be monitored, particularly internal snowpack temperature. As demonstrated in Chapter 5, snowmelt was under-simulated during and immediately after a snowfall event, when the

temperature of the snow surface decreased significantly over a short time period. This resulted in a high snowpack cold content and low energy available for snowmelt. However, the low snow surface temperature likely did not penetrate far into the snowpack during this short period; thus, average snowpack temperatures were estimated to be colder than in reality. High-resolution measurements of internal snowpack temperature would increase the accuracy of the average snowpack temperature used in the calculation of snowpack cold content.

b. The installation of a network of net radiometers across the forest stand would assist in measuring the spatial distribution of short-wave and long-wave radiation, and validating model output of net radiation. In Chapter 5, the poor comparison between simulated and measured net radiation in the healthy stand may have been a function of: (1) noisy net radiometer measurements at fine temporal scale under a heterogeneous forest canopy; (2) inaccurate model representation of short-wave radiation transmission through the complex canopy matrix during daylight hours; and/or, (3) model over-simulation of long-wave emissions from the forest canopy. A net radiometer network would help to quantify which of these three hypotheses led to the poor comparison. The model was also very sensitive to canopy transmissivity; thus collecting multiple measurements to estimate an average value of this parameter beneath a heterogeneous forest canopy may improve the comparison between simulated and measured net radiation.

c. Quantifying long-wave radiation emission from different dead tree types in the burned forest stand and their importance in the snowmelt energy balance. Chapter 6 described field observations during snow surveys that noted snow-free areas around blackened trees larger than those around burned trees that had shed their bark and become silver-grey. It was hypothesized that the lower albedo of the blackened trees would absorb more short-wave radiation, resulting in higher forest canopy and tree trunk temperatures and subsequent greater long-wave emission to the snow surface relative to the silver-grey coloured tree trunks. More accurate measurements of forest canopy and tree trunk temperature of different types of standing dead trees are required to validate this hypothesis.

d. Accurate snowmelt lysimeter measurements to properly quantify snowmelt water output from the snowpack. In Chapter 4, the construction and installation of snowmelt lysimeters were described. Snowmelt data from these lysimeters would have been the most accurate dataset to validate the model output; however, the success of the lysimeters was compromised by environmental conditions and event logger and/or tipping bucket failure. Lysimeter measurements from 2009 may have had a better fit with simulated snowmelt in the burned stand, as the measured snowmelt record from the lysimeter would have integrated snow re-distribution and sublimation into the snowmelt record.

3) This thesis presents results from a severely burned forest stand where the forest canopy was almost completely removed. Depending on the severity of the

wildfire, the amount of defoliated forest canopy will vary. Also, some wildfires are primarily ground fires that only burn the understory vegetation, litter layer, tree roots or the organic soils, while the forest canopy remains intact. Additional studies are required to evaluate the impacts of a range of burn severities on snowmelt processes.

4) Collection of additional years of data to further quantify the impact of inter-annual hydro-climatic variability and forest regeneration and/or continued forest structure change (including blowdown) after wildfire on snow processes. Chapter 6 described field observations from 2010 that indicated additional blowdown in the burned stand since forest measurements were completed in 2009. Therefore, the simulation of net radiation in 2010 may have missed key forest structural changes between years that would assist in quantifying net long-wave radiation processes and forest structure impacts on net radiation over time.

5) Collecting the same field data in a forest clearing near the burned and healthy stands. Comparing snowmelt processes between a cleared, a burned, and a healthy stands would make it easier to compare results from this thesis to other studies that have compared disturbed forests to clearings. These comparisons would also provide additional insights into the impacts of forest management options such as post-wildfire salvage harvesting.

6) Stand scale data could be used to parameterize large scale (e.g., watershed) runoff models and stand scale modelling results could be used to assess if assumptions inherent in large scale runoff models are correct. This would increase the

accuracy of large scale models evaluating runoff processes from disturbed forest stands.

This thesis presented a model designed to simulate sub-canopy snowmelt at a point based on both field data and information from the literature. Snowmelt simulated with this model compared well with measured snowmelt, providing confidence in the model's ability to simulate snowmelt energy balance processes in sub-canopy environments provided wind redistribution and sublimation are not major drivers in the local energy balance. This allowed for the quantification of wildfire disturbance effects on snow accumulation and melt. Removal of the forest canopy in burned stands resulted in significantly different snow processes in burned relative to healthy forest stands. Although results were comparable to cleared forest stands, burned forest stands should be considered a separate forest type. Stand scale data from burned stands should be used to parameterize larger scale watershed models and stand scale results should be used to validate assumptions inherent in these models. Although this thesis provides insights into the effect of wildfire on snow accumulation, the snowmelt energy balance, and the rate and timing of snowmelt at the stand scale, additional studies could improve stand scale snowmelt models and large scale runoff models in both disturbed and healthy forest environments.

References

Adams, H. D., Macalady, A. K., Breshears, D. D., Allen, C. D., Stephenson, N. L., Saleska, S. R., Huxman, T. E., & McDowell, N. G. (2010). Climate-induced tree mortality: earth system consequences. *EOS*, 91(17): 153-154.

Adams, W. P., & Barr, D. R. (1974). *Techniques and equipment for measurement of snow cover, including stratigraphy*, (Occasional Papers 3). Measurement in Physical Geography: Trent University: 11-26 pp.

Alberta Environment. (2009). *Rankings for June 2009 Mountain Snow Courses for Oldman River Basin*. Retrieved from http://environment.alberta.ca/forecasting/data/snow/jun2009/oldscrank.pdf.

Alberta Environment. (2010). *Rankings for June 2009 Mountain Snow Courses for Oldman River Basin*. Retrieved from http://environment.alberta.ca/forecasting/data/snow/jun2010/oldscrank.pdf.

Alberta Sustainable Resource Development. (2010). *Forest Regions of Alberta*. Retrieved from http://www.srd.alberta.ca/BioDiversityStewardship/Forests/Default.aspx.

Allen, C. D., Macalady, A. K., Chenchouni, H., Bachelet, D., McDowell, N., Vennetier, M., Kitzberger, T., Rigling, A., Breshears, D. D., Hogg, E. H., Gonzalez, P., Fensham, R., Zhang, Z., Castro, J., Demidova, N., Lim, J. H., Allard, G., Running, S. W., Semerci, A., & Cobb, N. (2010). A global overview of drought and heat-induced tree mortality reveals emerging climate change risks for forests. *Forest Ecology and Management*, 259(4): 660-684.

Anderson, E. A. (1973). *National Weather Service River Forecast System-Snow Accumulation and Ablation Model*, (NOAA Technical Memo, NWS Hydro-17). U.S. National Weather Service: Silver Springs, Maryland.

Andreadis, K. M., Storck, P., & Lettenmaier, D. P. (2009). Modeling snow accumulation and ablation processes in forested environments. *Water Resources Research*, 45: doi: W05429 05410.01029/02008wr007042.

Andreas, E. L. (2002). Parameterizing scalar transfer over snow and ice: A review. *Journal of Hydrometeorology*, 3(4): 417-432.

Baldocchi, D. B., Matt, D. R., Hutchison, B. A., & McMillen, R. T. (1984). Solar radiation within an oak-hickory forest: an evaluation of the extinction coefficients for several radiation components during fully-leafed and leafless periods. *Agricultural and Forest Meteorology*, 32: 307-322.

Baldocchi, D. D., Hicks, B. B., & Meyers, T. P. (1988). Measuring biosphere-atmosphere exchanges of biologically related gases with micrometeorological methods. *Ecology*, 69(5): 1331-1340.

BC Ministry of Forests and Range (2007). *Vegetation Resource Inventory Ground Sampling Procedures*, Victoria, BC, 218 pp.

Bergström, S. (1995). The HBV model. In: V. P. Singh. (Eds.), *Computer Models of Watershed Hydrology*. Water Resources Publication: Highlands Ranch, Colorado, pp. 443-476.

Beven, K. J. (2001). *Rainfall-runoff Modelling: The Primer*. John Wiley & Sons Ltd: West Sussex, England.

Bewley, D., Alila, Y., & Varhola, A. (2010). Variability of snow water equivalent and snow energetics across a large catchment subject to Mountain Pine Beetle infestation and rapid salvage logging. *Journal of Hydrology*, 388(3-4): 464-479.

Blonquist, J. M., Tanner, B. D., & Bugbee, B. (2009). Evaluation of measurement accuracy and comparison of two new and three traditional net radiometers. *Agricultural and Forest Meteorology*, 149(10): 1709-1721.

Bohren, C. F., & Thorud, D. B. (1973). Two theoretical models of radiation heat transfer between forest trees and snowpacks. *Agricultural Meteorology*, 11: 3-16.

Boon, S. (2007). Snow accumulation and ablation in a beetle-killed pine stand, northern Interior BC. *BC Journal of Ecosystem Management*, 8: 1-13.

Boon, S. (2009). Snow ablation energy balance in a dead forest stand. *Hydrological Processes*, 23(18): 2600-2610.

Braithwaite, R. J. (1984). Calculation of degree-days for glacier-climate research. *Zeitschrift für Gletscherkunde und Glazialgeologie*, 20: 1-8.

Brock, B. W., & Arnold, N. S. (2000). A spreadsheet-based (Microsoft Excel) point surface energy balance model for glacier and snow melt studies. *Earth Surface Processes and Landforms*, 25: 649-658.

Brock, B. W., Willis, I. C., & Sharp, M. J. (2000). Measurement and parameterization of albedo variations at Haut Glacier d'Arolla, Switzerland. *Journal of Glaciology*, 46(155): 675-688.

Buttle, J. M., Creed, I. F., & Moore, R. D. (2009). Advances in Canadian Forest Hydrology, 2003-2007. *Canadian Water Resources Journal*, 34(2): 113-126.

Buttle, J. M., & McDonnell, J. J. (1987). Modelling the areal depletion of snowcover in a forested catchment. *Journal of Hydrology*, 90: 43-60.

Byrne, J., Kienzle, S., Johnson, D., Duke, G., Gannon, V., Selinger, B., & Thomas, J. (2006). Current and future water issues in the Oldman River Basin of Alberta, Canada. *Water Science and Technology*, 53(10): 327-334.

Campbell Scientific (Canada) Corp. (2008). *CNR1 Net Radiometer Instruction Manual*. Retrieved from http://www.campbellsci.com.au/documents/manuals/cnr1.pdf.

Carlyle-Moses, D. (2007). Preliminary finds on canopy and bryophyte forest floor interception loss of growing-season rainfall at Mayson Lake. In: *Program and Abstracts of the Mountain Pine Beetle and Watershed Hydrology Workshop: Preliminary Results of Research from BC, Alberta, and Colorado*, Kelowna, British Columbia, pp. 23-24.

Chambers, J. M., Cleveland, M. S., Kleiner, B., & Tukey, P. A. (1983). *Graphical Methods for Data Analysis*. Duxbury Press, Wadsworth & Brooks/Cole: Boston, Massachusetts.

Chang, M. (2003). *Forest Hydrology: An Introduction to Water and Forests.* CRC Press: New York, New York.

del la Casiniere, A. C. (1974). Heat exchange over a melting snow surface. *Journal of Glaciology*, 13: 55-72.

Derby, R. W., & Gates, D. M. (1966). Temperature of tree trunks-calculated and observed. *American Journal of Botany*, 53(6P1): 580-587.

DeWalle, D. R., & Range, A. (2008). *Principles of Snow Hydrology*. Cambridge University Press: New York, New York.

Dingman, S. L. (2002). *Physical Hydrology*. 2nd Edition, Prentice-Hall Inc.: Upper Saddle River, New Jersey.

Duarte, H. F., Dias, N. L., & Maggiotto, S. R. (2006). Assessing daytime downward longwave radiation estimates for clear and cloudy skies in Southern Brazil. *Agricultural and Forest Meteorology*, 139(3-4): 171-181.

Dunham, J. B., Young, M. K., Gresswell, R. E., & Rieman, B. E. (2003). Effects of fire on fish populations: landscape perspectives on persistence of native fishes and nonnative fish invasions. *Forest Ecology and Management*, 178: 183-196.

Essery, R., Pomeroy, J., Ellis, C., & Link, T. (2008). Modelling longwave radiation to snow beneath forest canopies using hemispherical photography or linear regression. *Hydrological Processes*, 22(15): 2788-2800.

Etchevers, P., Martin, E., Brown, R., Fierz, C., Lejeune, Y., Bazile, E., Boone, A., Dai, Y., Essery, R., Fernandez, A., Gusev, Y., Jordan, R., Koren, V., Kowalcyzk, E., Nasonova, N. O., Pyles, R. D., Schlosser, A., Shmakin, A. B., Smirnova, T. G., Strasser, U., Verseghy, D.,Yamazaki, T., & Yang, Z. L. (2004). Validation of the energy budget of an alpine snowpack simulated by several snow models (SnowMIP project). *Annals of Glaciology*, 38: 150-158.

Fang, X., & Pomeroy, J. W. (2007). Snowmelt runoff sensitivity analysis to drought on the Canadian prairies. *Hydrological Processes*, 21(19): 2594-2609.

Faria, D. A., Pomeroy, J. W., & Essery, R. L. H. (2000). Effect of covariance between ablation and snow water equivalent on depletion of snow-covered area in a forest. *Hydrological Processes*, 14(15): 2683-2695.

Farnes, P. E. (1996). Impact of 1988 Yellowstone fires on snowmelt water yields. In: J. M. Greenlee. (Eds.), *The Ecological Implications of Fire in Greater Yellowstone*. International Association of Wildland Fire: Fairfield, Washington, pp. 39-42.

Fausch, K. D., Taniguchi, Y., Nakano, S., Grossman, G. D., & Townsend, C. R. (2001). Flood disturbance regimes influence rainbow trout invasion success among five holartic regions. *Ecological Applications*, 11: 1438-1455.

Federer, C. A. (1971). Solar radiation absorption by leafless hardwood forests. *Agricultural and Forest Meteorology*, 9(1971/1972): 3-20.

Flannigan, M. D., Logan, K. A., Amiro, B. D., Skinner, W. R., & Stocks, B. J. (2005). Future area burned in Canada. *Climatic Change*, 72(1-2): 1-16.

Floyd, W., & Weiler, M. (2008). Measuring snow accumulation and ablation dynamics during rain-on-snow events: innovative measurement techniques. *Hydrological Processes*, 22(24): 4805-4812.

Fontaine, T. A., Cruickshank, T. S., Arnold, J. G., & Hotchkiss, R. H. (2002). Development of a snowfall-snowmelt routine for mountainous terrain for the soil water assessment tool (SWAT). *Journal of Hydrology*, 262: 209-223.

Frazer, G. W., Canham, C. D., & Lertzman, K. P. (1999). *Gap Light Analyzer (GLA) Version 2D0: User Manual and Program Documentation*, Burnaby, British Columbia, 40 pp.

Geiger, R., Aron, R. H., & Todhunter, P. (2003). *The Climate Near the Ground*. Rowman & Littlefield Publishers: Lanham, Maryland.

Gelfan, A. N., Pomeroy, J. W., & Kuchment, L. S. (2004). Modeling forest cover influences on snow accumulation, sublimation, and melt. *Journal of Hydrometeorology*, 5(5): 785-803.

Golding, D. L., & Swanson, R. H. (1986). Snow distribution patterns in clearings and adjacent forest. *Water Resources Research*, 22: 1931-1940.

Gray, D. M., & Landine, P. G. (1988). An energy-budget snowmelt model for the Canadian prairies. *Canadian Journal of Earth Sciences*, 25(8): 1292-1303.

Gray, D. M., & Prowse, T. D. (1993). Snow and floating ice. In: D. R. Maidment. (Eds.), *Handbook of Hydrology*. McGraw-Hill: New York, New York, pp. 7.1-7.58.

Greuell, W., & Konzelmann, T. (1994). Numerical modelling of the energy balance and the englacial temperature of the Greenland Ice Sheet. Calculations for the ETH-camp location (West Greenland, 1155m a.s.l.). *Global and Planetary Change*, 9(1-2): 91-114.

Hanks, R. J., & Ashcroft, G. L. (1980). *Applied Soil Physics: Soil Water and Temperature Applications*. Springer-Verlag: Berlin, New York.

Hardy, J. P., Davis, R. E., Jordan, R., Li, X., Woodcock, C., Ni, W., & McKenzie, J. C. (1997). Snow ablation modeling at the stand scale in a boreal jack pine forest. *Journal of Geophysical Research-Atmospheres*, 102(D24): 29397-29405.

Hardy, J. P., Groffman, P. M., Fitzhugh, R. D., Henry, K. S., Welman, A. T., Demers, J. D., Fahey, T. J., Driscoll, C. T., Tierney, G. L., & Nolan, S. (2001). Snow depth manipulation and its influence on soil frost and water dynamics in a northern hardwood forest. *Biogeochemistry*, 56(2): 151-174.

Hauer, F. R., Stanford, J. A., & Lorang, M. S. (2007). Pattern and process in Northern Rocky Mountain headwaters: Ecological linkages in the headwaters of the Crown of the Continent. *Journal of the American Water Resources Association*, 43(1): 104-117.

Hayashi, M., Hirota, T., Iwata, Y., & Takayabu, I. (2005). Snowmelt energy balance and its relation to foehn events in Tokachi, Japan. *Journal of the Meteorological Society of Japan*, 83(5): 783-798.

Hedstrom, N. R., & Pomeroy, J. W. (1998). Measurements and modelling of snow interception in the boreal forest. *Hydrological Processes*, 12(10-11): 1611-1625.

Hélie, J. F., Peters, D. L., Tattrie, K. R., & Gibson, J. J. (2005). *Review and Synthesis of Potential Hydrologic Impacts of Mountain Pine Beetle and Related Harvesting Activities in British Columbia*, (MPBI Working Paper 2005-23). NRCAN CFS-PFC: Victoria, British Columbia, 26 pp.

Hicke, J. A., & Jenkins, J. C. (2008). Susceptibility of lodgepole pine to mountain pine beetle attach: Mapping stand structure across the western United States. *Forest Ecology and Management*, 255: 1536-1547.

Hill, T., & Lewicki, P. (2007). *Statistics Methods and Applications*. StatSoft: Tulsa, Oklahoma.

Hock, R. (1999). A distributed temperature-index ice-and snowmelt model including potential direct solar radiation. *Journal of Glaciology*, 45(149): 101-111.

Hosler, C. L., Jense, D. C., & Goldshlak, L. (1957). On the aggregation of ice crystals to form snow. *Journal of Meteorology*, 14: 415-420.

Intergovernmental Panel on Climate Change (2008). *Climate Change and Water.*, (Technical Paper VI). Cambridge University Press: New York, New York, 214 pp.

Jarvis, P. G., James, G. B., & Landsberg, J. J. (1976). Chapter 7: coniferous forest. In: J. L. Monteith. (Eds.), *Vegetation and atmosphere case studies*. Academic Press: London, pp. 171-240.

Jordan, R. (1991). *A One-dimensional Temperature Model for a Snow Cover: Technical Documentation for SNTHERM89.*, (Special Report 91-16). United States Army Corps of Engineers: Hanover, New Hampshire, pp.

Jost, G., Weiler, M., Gluns, D. R., & Alila, Y. (2007). The influence of forest and topography on snow accumulation and melt at the watershed-scale. *Journal of Hydrology*, 347(1-2): 101-115.

Kattelmann, R. C. (1984). Snowmelt lysimeters: design and use. In: *Proceeding of the 52nd Western Snow Conference*, Sun Valley, Idaho, pp. 68-79.

Klute, A. (1986). *Method of Soil Analysis*. Soil Science Society of America Inc,: Madison, Wisconsin.

Koivusalo, H., & Kokkonen, T. (2002). Snow processes in a forest clearing and in a coniferous forest. *Journal of Hydrology*, 262(1-4): 145-164.

Krause, P., Boyle, D. P., & Bäse, F. (2005). Comparison of different efficiency criteria for hydrological model assessment. *Advances in Geoscience*, 5: 89-97.

Kulig, J. C., Edge, D., Reimer, W. B., Townshend, I., & Lightfoot, N. (2009). Levels of risk: Perspectives from the Lost creek fire. *The Australian Journal of Emergency Management*, 40(2): 33-39.

Leach, J. A., & Moore, R. D. (2010). Above-stream microclimate and stream surface energy exchanges in a wildfire-disturbed riparian zone. *Hydrological Processes*, 24: 2369-2381.

Li, L., & Pomeroy, J. (1997). Estimates of threshold wind speeds for snow transport using meteorological data. *Journal of Applied Meteorology*, 36: 205-213.

Link, T. E., & Marks, D. (1999). Point simulation of seasonal snowcover dynamics beneath boreal forest canopies. *Journal of Geophysical Research*, 104(D22): 27, 841-827, 857.

Liston, G. E. (1995). Local advection of momentum, heat, and moisture during the melt of patchy snow covers. *Journal of Applied Meteorology*, 34(7): 1705-1715.

Littell, J. S., McKenzie, D., Peterson, D. L., & Westerling, A. L. (2009). Climate and wildfire area burned in western U. S. ecoprovinces, 1916-2003. *Ecological Applications*, 19(4): 1003-1021.

López-Moreno, J. I., & Stähli, M. (2008). Statistical analysis of the snow cover variability in a subalpine watershed: Assessing the role of topography and forest, interactions. *Journal of Hydrology*, 348(3-4): 379-394.

Lundberg, A., & Halldin, S. (1994). Evaporation of intercepted snow- analysis of governing factors. *Water Resources Research*, 30(9): 2587-2598.

MacDonald, R. J., Byrne, J., & Kienzle, S. (2009). A physically based daily hydrometeorological model for complex mountain terrain. *Journal of Hydrometeorology*, 10: 1430-1446.

Macias Fauria, M., & Johnson, E. A. (2008). Climate and wildfires in the North American boreal forest. *Philosophical Transactions of the Royal Society B: Biological Sciences*, 363(1501): 2317-2329.

Male, D. H., & Gray, D. M. (1981). Snowcover ablation and runoff. In: D. M. Gray. (Eds.), *Handbook of Snow*. The Blackburn Press: Caldwell, New Jersey, pp. 360-436.

Marks, D., Domingo, J., Susong, D., Link, T., & Garen, D. (1999). A spatially distributed energy balance snowmelt model for application in mountain basins. *Hydrological Processes*, 13(12-13): 1935-1959.

Marks, D., Kimball, J., Tingey, D., & Link, T. (1998). The sensitivity of snowmelt processes to climate conditions and forest cover during rain-on-snow: a case study of the 1996 Pacific Northwest flood. *Hydrological Processes*, 12(10-11): 1569-1587.

Martinec, J., & Rango, A. (1986). Parameter values for snowmelt runoff modeling. *Journal of Hydrology*, 84: 197-219.

McGregor, G. R., & Gellatly, A. F. (1996). The energy balance of a melting snowpack in the French Pyrenees during warm anticyclonic conditions. *International Journal of Climatology*, 16(4): 479-486.

McKay, D. C., & Thurtell, G. W. (1978). Measurements of energy fluxes involved in energy budget of a snow cover. *Journal of Applied Meteorology*, 17(3): 339-349.

Melloh, R. (1999). *A Synopsis and Comparison of Selected Snowmelt Algorithms*, (CRREL Report 99-8). US Army Corps of Engineers, Cold Regions Research & Engineering Laboratory: 24 pp.

Melloh, R. A., Hardy, J. P., Davis, R. E., & Robinson, P. B. (2001). Spectral albedo/reflectance of littered forest snow during the melt season. *Hydrological Processes*, 15(18): 3409-3422.

Metcalfe, R. A., & Buttle, J. M. (1998). A statistical model of spatially distributed snowmelt rates in a boreal forest basin. *Hydrological Processes*, 12: 1701-1722.

Mitchell, R. G., & Preisler, H. K. (1998). Fall rate of lodgepole pink killed by the mountain pine beetle in central Oregon. *Western Journal of Applied Forestry*, 13: 23-26.

Moore, R. D. (1983). On the use of bulk aerodynamic formulas over melting snow *Nordic Hydrology*, 14(4): 193-206.

Murray, C. D., & Buttle, J. M. (2003). Impacts of clearcut harvesting on snow accumulation and melt in a northern hardwood forest. *Journal of Hydrology*, 271(1-4): 197-212.

Murray, C. D., & Buttle, J. M. (2005). Infiltration and soil water mixing on forested and harvested slopes during spring snowmelt, Turkey Lakes Watershed, central Ontario. *Journal of Hydrology*, 306(1-4): 1-20.

Nash, J. E., & Sutcliffe, J. V. (1970). River flow forecasting through conceptual models. Part 1: a discussion of principles. *Journal of Hydrology*, 10(3): 282-290.

Natural Resources Canada. (2007). *Forest Ecozones of Canada*. Retrieved from http://ecosys.cfl.scf.rncan.gc.ca/classification/classif05-eng.asp.

Ni, W. G., Li, X. W., Woodcock, C. E., Roujean, J. L., & Davis, R. E. (1997). Transmission of solar radiation in boreal conifer forests: Measurements and models. *Journal of Geophysical Research-Atmospheres*, 102(D24): 29555-29566.

Nkemdirim, L. C. (1996). Canada's chinook belt. *International Journal of Climatology*, 16(4): 441-462.

Nkemdirim, L. C., & Weber, L. (1998). Comparison between the droughts of the 1930s and 1980s in the Southern Prairies of Canada. *Journal of Climate*, 12: 2434-2450.

Nobis, M., & Hunziker, U. (2005). Automatic thresholding for hemispherical canopy-photographs based on edge detection. *Agricultural and Forest Meteorology*, 128(3-4): 243-250.

Obukhov, A. M. (1971). Turbulence in an atmosphere with a non-uniform temperature. *Boundary-Layer Meteorology*, 2: 7-29.

Oke, T. R. (1987). *Boundary Layer Climates*. Routledge: London, New York.

Oldman Watershed Council (2010). *Oldman River State of the Watershed Report 2010*, Oldman Watershed Council: Lethbridge, Alberta, 284 pp.

Overpeck, J. T., Rind, D., & Goldberg, R. (1990). Climate-induced changes in forest disturbance and vegetation. *Nature*, 343(6253): 51-53.

Parviainen, J., & Pomeroy, J. W. (2000). Multiple-scale modelling of forest snow sublimation: initial findings. *Hydrological Processes*, 14(15): 2669-2681.

Pellicciotti, F., Helbing, J., Rivera, A., Favier, V., Corripio, J., Araos, J., Sicart, J. E., & Carenzo, M. (2008). A study of the energy balance and melt regime on Juncal Norte Glacier, semi-arid Andes of central Chile, using melt models of different complexity. *Hydrological Processes*, 22(19): 3980-3997.

Podur, J., Martell, D. L., & Knight, K. (2002). Statistical quality control analysis of forest fire activity in Canada. *Canadian Journal of Forest Research*, 32(2): 195-205.

Pomeroy, J., Essery, R., Hardy, J., Rowlands, A., & Marks, D. (2003). Uncertainty in estimating longwave fluxes to snow under forest canopies. *Geophysical Research Abstracts*, 5: 12810.

Pomeroy, J., & Goodison, B. E. (1997). Winter and snow. In: W. G. Bailey, T. R. Oke and W. R. Rouse. (Eds.), *The Surface Climates of Canada*. McGill-Queen's University Press: Montreal, Quebec, pp. 68-100.

Pomeroy, J., & Gray, D. M. (1995). *Snowcover Accumulation, Relocation, and Management*, (National Hydrology Research Institute Science Report No.7). Minister of Supply and Services Canada: Saskatoon, Saskatchewan, 135 pp.

Pomeroy, J., Gray, D. M., Brown, T., Hedstrom, N., Quinton, W. L., Granger, R. J., & Carey, S. K. (2007). The cold regions hydrological model: a platform for basing process representation and model structure on physical evidence. *Hydrological Processes*, 21: 2650-2667.

Pomeroy, J., & Schmidt, R. A. (1993). The use of fractal geometry in modelling intercepted snow accumulation and sublimation. In: *Proceeding of the 50th Annual Eastern Snow Conference*, Quebec City, Quebec, pp. 231-239.

Pomeroy, J. W., & Granger, R. J. (1997). Sustainability of the western Canadian boreal forest under changing hydrological conditions .1. Snow accumulation and ablation. In: D. Rosbjerg, N. E. Boutayeb, A. Gustard and Z. W. Kundzewicz. (Eds.), *Sustainability of Water Resources Under Increasing Uncertainty*. Int Assoc Hydrological Sciences: Wallingford, United Kingdom, pp. 237-242.

Pomeroy, J. W., Gray, D. M., Hedstrom, N. R., & Janowicz, J. R. (2002). Prediction of seasonal snow accumulation in cold climate forests. *Hydrological Processes*, 16(18): 3543-3558.

Pomeroy, J. W., Gray, D. M., Shook, K. R., Toth, B., Essery, R. L. H., Pietroniro, A., & Hedstrom, N. (1998). An evaluation of snow accumulation and ablation processes for land surface modelling. *Hydrological Processes*, 12(15): 2339-2367.

Pomeroy, J. W., Marks, D., Link, T., Ellis, C., Hardy, J., Rowlands, A., & Granger, R. (2009). The impact of coniferous forest temperature on incoming longwave radiation to melting snow. *Hydrological Processes*, 23(17): 2513-2525.

Prata, A. J. (1996). A new long-wave formula for estimating downward clear-sky radiation at the surface. *Quarterly Journal of the Royal Meteorological Society*, 122: 1127-1151.

Price, A. G. (1977). *Snowmelt Runoff Processes in a Subarctic Area*, (McGill Sub-Arctic Research Paper No.29, Climatological Research Series No.10). McGill University, Department of Geography: Montreal, Quebec, 106 pp.

Price, A. G., & Dunne, T. (1976). Energy-balance computations of snowmelt in a subarctic area. *Water Resources Research*, 12(4): 686-694.

Quick, M. C., & Pipes, A. (1977). UBC Watershed model. *Hydrological Sciences Bulletin*, 22(1): 153-161.

Rauner, J. L. (1976). Chapter 8: deciduous forests. In: J. L. Monteith. (Eds.), *Vegetation and the Atmosphere Case Studies*. Academic Press: London, pp. 241-264.

Reba, M. L., Link, T. E., Marks, D., & Pomeroy, J. (2009). An assessment of corrections for eddy covariance measured turbulent fluxes over snow in mountain environments. *Water Resources Research*, 45: doi:10.1029/2008wr007045.

Reifsnyder, W. E., & Lull, H. W. (1965). *Radiant Energy in Relation to the Forest*, (USDA Agricultural Technical Bulletin No. 1344 (Reprinted by AMS Press, 1979)). 111 pp.

Rood, S. B., Samuelson, G. M., Weber, J. K., & Wywrot, K. A. (2004). Twentieth-century decline in streamflows from the hydrographic apex of North America. *Journal of Hydrology*, 306: 215-233.

Roujean, J. L. (1999). Two-story equations of transmission of solar energy (TSETSE) in open boreal conifer tree stands. *Jounal of Geophysical Research*, 104(D22): 27869-27879.

Saunders, I. R., & Byrne, J. M. (1994). Annual and seasonal climate and climatic changes in the Canadian prairies simulated by the CCC-GCM. *Atmosphere-Ocean*, 32(3): 621-641.

Schindler, D. W., & Donahue, W. F. (2006). An impending water crisis in Canada's western prairie provinces. *Proceedings of the National Academy of Sciences of the United States of America*, 103(19): 7210-7216.

Schmidt, R. A. (1980). Threshold wind-speeds and elastic impact in snow transport. *Journal of Glaciology*, 26(94): 453-467.

Schmidt, R. A., Jairell, R. L., & Pomeroy, J. W. (1988). Measuring snow interception and loss from an artificial conifer. In: *Proceedings of the 56th Annual Western Snow Conference*, Kalispell, Montana, pp. 166-169.

Schmidt, R. A., & Pomeroy, J. (1990). Bending of a conifer branch at subfreezing temperatures: Implications for snow interception. *Canadian Journal of Forest Research*, 20: 1250-1253.

Schmidt, R. A., & Troendle, C. A. (1992). Sublimation of intercepted snow as a global source of water vapour. In: *Proceedings of the 60th Annual Western Snow Conference*, Jackson, Wyoming, pp. 1-9.

Shapiro, S. S., Wilk, M. B., & Chen, H. J. (1968). A comparative study of various tests for normality. *Journal of American Statistical Association*, 63(324): 1343-1372.

Shook, K. R., Gray, D. M., & Pomeroy, J. (1993). Temporal variations in snowcover area during melt in prairie and alpine environments. *Nordic Hydrology*, 24: 183-198.

Sidle, R. C. (2006). Field observations and process understanding in hydrology: essential components in scaling. *Hydrological Processes*, 20(1439-1445).

Silins, U., Bladon, K. D., Stone, M., Emelko, M. B., Boon, S., Williams, C., Wagner, M., & Howery, J. (2009a). *Southern Rockies Watershed Project: Impact of Natural Disturbance by Wildfire on Hydrology, Water Quality, and Aquatic Ecology of Rocky Mountain Watersheds Phase 1 (2004-2008)*, 88 pp.

Silins, U., Stone, M., Emelko, M. B., & Bladon, K. D. (2009b). Sediment production following severe wildfire and post-fire salvage logging in the Rocky Mountain headwaters of the Oldman River Basin, Alberta. *Catena*, 79(3): 189-197.

Silins, U., & Wagner, M. (2007). *Southern Rockies Watershed Project 2nd interim report*, 44 pp.

Sivapalan, M., Takeuchi, K., Franks, S. W., Gupta, V. K., Karambiri, H., Lakshmi, V., Liang, X., McDonnell, J. J., Mendiondo, E. M., O'Connell, P. E., Oki, T., Pomeroy, J. W., Schertzer, D., Uhlenbrook, S., & Zehe, E. (2003). IAHS decade on predictions in ungauged basins (PUB), 2003-2012: Shaping an exciting future for the hydrological sciences. *Hydrological Sciences Journal*, 48(6): 857-880.

Spittlehouse, D. L., & Winker, R. D. (1996). Forest canopy effects on sample size requirements in snow accumulation and melt comparisons. In: *Proceedings of the 64th Annual Western Snow Conference*, Bend, Oregon, pp. 39-46.

Spittlehouse, D. L., & Winkler, R. D. (2002). Modelling snowmelt in a forest and clearcut. In: *Proceedings of the 25th Conference on Agricultural and Forest Meteorology*, Norfolk, Virginia, pp. 121-122.

Storck, P., Lettenmaier, D. P., & Bolton, S. M. (2002). Measurement of snow interception and canopy effects on snow accumulation and melt in a mountainous maritime climate, Oregon, United States. *Water Resources Research*, 38(11): doi:10.1029/2002WR001281.

Sturm, M., Holmgren, J., König, M., & Morris, K. (1997). The thermal conductivity of seasonal snow. *Journal of Glaciology*, 43(143): 26-41.

Suzuki, K., Kodama, Y., Yamazaki, T., Kosugi, K., & Nakai, Y. (2008). Snow accumulation on evergreen needle-leaved and deciduous broad-leaved trees. *Boreal Environment Research*, 13(5): 403-416.

Swank, W. T., Vose, J. M., & Elliott, K. J. (2001). Long-term hydrologic and water quality responses following commercial clearcutting of mixed hardwoods on a southern Appalachian catchment. *Forest Ecology and Management*, 143(1-3): 163-178.

Swanson, F. J., Johnson, S. L., Gregory, S. V., & Acker, S. A. (1998). Flood disturbance in a forested mountain landscape. *BioScience*, 48(9): 681-689.

Toews, D. A. A., & Gluns, D. R. (1986). Snow accumulation and ablation on adjacent forested and clearcut sites in southeastern British Columbia. In: *Proceedings of the 54th Annual Western Snow Conference*, Phoenix, Arizona, pp. 101-111.

United States Army Corps of Engineers (1956). *Snow Hydrology: Summary Report of the Snow Investigations*, Portland, Oregon, 437 pp.

Walter, M. T., Brooks, E. S., McCool, D. K., King, L. G., Molnau, M., & Boll, J. (2005). Process-based snowmelt modeling: does it require more input data than temperature-index modeling? *Journal of Hydrology*, 300(1-4): 65-75.

Westerling, A. L., Gershunov, A., Brown, T. J., Cayan, D. R., & Dettinger, M. D. (2003). Climate and wildfire in the western United States. *Bulletin of the American Meteorological Society*, 84(5): 595.

Westerling, A. L., Hidalgo, H. G., Cayan, D. R., & Swetnam, T. W. (2006). Warming and earlier spring increase western U.S. forest wildfire activity. *Science*, 313: 940-943.

Winkler, R. D. (2001). *The Effects of Forest Structure on Snow Accumulation and Melt in South-central British Columbia*. Doctor of Philosophy. University of British Columbia, Vancouver, British Columbia.

Winkler, R. D., & Boon, S. (2009). A summary of research into the effects of mountain pine beetle related stand mortality on snow accumulation and ablation in BC. In: *Proceedings of the 77th Annual Western Snow Conference*, Canmore, Alberta, pp. 83-93.

Winkler, R. D., Boon, S., Zimonick, B., & Baleshta, K. (2010). Assessing the effects of post pine beetle forest litter on snow albedo. *Hydrological Processes*, 24: 803-812.

Winkler, R. D., Spittlehouse, D. L., & Golding, D. L. (2005). Measured differences in snow accumulation and melt among clearcut, juvenile, and mature forests in southern British Columbia. *Hydrological Processes*, 19(1): 51-62.

Wiscombe, W. J., & Warren, S. G. (1980). A model for the spectral albedo of snow. I: Pure snow. *Journal of Atmospheric Science*, 37: 2712-2733.

Woo, M., & Giesbrecht, M. A. (2000). Simulation of snowmelt in a subarctic spruce woodland: 1. Tree model. *Water Resources Research*, 36(8): 2275-2285.